Response to Anonymous Referee #1

The referee's comments are in italics, our responses in plain font.

While not explicitly stated in the manuscript (except indirectly in the title), it appears to me that this paper is an introduction article to the ATTO special issue rather than a regular research article. At such, the paper is very well written and easy to read. I do not find any errors in the paper, so my comments are mainly related to structural and technical issues. Once the authors have addressed the comments given, I recommend accepting this paper for publication in ACP.

We thank the referee for his/her constructive comments. We have added a paragraph at the end of the introduction that makes it clear that this paper is intended as introduction and overview for a special issue.

General issues

The objectives, given in the end of section 1, remain a bit unclear when reading the paper for the first time. What are these objectives representing? Objectives of the whole research being done in ATTO, or even more generally in the Amazon basin? Objective of the research planned to be published in this special issues, or something else? Please define this clearly in the text. The current list of objectives ranges from aiming to solve purely scientific questions to mainly technical issues (carrying out various kinds of measurement). The whole paper would definitely be more appealing to readers if the authors could somehow divide the list of objective into 2-3 separate categories (e.g. "scientific aims", "technical goals" etc.).

We have now made it clear that these are the scientific objectives of the ATTO project. We have reorganized and tightened up the description of the objectives, reducing their number to seven. At this point, there are no objectives of a purely technical nature, so that a division of the list, as proposed by the reviewer, is not practical.

The type of this paper should be reflected in the section titles. Therefore, I do not think that the titles of sections 4 and 5 are appropriate. For example, some of the subsections in section 4 do not contain results at all (e.g. 4.1.2) but rather describe what is being done in practice. I suggest renaming the title of section 4 something like "4. Ongoing research and preliminary results". Likewise, the conclusions made from the ongoing measurements are preliminary rather than end products of this project. I would be more comfortable with the title "5. Summary and future outlook".

We have adopted the headings proposed by the reviewer.

While I am in favor of keeping section 3 as brief as possible, some addition information might be useful for the readers. Section 3.4: what is the accuracy of trace gas measurements, especially in terms of the detection limit for concentrations? Sections 3.6.1 and 3.6.2: Are the instruments measuring aerosol number size distributions, optical properties and CCN under regular quality control and have any of these instruments been in instrument inter-comparison experiments?

Section 3.4: Information on the precision and detection limits has been added.

Sections 3.6.1 and 3.6.2: We are conducting regular quality checks with all aerosol sizing instruments and CPCs, including flow checks, zero tests, and intercomparisons with ambient aerosol and monodisperse PSL cells. Exemplary plots are already included in the manuscript (Fig. 26). In general, all instruments are calibrated frequently as part of the maintenance routines, e.g., the CCNC with size selected monodisperse ammonium sulfate particles and the nephelometer with CO_2 as reference gas. The MAAP and aethalometer are subject to frequent intercomparisons with the other optical instruments. For example, two aethalometers and the MAAP were operated side-by-side during an intensive campaign in Nov/Dec 2014. The BC concentrations from the individual instruments agreed well. The SP2 instrument was carefully intercalibrated with another SP2 during the GoAmazon-2014 campaign. This information has been added to the text.

Technical issues

Page 11634 and Figs. 8-11: What does SD function mean? Please define.

SD means standard deviation. We had that spelled out in the manuscript, but ACP changed it to SD without telling us!

Pages 11637 and 11638: The authors use terms "intermittent events" and "GW events" and sometimes simply events (line 14 on page 11638). What is the difference? Is one of those subset of the other, or are they totally different phenomena.

Oscillatory behavior in the nocturnal boundary layer (Van de Wiel et al., 2002) can be generated by intermittent turbulence, for example due to downward bursts from turbulence created aloft (Mahrt, 1999), or by the action of gravity waves upon the turbulent flow (Zeri and Sá, 2011). The first case is discussed in section 4.2.4, where the term "intermittent events" is used (or sometimes just "events", where the context is clear). The second case, the effect of gravity waves on the stable boundary layer, is discussed in section 4.2.5, where the term "gravity wave events" is used. These two sections have been reorganized to make this distinction clear and definitions have been added.

In principle, the figure captions should be understandable by themselves. Therefore, I recommend spelling out SD, TKE and GW in the captions of fFgs. 8-11, 13 and 14.

Done

There is a very large number of figures. Are all of them necessary and could some of them combined together (for example, Figs. 17-19 could form 3 panels of one figure).

We combined Figs. 8-10 and Figs. 17-19 into one Figure each.

Response to Anonymous Referee #2

The referee's comments are in italics, our responses in plain font.

This manuscript states that it provides an overview of the first results from the Amazon Tall Tower Observatory (ATTO). The ACPD short title is "ATTO overview".

Ongoing and future ATTO results will be an incredible addition to Amazonian science. That said, the manuscript in its present form in my own view does not do justice to the project, and I give a rating of "fair" to this ACPD manuscript.

The present version of the manuscript appears to me to lack a simple statement as to its purpose. Why do we need this manuscript? The absence of this motivational statement makes preparation of the review quite difficult because I do not know exactly what criteria to evaluate in deciding if the authors have achieved their purpose. Based on the title, a logical inference is to formulate criteria based on the quality of a description of the need for a tall tower and a presentation of early results. The actual manuscript, however, is much different from such criteria, especially with regard to the description of a need.

We thank the referee for his/her constructive comments. We have added a paragraph at the end of the introduction that makes it clear that this paper is intended as an introduction to and overview for a special issue. The Amazon Tall Tower Observatory is actually more than the tall tower itself, rather, it comprises several smaller towers for pilot and process studies as well as the ecosystem surrounding the towers. This paper is intended to provide the scientific context of ATTO and to serve as an overview paper for the pilot studies. A future paper will discuss the details of the tall tower.

Here are some suggestions:

1. Foremost, there should be a description of the tall tower and its motivation. The actual manuscript emphasizes long-term measurements. This is not a new theme for Amazonia. Those efforts have been under way through many projects, most notably LBA for climate change as well as multiple forestry studies.

As stated above, there will be a future paper with the details of the tall tower. Nevertheless, we have added some text regarding the motivation for the construction of the tall tower in the introduction.

2. The motivation for the tall tower is really marginalized in the actual manuscript. Only the sections on turbulence (sections 4.2.x) provide some intellectual motivation for the tallness of the tower. I think instead the introduction should do this job. Why do we need a 325 m tower and what do we get out of it? The manuscript does not presently answer this question. As an example, how about to show the fetch of a 325 m compared to shorter towers in Amazonia, and how about to discuss what that means for a definitive answer about CO2 uptake or release?

See the response to comment 1) above.

3. This manuscript does not discuss measurements from the tall tower. The manuscript states that the tall tower will be completed in 2015. Again, the entire motivation for the manuscript is not clear.

See the response to the introductory comment above.

4. The introduction of the manuscript reads like a review paper, a book chapter, or perhaps the introduction to a proposal, rather than a research article. ATTO itself is not mentioned until the end of the long introduction, at which point a list of 9 objectives is summarily presented. How about a complete deletion of the present introduction with a re-work toward a clear motivation for what a tall tower can and will accomplish (this is what is novel), with a downgrade on emphasis of long-term measurements (which are needed but not novel, i.e., this idea is common place and there are various type of long-term measurements already underway for years to decades at other sites).

The introduction serves to introduce the reader of the special volume to the scientific background and context of the ATTO project. Therefore, to provide this background to a broad range of scientists from many disciplines it is written as a “mini-review”. It is also meant as a common point of reference for the specialist papers in the special issue. While the need for long-term measurements may be well known, it is nevertheless important to emphasize this point for a site that is intended to operate for decades. Besides, to our knowledge there are no continuous long-term high-accuracy measurements of trace gases and aerosols in the Amazon region. The

introduction now contains a section discussing the motivation and concept of the tall tower and an improved description of the objectives.

5. Parts of section 2 are strange for a research article. Sections 2.2, 2.3, and 2.5 seem to be drawn from a narrative of a travel report. I would suggest for consideration that these sections can be entirely removed and that the manuscript would be focused and improved in consequence.

As mentioned before, this paper is meant to be a common resource for specialist papers in the ATTO Special Issue. As such, the description of logistical details is appropriate. The text has been tightened up somewhat, however.

6. Subsections of section 3 are highly heterogeneous in content and quality. Some of them go into much more detail than would be needed in an overview paper, such as repeating in full paragraphs what are standard operating procedures for instruments and techniques (e.g., consider using just a single reference in place of a paragraph). In my view, section 3 should only going into details about aspects that are unique and different to ATTO.

Here, there is a divergence of opinions among reviewers. While reviewer 1 feels that the methods section is quite brief and requests some more details, this reviewer thinks there is too much detail in some sections. Given that this paper is a team effort and contains contributions from many disciplines, a certain degree of heterogeneity seems unavoidable. For example, the discussion of the CO_2/CH_4/CO analyzers needs to be quite detailed, because the performance of the analyzers is specific to individual instruments and traceability is essential to quality assurance of these key data. Similarly, inlet setups are described in detail as they are crucial to the validity of the measurements, and a detailed discussion here allows common referencing in the specialist papers. The methods section was edited throughout for brevity and clarity.

7. Section 4 relates to results and discussion. Again, these sections are highly heterogeneous in presentation and quality.

7a. Section 4.2.4 is an example of what in my view was really done well. This section provides new information based on measurements that are specific to the ATTO site. Sections 4.2.5, 4.2.6, and 4.2.7 are also exemplarily positive in that they provide new and specific information about the ATTO site that promise to be useful as studies there continue in the future, as

well as interesting at present to a reader. Each of these sections has a nice concluding take-home statement for the reader about ATTO specific information.

We thank the reviewer for these positive remarks.

7b. Let me now give a negative example. Section 4.1.2 essentially provides no research information. It should be deleted.

At the time the ACPD version of the manuscript was written, this project was in its very early stages. Many of the measurements reported here therefore represent an attempt to define an initial baseline against which the extended records can be evaluated in the future. Nevertheless, significant results have been obtained in the meantime, which are briefly presented in the revised version.

7c. My quick review is that helpful, informative sections with new research results include: 4.3.2 and 4.3.3. Sections that really do not say anything by way of new data or new insights compared to existing literature (as cited in the manuscript itself) include: 4.3.1, 4.3.4, 4.3.5, 4.3.6, 4.3.7, and 4.3.8.

In the following, we point out what is new in terms of data and insights in those sections that the reviewer did not feel contained enough novel material:

4.3.1: There are no previously published high-accuracy measurements of CO_2, CH_4, or CO in the Amazon forest (or any tropical forest that I am aware of) that span more than the time of an intensive campaign. Even these campaign data are usually not continuous measurements. For CO, for example, only some fragmentary profiles with outdated techniques are in the literature. There are also no continuous data from any mid-continental tropical site for these trace gases. The only comparable data are from flask sampling programs. The ATTO results present clear evidence for a CO source at ground level in the rainforest, something that was only speculated about earlier. They also indicate strong episodic CH_4 sources that remain unexplained.

4.3.4: Systematic measurements of the aerosol optical properties in the central Amazon are still scarce. The only comparable data set is that of Rizzo et al. (2013). Since their site has a significantly greater likelihood of contamination from the Manaus area, having a more remote site for comparison is very important. This section also contains a discussion of the absorption Ångstrom exponent, for which no systematic previous data exist from a remote tropical forest

region. We also present the first results of measurements of refractory black carbon by the SP2 instrument in this type of environment, which produce some quite surprising and not yet fully explained results. Our measurements suggest very strong absorption enhancements in Amazonian particles relative to fresh soot particles, which are likely related to thick coatings with biogenic or pyrogenic organic matter.

4.3.5: Compared to the huge amounts of data available from, for example, Europe and North America, the moist tropics are still a highly undersampled region. Previous studies were limited to short campaign periods and did not cover the full seasonal and intraseasonal variability of size distributions. While this section contains a significant amount of confirmatory information, it is nevertheless important to document that the comprehensive data sets obtained at ATTO agree with the more spotty information obtained previously. Furthermore, this section contains some aspects of the long-term measurements of fluorescent biological particles, which are unique for the Amazon ecosystem. It emphasizes the dominance of fluorescent supermicron bioaerosols in the coarse mode size range in the Amazon. These are the first reported measurements of fluorescent particles with the WIBS system from the Amazon.

4.3.6: Again, there are no previous measurements from Amazonia by an aerosol mass spectrometer that extend over more than a few weeks in the wet season. In the revised manuscript, we include monthly average ACSM data that show the changes in aerosol composition and concentration throughout the annual cycle.

We present here the first measurements of iron oxidation states and solubility in aerosols from a comparable environment. The measurements of crustal elements reported here may be more of a confirmation of previous work, but are reported to provide a comprehensive overview of work going on at ATTO.

4.3.7: In general, there are only a small number of studies that focus on the microstructure of Amazonian aerosols, which is important for understanding their micro-physical properties. Moreover, the previous single-particle studies in central Amazonia have focused on the wet season. Here we present exemplary results that show dry-season aerosols with significant contributions from aged biomass burning and fossil fuel burning. The data presented here show the high degree of mixing and atmospheric aging of the particles. It further emphasizes the thick coating on BC cores, with important implications for the optical properties of the aerosol. The STXM

images from the wet season show the characteristics of coarse-mode primary biological particles. These types of results have not been published previously.

4.3.8: We are surprised that the reviewer feels that this section does not contain new information. We are not aware of a previous publication that quantifies the amounts of monoterpene and sesquiterpene oxidation products in tropical forest aerosols. However, to better point out the new scientific aspects this section has been revised and updated.

7d. Figure 1 is essential. Figure 2 seems extraneous. And so on. Are 35 figures justified? Or could a very nice job be done with half as many or fewer? Some of the figures represent statistical studies of a full season (which seems appropriate to an overview manuscript) while other figures seem anecdotal to a single or a few days studies (which seems inappropriate to an overview manuscript).

We disagree with the reviewer concerning Figure 2. Since ATTO is intended to be an observatory with the objective of detecting large-scale, long-term trends, it is important to show the potential sources and sinks of biogenic and anthropogenic species in the fetch region. We represent the anthropogenic sources by mapping population density and the biogenic sources by ecosystem type. The mapped region has been deliberately kept fairly large to provide context. For example, how does the populated region in NE Brazil, which is in the normal fetch of ATTO during the dry season compare to the Sao Paulo region, which rarely affects the central Amazon?

Having figures that display long-term measurements as well as results from intensive campaigns reflects the concept of the ATTO observatory to be both a long-term monitoring site and to host intensive campaigns. Given the large number of studies ongoing at ATTO, we feel that the most effective way of providing an overview is to present a relatively short text and one or a few plots for each program component. We did combine some of the figures into a single plot, however.

7e. I expect the authors will disagree on some of my classifications of good and bad examples and provide good explanations, but I think they will agree with at least some of the classifications and recognize in all cases opportunities for significant improvements. My point here is not really to attempt to be directive in any way about what should stay in or what should go out in a seriously revised manuscript. Rather, I hope that the authors will make revisions with an eye toward cutting the length of the text significantly and focusing on what is really new and dif-

ferent for an overview of the first results from ATTO. The manuscript probably would have benefited from a few more rounds of internal revisions before being sent to peer review. I would encourage the new flavor of the manuscript to emphasize why a TALL tower is motivated or interesting.

We hope that the revised version will have addressed at least most of the reviewer's concern. Producing a synthesis with such a large number of co-authors and such a large and diverse portfolio is not an easy task. As pointed out before, the motivation for the tall tower has now been included, but specifics and results from the tall tower will be provided in a future paper.

The ATTO project will be a source of excellent observations and associated science in the years and decades ahead. It would be valuable to the ATTO community for this first manuscript to be really streamlined and focused if it is to continue to ACP so that it can be of a final quality equal to the ATTO project itself. Please accept my criticisms in that context.

Response to Referee #3 (D. Fitzjarrald)

We thank the referee for his constructive comments. The referee's comments are in italics, our responses in plain font.

Having labored in the Amazon rainforest environment at intervals during a period of 30 years, I can well appreciate the remarkable effort that went into the making of this facility.

I have worked personally with many of the authors on other projects. I think that too many topics and indeed, many separate potential papers or notes, were combined in this mighty one-hundred-and-twenty-seven-page manuscript. This is more than an "Overview", but less than a proper publication for each topic. Releasing these half-results now runs the risk of preventing the original scientists from presenting their specialized work separately.

Given the large number of studies ongoing at ATTO, we feel that the most effective way of providing an overview is to present a relatively short text and one or a few plots for each program component. This is the "standard" way of producing an overview paper for a special issue. There would be no objective basis for arbitrarily excluding some of the ATTO subprojects. The authors see no risk of this publication precluding future specialized papers. The overview is also intended to provide a broad context for readers unfamiliar with work in the disciplines other than their own.

This is compounded by the distinct impression this journal gives that the paper is essentially already accepted, even as it remains in some odd limbo as it awaits some correction and blessing.

It appears that the reviewer is not familiar with the two-stage publication and open review process of ACPD/ACP. Please see

http://www.atmospheric-chemistry-and-physics.net/peer_review/interactive_review_process.html

One mystery about this paper it may be too soon to report on results from ATTO, since no data has been obtained from the ATTO centerpiece, the 325 m tower. Why is this paper with preliminary results coming out before the tall tower is commissioned? Why not simply describe the project, justify its siting, instrumentation and height, and pass lightly over both the boilerplate justification and early finding from the smaller towers?

We apologize for not having made the purpose of this paper more transparent. As pointed out in the response to Reviewer 1, the Amazon Tall Tower Observatory is actually more than just the tall tower itself, rather, it comprises several smaller towers for pilot and process studies as well as the ecosystem surrounding the towers. This paper is intended to provide the scientific context of ATTO and to serve as an overview paper for the pilot studies. A future paper will discuss the details of the tall tower. We have added a paragraph at the end of the introduction that makes it clear that this paper is intended as an introduction and overview for a special issue.

The justifications as to why there is a need for long-term continuous measurements in the first thirteen pages are not clearly focused on the ATTO concept. The authors take side trips to explain details of the importance of the Amazon Basin to global biodiversity and climate change; these should be dealt with by references to other review articles already in the literature.

The introduction serves to introduce the reader of the special volume to the scientific background and context of the ATTO project. Therefore, it is written as a "mini-review", to provide this background to a broad range of scientists from many disciplines. It is also meant as a common point of reference for the specialized papers in the special issue. While the need for long-term measurements may be well known, it is nevertheless important to emphasize it for a site that is intended to operate for decades.

The reader deserves a more specific argument—more than generalities highlighting the importance of the Amazon Basin—that defends the idea that a 328-m tall tower be installed in such a hostile environment. It is necessary, but not sufficient to note that there are other tall towers monitoring the lower atmosphere at other parts of the world. The reader deserves to know why the ATTO tower was sited at this particular, relatively remote site.

The introduction now contains a section discussing the motivation and concept of the tall tower, the site selection criteria, and an improved description of the objectives.

What is the purpose of the smaller towers around the tall one? (The local canopy data presented in this paper all come from these towers.)

They were established to conduct process studies with minimal disturbance of the forest ecosystem, as is unavoidable with a large structure such as the tall tower, and to begin research

during the time that it took to get the tall tower constructed. This enabled about four years of process studies and pilot research at the ATTO site, which are being introduced in this overview.

Why is the local topography and map of adjacent water bodies only included deep into the manuscript, as part of one finding about gravity waves? These topics need to be presented right at the beginning, so that this paper can serve its rightful purpose as a reference to papers that follow, so that this information need not be endlessly repeated.

We agree, and have added a map with local topography and a brief discussion of the soils and geology earlier in the paper (Section 2.1).

To repeat: The authors would be well served to make a short description of the vertical structure of the atmosphere—and its diurnal variability—is presented. Such at least would allow the reader to understand why one has to make such a tall tower.

Boundary-layer phenomena that can be investigated using the tall tower are now discussed in the introduction. For a description of the boundary layer behavior we included a reference to Fisch et al. (2004).

The reader sees no reference to the successes and difficulties that have occurred at other tall tower installations (BAO, Cabauw, ZOTTO in Russia).

This will be included in a future paper specifically addressing the tall tower.

One important issue is the likely percentage of good turbulence data that has been obtained from tall towers in other 'remote' sites. This reader sees no reference to what degree the preliminary measurements have been continuous. (In the preliminary results, many findings based on 2-3 weeks of work are presented at representative.)

Continuous micrometeorological measurements have been made since September 2012, with some interruptions due to technical problems. This information has been included in Section 3.3.

What this reader found here resembles a forced marriage collection of 'white papers' written over some time to accompany meetings planning this tower and/or (perhaps) selling the concept to funding agencies.

In fact, all the text contained in this manuscript was specifically written for this paper.

In short, the reader gets a heavy dose of interesting, perhaps important facts, but facts that are tangential to the issue at hand. The authors need to describe the site, explain why it was placed where it was, and what peculiarities it exhibits. I'm thinking of vegetation diversity, geographical diversity, and behavior of local wind systems. As one example, does proximity to the large Balbina dam and reservoir perturb any measurements? How would the authors know?

We have described the site in quite some detail and have now added additional detail on site selection and characteristics. Vegetation diversity is described in 4.1.1; geomorphology in section 2.1 (new text); local wind systems in 4.2.1. The influence of the Balbina Reservoir has not been detected in chemical tracers (e.g., CH_4) or wind measurements.

Perhaps the size of the text is merely a symptom of the enthusiasm that led to the tower's construction, but the founds ought to be restrained a little, to avoid the hubris that leads to 'monumental science'. There is not yet enough output to justify a celebration. The reader deserves to receive an overview that discusses ATTO, not an encyclopedia of everything all shoved together as it would be in a loosely gathered notebook. If the fifty-six authors want to write such a tome, they should write a book, with chapters for the sundry specialties OR they should commandeer a journal for a dedicated issue.

In fact, this is a paper that introduces just such a dedicated issue, and that is intended to serve as a common reference for the specialized papers.

I hope that in revision the paper more closely resembles a reference work that allows the reader to understand why the tower was placed where it was, how the height of the tower was determined, what thinking went behind the construction of the smaller, satellite towers.

This has been included in the revised manuscript (see above).

I imagine that the revised paper will make a reasonable assessment of the percentage of time that continuous measurements can be achieved.

Such an assessment would be different for all the variables measured at the site and would dramatically increase the size of this already large paper.

Such a paper would lighten the load of the many authors who will follow and report on their new findings. The justification for the ATTO and how it came to be at this site can simply be referred to. Only some of these findings—perhaps long-term concentration measurements of

trace gases and aerosols—will be relevant to the Basin as a whole; many more will be of necessity local area case studies.

Indeed, ATTO is meant to be both a site for long-term measurements and local process studies.

Specific comments.

1. Any subsequent drafts should provide line numbers to aid the harried reviewer.

We don't understand. The ACPD version has both line and page numbers.

p. 7. "Efforts to upscale local measurements to larger scales have also lead to inconclusive and often contradictory results." Where do the authors explain how adding a single point measurements will improve this situation?

This statement is part of a general discussion on carbon cycle investigations. We did not imply that ATTO by itself would be the answer to this problem. But the establishment of long-term mid-continental baseline stations has been shown to significantly reduce uncertainties in the carbon budget. See the paper by Gloor et al. (2001), now discussed in the Introduction section 1.5.

p. 8. "Seen together, these studies suggest that the Amazon Basin teeters on a precarious balance…" Again, these generalizations would be interesting if they were not distracting from the mission at hand. They belong in an overview paper; perhaps they come from one.

This is the overview paper.

p. 8. "While remote sensing can provide important information on the response of the Amazon forest to changing climate and ecological factors, the recent controversy about the effects of seasonal change and drought on the "greenness" of the forest illustrates how important long-term ground based observations are to our understanding of the Amazon system…" This is a true statement, as far as it goes. Much of this 'green-up' controversy has to do with the situation further east in the Basin, where the dry season is more intense and prolonged. The authors are 'selling' the utility of a tall tower in the central Basin. They are justifying it in much the same way as one would justify having a much smaller tower, of the type that is in use in this region already. What they need to do is emphasize the scientific riches that are in store for those who

have long-term observations at 325 meters, about one fourth of the thickness of the daytime convective boundary layer.

This is now discussed in section 1.5, and will be included in more detail in a forthcoming paper specifically addressing the tall tower.

5. p. 15. Suggested changes to the objectives, all designed to rein in hyperbole:

The Objectives have been tightened up and rewritten.

1) To understand the carbon budget of one specific site in the Amazonian rain forest under changing climate conditions and anthropogenic influences.

Actually, because the tall tower has a CO_2 concentration footprint on the order of 10^6 km^2, it represents more than one specific site. See new text in Section 1.5.

2) To continuously observe anthropogenic and biogenic greenhouse gases in the lower troposphere, within the planetary boundary layer by day and outside it at night, in order to help constrain inverse methods for deriving continental source and sink strengths and their changes over time.

Changed as suggested.

3) To continuously measure trace gases and aerosols for improvement of our understanding of atmospheric chemistry and physics in the Amazon and further allow a continuous assessment of the effects of land use change that occur upwind of ATTO on the atmosphere and climate.

Now part of the newly formulated Objective 1.

4) To simultaneously measure anthropogenic and biogenic trace gases, contributing to our understanding of natural and anthropogenic effects on the atmosphere and climate. Measurements of isotopic composition will be made to help distinguish anthropogenically and biologically induced fluxes.

OK

5) To investigate key atmospheric processes, with emphasis on the atmospheric oxidant cycle, the trace gas exchange between forest and atmosphere, and the life cycle of the Amazonian aerosol.

6) To determine vertical trace gas and aerosol gradients from the tower top to the ground to estimate biosphere-atmosphere exchange rates.

7) To study turbulence and transport processes in the lower atmospheric boundary layer, as well as to understand the extent and characteristics of the roughness sublayer over the forest.

8) To develop and validate dynamic vegetation models, atmospheric boundary layer models, and inverse models for the description of heat, moisture, aerosol, and trace gas fluxes.

9) To provide single-point ground truth to help evaluate satellite estimates of greenhouse gas concentrations and temperature and humidity profiles

Modified to reflect the point that this is one site.

6. p. 20. Are raw turbulence and trace gas data archived? Will these be available to the community?

Yes. This is now stated in section 3.3.

7. p. 31. "The variation of the wind roses between daytime and nighttime was insignificant." This reader doesn't believe this. Please present hourly hodographs to show possible breeze influences.

This statement was based on an initial analysis of wind roses for daytime and nighttime. We have now plotted hourly wind roses for each season (see Figure 1 below, time in UTC) and cannot detect a lake breeze system. Such a system would be characterized by dominant flows from the north-western sector (Balbina reservoir) during daytime, which is clearly not the case. However, the wind roses show a slight diurnal variation with small contributions from the North, West and South during nighttime, when the nocturnal boundary layer is decoupled, in both seasons. In contrast, during daytime the wind blows nearly all the time from the East (dry season) and Northeast (wet season) with much higher wind speeds.

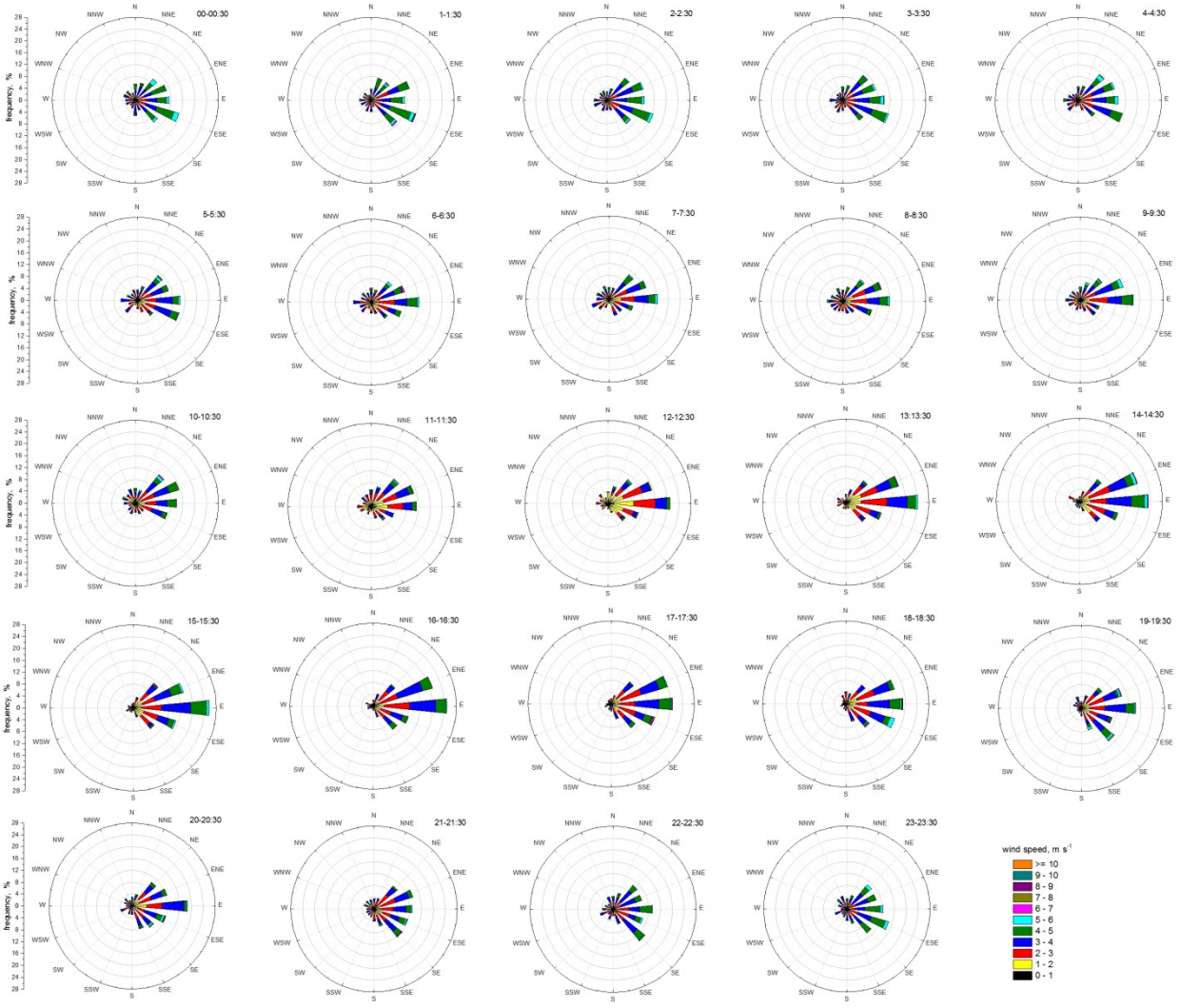
00-00:30
1-1:30
2-2:30
3-3:30
4-4:30
5-5:30
6-6:30
7-7:30
8-8:30
9-9:30
10-10:30
11-11:30
12-12:30
13-13:30
14-14:30
15-15:30
16-16:30
17-17:30
18-18:30
19-19:30
20-20:30
21-21:30
22-22:30
23-23:30
frequency, %
N
NNE
NE
ENE
E
ESE
SE
SSE
S
SSW
SW
WSW
W
WNW
NW
NNW
wind speed, m s-1
>= 10
9 - 10
8 - 9
7 - 8
6 - 7
5 - 6
4 - 5
3 - 4
2 - 3
1 - 2
0 - 1

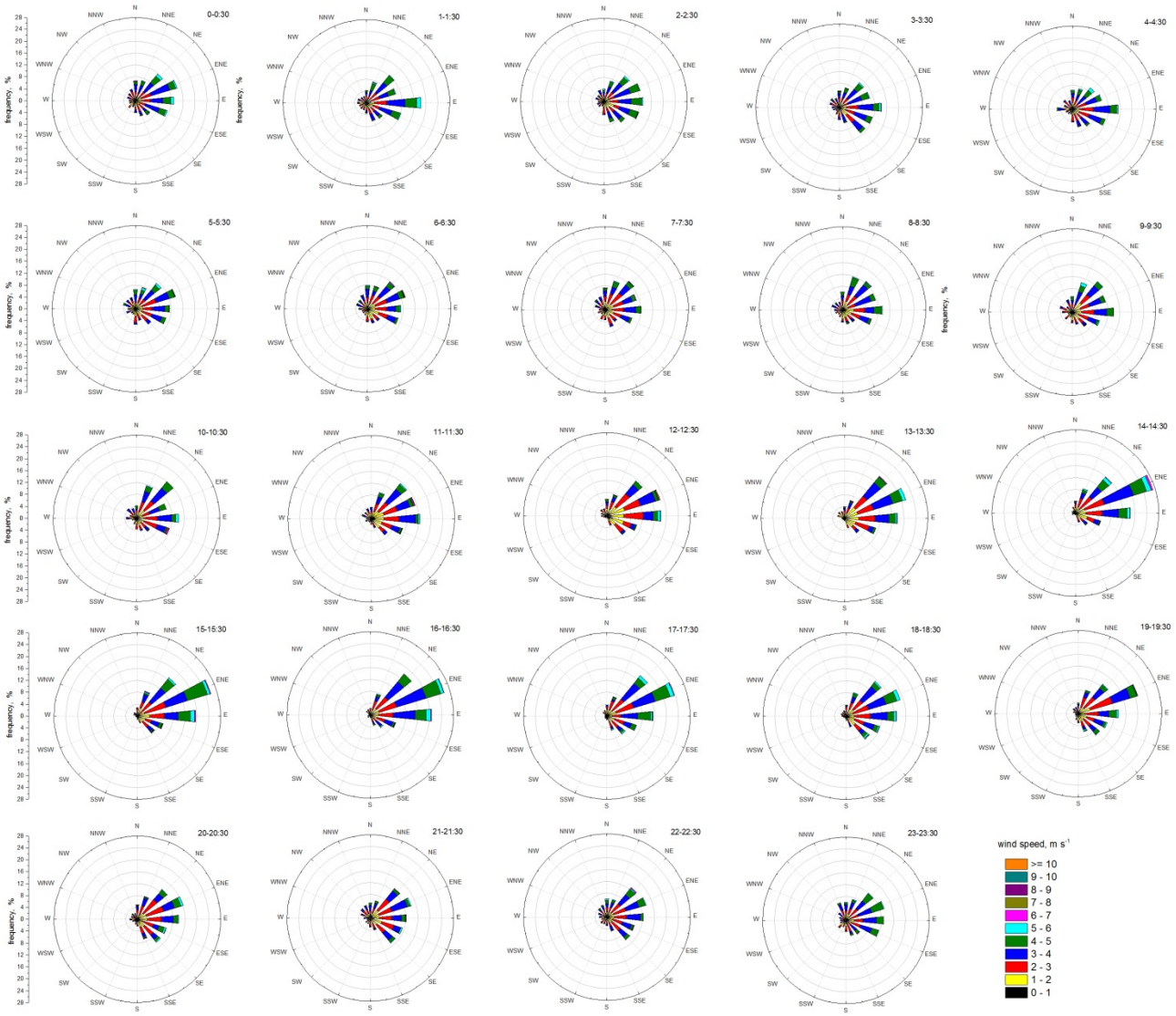

Figure 1: Half-hourly wind roses at 80 m at the ATTO site. The upper diagram shows the dry-season average, the lower diagram the rainy season average.

8. p. 32. (Figure 6) I don't see that the vertical spacing of temperature sensors is adequate to describe the stability regimes within the canopy. One cannot properly resolve the stability at canopy top and near the forest floor with the observation levels shown. How will this be addressed in the long term?

The referee is right in that the vertical spacing of the temperature sensors (6 levels throughout the canopy) might not be sufficient to resolve the shape of the temperature profile and, therefore, the exact heights of the diurnal maxima and minima. Nevertheless, the observed minima and maxima reflect the regimes of cooling and heating of the canopy as described in the text, which are in agreement with general observations in forest canopies. Nevertheless, our concept for upgrading the measurements within the framework of equipping the ATTO tower includes a higher vertical resolution of the profile throughout the canopy.

9. p. 40. Text following: "Figure 15a shows a topographic image of the experimental site with colors ranging from blue to red representing the altimetry values in meters above sea level." It turns out that the forest floor topography has an important influence on the CO2 balance, at length scales well smaller than 30 km, as the work of co-author Julio Tóta has shown. Somewhere in the site description this information should show up. Indeed, one shouldn't have to wait until p. 40 to learn of this site peculiarity.

We have added a new Figure (Fig. 1b) and some text in the manuscript (Section 2.1) to introduce this topic earlier in the revised version. The topography surrounding ATTO is actually not a site peculiarity, but the dominant landscape form in the central Amazon Basin. Regrettably, but unavoidably, this is not an ideal type of terrain from the perspective of micrometeorological flux measurements, because it induces significant upslope and downslope circulations (Tota et al., 2012). The effects of local topography on the local flux measurements from the small towers are the subject of ongoing investigations.

It must be pointed out, however, that the main objective of the tall tower with respect to greenhouse gas and aerosol monitoring is the measurement of concentrations above the level of local circulations. In this context, measurements from tall towers, such as ATTO, have the advantage of being less influenced by the surface layer variability due to diurnal changes in photosynthesis and respiration, as well as ecosystem and terrain heterogeneity. This results in smoothening of the large daily cycles of near-surface signals and efficiently integrates over daily cycles and small-scale heterogeneities, and facilitates the detection of long-term changes in the background atmospheric composition.

Tota, J., Fitzjarrald, D. R., and da Silva Dias, M. A. F., Amazon rainforest exchange of carbon and subcanopy air flow: Manaus LBA Site - A complex terrain condition: Scientific World Journal, 2012, 165067, doi:10.1100/2012/165067, 2012.

The Amazon Tall Tower Observatory (ATTO): Overview of pilot measurements on ecosystem ecology, meteorology, trace gases, and aerosols

Deleted: The Amazon Tall Tower Observatory (ATTO) in the remote Amazon Basin: Overview of first results from ecosystem ecology, meteorology, trace gas, and aerosol measurements¶

M. O. Andreae[1,2], O. C. Acevedo[3], A. Araùjo[4], P. Artaxo[5], C. G. G. Barbosa[6], H. M. J. Barbosa[5], J. Brito[5], S. Carbone[5], X. Chi[1], B. B. L. Cintra[7], N. F. da Silva[7], N. L. Dias[6], C. Q. Dias-Júnior[8,11], F. Ditas[1], R. Ditz[1], A. F. L. Godoi[6], R. H. M. Godoi[6], M. Heimann[9], T. Hoffmann[10], J. Kesselmeier[1], T. Könemann[1], M. L. Krüger[1], J. V. Lavric[9], A. P. Lopes[15], A. O. Manzi[11], D. L. Martins[15], E. F. Mikhailov[1,20], D. Moran-Zuloaga[1], B. W. Nelson[15], A. C. Nölscher[1], D. Santos Nogueira[12], M. T. F. Piedade[7], C. Pöhlker[1], U. Pöschl[1], C. A. Quesada[15], L. V. Rizzo[5], C.-U. Ro[13], N. Ruckteschler[1], L. D. A. Sá[14], M. de Oliveira Sá[15], C. B. Sales[11,16], R. M. N. dos Santos[17], J. Saturno[1], J. Schöngart[1,7], M. Sörgel[1], C. M. de Souza[11,18], R. A. F. de Souza[17], H. Su[1], N. Targhetta[7], J. Tóta[17,19], I. Trebs[1,*], S. Trumbore[9], A. van Eijck[10], D. Walter[1], Z. Wang[1], B. Weber[1], J. Williams[1], J. Winderlich[1,9], F. Wittmann[1], S. Wolff[1,11], A. M. Yáñez-Serrano[1,11]

[1]Max Planck Institute for Chemistry, Biogeochemistry, Multiphase Chemistry, and Air Chemistry Departments, P. O. Box 3060, 55020, Mainz, Germany

[2]Scripps Institution of Oceanography, University of California San Diego, La Jolla, CA 92037, U. S. A.

[3]Universidade Federal Santa Maria, Dept. Fisica, BR-97119900 Santa Maria, RS, Brazil

[4]Empresa Brasileira de Pesquisa Agropecuária (EMBRAPA), Trav. Dr. Enéas Pinheiro, Belém-PA, CEP 66095-100, Brasil

[5]Instituto de Física, Universidade de São Paulo (USP), Rua do Matão, Travessa R, 187, CEP 05508-900, São Paulo, SP, Brasil

[6]Department of Environmental Engineering, Federal University of Paraná UFPR, Curitiba, PR, Brazil

[7]Instituto Nacional de Pesquisas da Amazônia (INPA), MAUA group, Av. André Araújo 2936, Manaus-AM, CEP 69067-375, Brasil
[8]Instituto Nacional de Educação, Ciência e Tecnologia do Pará (IFPA/Bragança), Pará, Brazil
[9]Max Planck Institute for Biogeochemistry, Hans-Knöll-Straße 10, 07745 Jena, Germany
[10]Department of Chemistry, Johannes Gutenberg University, Mainz, Germany
[11]Instituto Nacional de Pesquisas da Amazônia (INPA), Clima e Ambiente (CLIAMB), Av. André Araújo 2936, Manaus-AM, CEP 69083-000, Brazil
[12]Centro Gestor e Operacional do Sistema de Proteção da Amazônia (CENSIPAM), Belém, Pará, on leave from Amazon Regional Center, National Institute for Space Research (INPE), Belém, Pará
[13]Department of Chemistry, Inha University, Incheon 402-751, Korea
[14]Centro Regional da Amazônia, Instituto Nacional de Pesquisas Espaciais (INPE), Belém, Pará, Brazil
[15]Instituto Nacional de Pesquisas da Amazônia (INPA), LBA, Av. André Araújo 2936, Manaus-AM, CEP 69067-375, Brazil
[16]Centro de Estudos Superiores de Parintins (CESP/UEA), Parintins, Amazonas, Brazil
[17]Universidade do Estado do Amazonas (UEA), Manaus, Amazonas, Brazil
[18]Universidade Federal do Amazonas (UFAM/ICSEZ-Parintins), Parintins, Amazonas, Brazil
[19]Universidade Federal do Oeste do Pará – UFOPA, Santarém, Pará, Brazil
[20]Atmospheric Physics Department, Institute of Physics, St. Petersburg State University, St. Petersburg, Russia
* now at: Luxembourg Institute of Science and Technology, Environmental Research and Innovation (ERIN) Department, L-4422 Belvaux, Luxembourg.

Correspondence to: M. O. Andreae (m.andreae@mpic.de)

Abstract

The Amazon Basin plays key roles in the carbon and water cycles, climate change, atmospheric chemistry, and biodiversity. It has already been changed significantly by human activities, and more pervasive change is expected to occur in the next decades. It is therefore essential to establish long-term measurement sites that provide a baseline record of present-day climatic, biogeochemical, and atmospheric conditions and that will be operated over coming decades to monitor change in the Amazon region, as human perturbations increase in the future.

The Amazon Tall Tower Observatory (ATTO) has been set up in a pristine rain forest region in the central Amazon Basin, about 150 km northeast of the city of Manaus. Two 80-m towers have been operated at the site since 2012, and a 325-m tower is nearing completion in mid-2015. An ecological survey including a biodiversity assessment has been conducted in the forest region surrounding the site. Measurements of micrometeorological and atmospheric chemical variables were initiated in 2012, and their range has continued to broaden over the last few years. The meteorological and micrometeorological measurements include temperature and wind profiles, precipitation, water and energy fluxes, turbulence components, soil temperature profiles and soil heat fluxes, radiation fluxes, and visibility. A tree has been instrumented to measure stem profiles of temperature, light intensity, and water content in cryptogamic covers. The trace gas measurements comprise continuous monitoring of carbon dioxide, carbon monoxide, methane, and ozone at 5 to 8 different heights, complemented by a variety of additional species measured during intensive campaigns (e.g., VOC, NO, NO_2, and OH reactivity). Aerosol optical, microphysical, and chemical measurements are being made above the canopy as well as in the canopy space. They include aerosol light scattering and absorption, fluorescence, number and volume size distributions, chemical composition, cloud condensation nuclei (CCN) concentrations, and hygroscopicity. In this paper, we discuss the scientific context of the ATTO observatory and present an overview of results from ecological, meteorological, and chemical pilot studies at the ATTO site.

Deleted: has

Moved (insertion) [1]

Moved up [1]: Two 80-m towers have been operated at the site since 2012, and a 325-m tower is nearing completion in mid-2015.

Deleted: aerosol

Deleted: Initial

Deleted: are presented in this paper

1 Introduction

A little over thirty years ago, Eneas Salati and Peter Vose published a landmark paper entitled "Amazon Basin: A System in Equilibrium" (Salati and Vose, 1984). Since then, a paradigm shift has occurred in the minds of the public at large as well as the scientific community, which is reflected in the title of a recent synthesis paper by a group of prominent Amazon researchers, "The Amazon Basin in transition" (Davidson et al., 2012). Despite its reassuring title, Salati and Vose's paper had already pointed at growing threats to the integrity of the Amazon ecosystem, mostly resulting from ongoing large-scale deforestation. Since then, deforestation has indeed continued and has only begun to abate in recent years (Lapola et al., 2014; Tollefson, 2015). It goes hand in hand with road construction and urbanization (Fraser, 2014), affecting ecosystems and air quality in many parts of the Basin. And, whereas Salati and Vose were concerned with climate change as a regional phenomenon driven by deforestation and its impact on the hydrological cycle, the focus now is on the interactions of global climate change with the functioning of the Amazon forest ecosystem (Keller et al., 2009). In the following sections, we will present the key roles the Amazon is playing in the global ecosystem, which form the rationale for setting up a long-term measuring station, including a tall tower, for monitoring its functioning and health.

Deleted: continued

Deleted: D

Deleted: ,

1.1 Carbon cycle

The Amazon Basin covers about one third of the South American continent and extends over about $6.9 \cdot 10^6$ km^2, of which about 80% is covered with rain forest (Goulding et al., 2003). It contains 90-120 Pg C in living biomass, representing about 84% of the aboveground biomass in Latin America and ca. 40% of all tropical forests worldwide (Baccini et al., 2012; Gloor et al., 2012). Another 160 Pg C are stored in the Amazon Basins's soils – putting this in perspective, the Amazon holds about half as much carbon as was in the Earth's atmosphere before the industrial revolution (Gloor et al., 2012). Given the magnitude of this carbon reservoir, it is clear that tropical forests in general, and the Amazon forest in particular, have the potential to play a crucial role in climate change because of their potential to gain or lose large amounts of carbon as a result of land use and climate change. A recent study shows a strong correlation between climate change

on the tropical continents and the rate at which CO_2 increases in the atmosphere, and indicates that the strength of this feedback has doubled since the 1970s (Wang et al., 2014). The interaction between physical climate and the biosphere represents one of the largest uncertainties in the assessment of the response of the climate system to human emissions of greenhouse gases.

Depending on the path land use change takes and the interactions between the forest biota and the changing climate, the Amazon can act as a net source or sink of atmospheric CO_2. The most recent global carbon budget estimates indicate that in the decade of 2004-2013 land use change worldwide resulted in a net carbon release of 0.9±0.5 Pg a^{-1}, or about 9% of all anthropogenic carbon emissions (Le Quéré et al., 2014). This represents a significant decrease since the 1960s, when land-use carbon emissions of 1.5±0.5 Pg a^{-1} accounted for 38% of anthropogenic CO_2. Part of this decrease in the relative contribution from land use change is of course due to the increase in fossil fuel emissions, but there has also been a significant decrease in deforestation in recent years, particularly in the Brazilian Amazon (Nepstad et al., 2014).

The "net" land use emissions, as presented above, are the sum of "gross" release and uptake fluxes, where deforestation represents the dominant gross source, whereas afforestation, regrowth, and uptake by intact vegetation are the main gross sinks. Using an approach based on forest inventories and land use budgeting, Pan et al. (2011) estimated that tropical land use change represented a net carbon source of 1.3±0.7 Pg a^{-1} in the 1990s and early 2000s, consisting of a gross tropical deforestation carbon emission of 2.9±0.5 Pg a^{-1} partially compensated for by a carbon sink in tropical forest regrowth of 1.6±0.5 Pg a^{-1}. A more recent comprehensive analysis of the role of land vegetation in the global carbon cycle concluded that carbon sources and sinks in the tropics are approximately balanced, with regrowth and CO_2-driven carbon uptake compensating the large deforestation source (Schimel et al., 2015). For the South American continent, a detailed budgeting study also concluded that, at present, carbon uptake by the biosphere approximately compensates the emissions from deforestation and fossil fuel burning, with a slight trend of the continent becoming a carbon source in the most recent period (Gloor et al., 2012).

Deleted: always

Deleted: and

Deleted: ,

Deleted: at present

Deleted: in

Attempts to verify these carbon budgets with measurements have remained inconclusive so far. The largest spatial scale is represented by global inversion models, which derive fluxes from concentration measurements and global transport models. An early attempt deduced a large tropical sink from inverse modeling (Stephens et al., 2007), whereas a more recent analysis suggests a net tropical carbon source of 1.1±0.9 Pg a^{-1} (Steinkamp and Gruber, 2013). Gloor et al. (2012) have reviewed the numerous attempts to deduce the South American carbon budgets from inverse modeling and came to the conclusion that they are not adequately constrained to produce meaningful results, a conclusion that they extend to the application of digital global vegetation models for larger time and space scales.

Efforts to upscale local measurements to larger scales have also lead to inconclusive and often contradictory results. Flux measurements using the eddy covariance technique initially suggested a fairly large carbon sink (1-8 t ha^{-1} a^{-1}) in intact Amazon forests (e.g., Grace et al., 1995; Carswell et al., 2002; de Araújo et al., 2002). But as more studies were conducted, this uncertainty range expanded, reaching from a sink of 8 t ha^{-1} a^{-1} to a source of 1.4 t ha^{-1} a^{-1}. It thus became clear that issues related to nighttime fluxes and terrain effects make upscaling of CO_2 fluxes from eddy covariance measurements difficult to impossible (de Araujo et al., 2010, and references therein). Nevertheless, such flux measurements are essential for understanding micrometeorological and ecological processes and for monitoring changes in the functioning of the forest ecosystem.

An alternative approach to upscaling from local to regional carbon balances is followed in the RAINFOR project, where initially some 140 forest plots have been monitored over decades for standing biomass (Phillips et al., 2009). This study suggested substantial carbon uptake by intact forest, interrupted by biomass loss during drought years. It has been proposed that a large fraction of the uptake extrapolated from the RAINFOR sites is compensated by carbon losses due to rare disturbance events, such as forest blow-downs resulting from severe thunderstorms (Chambers et al., 2013, and references therein). The latest analysis from the RAINFOR project, now based on 321 plots and 25 years of data, indicates that the Amazon carbon sink in intact forest has declined by one-third during the past

Deleted: o
Deleted: 2
Deleted: o
Deleted: 2
Deleted: o
Deleted: 2
Deleted: ,
Deleted: and i

decade compared to the 1990s. This appears to be driven by increased biomass mortality, possibly caused by greater climate variability and feedbacks of faster growth on mortality (Brienen et al., 2015). Like flux-tower measurements, biomass inventories also miss the contributions of wetlands and water bodies to the carbon flux, which may make a substantial contribution to CO_2 outgassing (Richey et al., 2002; Abril et al., 2014).

An intermediate scale between global inverse modeling and plot-size flux and inventory studies is captured by aircraft CO_2 soundings through the lowest few km of the troposphere. This method averages regional fluxes on scales of tens to hundreds of km. Early measurements made during the 1987 ABLE-2 experiment were reanalyzed by Chou et al. (2002) and suggested a near-neutral carbon balance for their study region near Manaus. A series of flights north of Manaus during the 2001 wet-to-dry transition season also revealed that daytime carbon uptake and nighttime release were in approximate balance (Lloyd et al., 2007). A 10-year aircraft profiling study conducted near Santarem in the eastern Amazon concluded that the fetch region was a small net carbon source (0.15 t ha^{-1} a^{-1}), mostly as a result of biomass burning, with no significant net flux to or from the forest biosphere (Gatti et al., 2010). In 2010, this study was extended to include the southern and western parts of the Amazon Basin (Gatti et al., 2014). The results from 2010, an unusually dry year, show the Amazon forest biosphere to be sensitive to drought, resulting in net carbon emission from the vegetation. The following year, 2011, was wetter than average, and the Basin returned to an approximately neutral carbon balance, with a modest biospheric sink compensating the biomass burning source. A detailed study on the carbon dynamics over the years 2009 to 2011 showed a complex response of the forest ecosystem to the drought episode, which not only affected net primary production (NPP) and tree mortality, but also the allocation of carbon to the canopy, wood, and root compartments (Doughty et al., 2015).

Seen together, these studies suggest that the Amazon Basin teeters on a precarious balance between being a source or sink of carbon to the world's atmosphere, with its future depending on the extent and form of climate change as well as on human actions. The region has already warmed by 0.5-0.6 °C, and warming

Deleted: of CO_2

Deleted: ,

Deleted: o

Deleted: ^{2}

Deleted: did

is expected to continue (Malhi and Wright, 2004). Together with the increased frequency of drought episodes (Saatchi et al., 2013), the occurrence of periods of net biospheric carbon emissions will be enhanced and the likelihood of destructive understory fires will increase (Gloor et al., 2013; Balch, 2014; Zeri et al., 2014). On the other hand, the observed 20% increase in Amazon River discharge may reflect increasing water availability to the vegetation (Gloor et al., 2013), which together with increasing atmospheric CO_2 may lead to more net carbon uptake by the intact forest vegetation (Schimel et al., 2015). While remote sensing can provide important information on the response of the Amazon forest to changing climate and ecological factors, the recent controversy about the effects of seasonal change and drought on the "greenness" of the forest illustrates how important long-term ground based observations are to our understanding of the Amazon system (Morton et al., 2014; Soudani and Francois, 2014; Zeri et al., 2014).

Deleted: an

Deleted: supply

Ultimately, the fate of the carbon stored in the Amazon Basin will depend on the interacting and often opposing effects of human actions, especially deforestation, global and regional climate change, and changing atmospheric composition (Soares-Filho et al., 2006; Poulter et al., 2010; Rammig et al., 2010; Davidson et al., 2012; Cirino et al., 2014; Lapola et al., 2014; Nepstad et al., 2014; Schimel et al., 2015; Zhang et al., 2015). Interactions of the carbon cycle with the cycles of other key biospheric elements, especially nitrogen and phosphorus, are also likely to play important roles (Ciais et al., 2013). This applies equally to two other greenhouse gases, methane (CH_4) and nitrous oxide (N_2O), both of which have important sources in the wetlands or soils of the Amazon (Miller et al., 2007; D'Amelio et al., 2009; Beck et al., 2012).

Deleted: Amazon

1.2 Water and energy cycle

The Amazon River has by far the greatest discharge of all the World's rivers — about 20% of the world's freshwater discharge, and five times that of the Congo, the next largest river in discharge. This reflects the immense amount of water that is cycling through the water bodies, soils, plants, and atmosphere of the Amazon Basin. As a result, the hydrological cycle of the Amazon Basin is crucial for providing the water that supports life within the Basin and even beyond its borders. Most moisture enters the Basin from the Atlantic Ocean with the trade

290 wind circulation, but recirculation of water through evapotranspiration maintains a
291 flux of precipitation that becomes increasingly more important as airmasses move
292 into the western part of the Basin (Spracklen et al., 2012). When reaching the An-
293 des, moisture becomes deflected southward, with the result that Amazonian evap-
294 oration even supports the rain-fed agriculture in Argentina (Gimeno et al., 2012).
295 As a result, perturbations of the Amazonian moisture flux and the effects of
296 smoke aerosols from fires in Amazonia on cloud processes can affect rainfall even
297 over the distant La Plata Basin (Camponogara et al., 2014; Zemp et al., 2014).

298 Evaporation of water from the Earth's surface also supports a huge energy
299 flux in the form of latent heat, which is converted to sensible heat and atmospheric
300 buoyancy when the water vapor condenses to cloud droplets. This heat transfer
301 represents one of the major forces that drive atmospheric circulation at all scales
302 (Nobre et al., 2009). Changes in land cover, e.g., conversion of forest to pasture,
303 alter the amount and type of clouds over the region (e.g., Heiblum et al., 2014)
304 and shift the proportion of rain that flows away as runoff versus the fraction that is
305 transformed to water vapor by evapotranspiration (Silva Dias et al., 2002; Da-
306 vidson et al., 2012; Gloor et al., 2013; and references therein). This in turn chang-
307 es local and regional circulation and rainfall patterns, and consequently deforesta-
308 tion has been predicted to reduce the potential for hydropower generation in Ama-
309 zonia (Stickler et al., 2013). When the scale of deforestation exceeds some 40% of
310 the Basin, these perturbations of the water cycle may change the functioning of
311 the entire Amazon climate and ecosystem (Coe et al., 2009; Nobre and Borma,
312 2009; Lawrence and Vandecar, 2015).

313 Our ability to prognosticate the possible outcomes for the Amazon ecosys-
314 tem in the coming decades is severely curtailed by limitations in the representa-
315 tion of key processes in climate/vegetation models, including the role of the An-
316 des and the teleconnections between the Amazon and the Atlantic and Pacific
317 Oceans. In addition, the biophysical response of the vegetation to changing water
318 supply and increasing CO_2 and temperature remains very poorly understood
319 (Davidson et al., 2012). Long-term measurements and process studies at key loca-
320 tions are urgently needed to improve our understanding of these interactions.

1.3 Biodiversity

The Amazon Basin contains the most species-rich terrestrial and freshwater ecosystems in the world (Hoorn et al., 2010; Wittmann et al., 2013). It houses at least 40,000 plant species, over 400 mammal species, about 1300 bird species, and countless numbers of invertebrate and microbe species (Da Silva et al., 2005), accounting for about 10-20% of all the world's species diversity. Of these, the great majority have not yet been described scientifically, and possibly never will be. The variety of species in the Amazon Basin is directly related to the variety of habitats, and consequently is threatened by any form of exploitation that is accompanied by habitat destruction, particularly land clearing and deforestation. The genetic information stored in these ecosystems and their biodiversity is beyond measure and may be of enormous economic significance. This diversity is now under great threat, mostly as a result of habitat loss due to deforestation and other land use changes (Vieira et al., 2008).

Deleted: has

Deleted: in

Much of the Amazon's aboveground biomass is in its trees, and a single hectare of the forest can be home to over 100 different tree species. Scientists still do not know how many tree species occur in the Amazon, and the current estimate of about 16,000 tree species is the result of an extrapolation from the existing scattered census data. Surprisingly, a relatively small number (227 species, or 1.4%) account for half of all individual trees (ter Steege et al., 2013), which therefore account for a large fraction of the Amazon's ecosystem services. This fact may greatly facilitate research in Amazonian biogeochemistry, for example studies on the trace gas exchange between plants and the atmosphere.

1.4 Atmospheric composition and self-cleansing

The tropical atmosphere has been referred to as the "washing machine of the atmosphere" by Paul Crutzen (pers. comm., 2013). Both, human activities and the biosphere, release huge amounts of substances such as nitrogen oxides (NO_x), carbon monoxide (CO), and volatile organic compounds (VOC) into the atmosphere, which must be constantly removed again to prevent accumulation to toxic levels. Most such gases are poorly soluble in water, and are thus not effectively washed out by rain. The self-purification of the atmosphere therefore requires

chemical reactions by which the trace substances are brought into water-soluble form. These reaction chains normally begin with an initial oxidation step in which the trace gas is attacked by a highly reactive molecule, such as ozone (O_3) or the hydroxyl radical (OH). Production of these atmospheric detergents requires UV radiation and water vapor, both of which are present in generous quantities in the tropics. It comes thus as no surprise, that the tropics are the region in which large fractions of many atmospheric trace gases, including CO and CH_4, are eliminated (Crutzen, 1987). Recent discoveries indicate that the atmospheric oxidant cycles in the boundary layer are even much more active than had been previously assumed, yet the mechanisms of these reactions are still a matter of active research (Lelieveld et al., 2008; Martinez et al., 2010; Taraborrelli et al., 2012; Nölscher et al., 2014).

Deleted: largely

Deleted: but

The functioning of this self-cleansing mechanism is challenged by human activities that change the emissions from the biosphere and add pollutants from biomass burning and industrial activities. This may convert the "washing machine" into a reactor producing photochemical smog with high concentrations of ozone and other atmospheric pollutants, and large quantities of fine aerosols – which in turn influence the formation of clouds and precipitation and thus modify the water and chemical cycles (Andreae, 2001; Pöschl et al., 2010). Increased ozone concentrations over Amazonia, resulting from biomass burning emissions, have also been implicated in plant damage, which may substantially decrease the carbon uptake by the Amazon forest (Pacifico et al., 2015).

The concentrations and types of aerosol particles over the Amazon Basin exhibit huge variations in time and space. In the absence of pollution from regional or distant sources, and especially in the rainy season, the Amazon has among the lowest aerosol concentrations of any continental region (Roberts et al., 2001; Andreae, 2009; Martin et al., 2010b; Pöschl et al., 2010; Andreae et al., 2012; Artaxo et al., 2013; Rizzo et al., 2013). Biogenic aerosols, either emitted directly by the biota or produced photochemically from biogenic organic vapors, make up most of this "clean-period" aerosol (Martin et al., 2010a). At the other extreme, during the biomass burning season in the southern Amazon, aerosol concentrations over large regions are as high as in the most polluted urban areas worldwide

(Artaxo et al., 2002; Eck et al., 2003; Andreae et al., 2004). These changes in the atmospheric aerosol burdens have strong impacts on the radiation budget, cloud physics, precipitation, and plant photosynthesis (Schafer et al., 2002; Williams et al., 2002; Andreae et al., 2004; Lin et al., 2006; Oliveira et al., 2007; Freud et al., 2008; Bevan et al., 2009; Martins et al., 2009; Vendrasco et al., 2009; Sena et al., 2013; Cirino et al., 2014). Episodic inputs of Saharan dust, biomass smoke from Africa, and marine aerosols transported over long distances with the trade winds further complicate the picture (Formenti et al., 2001; Ansmann et al., 2009; Ben-Ami et al., 2010; Baars et al., 2011). This complexity of aerosol sources is one important reason why the mechanisms that lead to the production of biogenic aerosols in Amazonia are still enigmatic (Pöhlker et al., 2012; Chen et al., 2015).

1.5 The Amazon Tall Tower Observatory (ATTO)

The foregoing sections have cast some spotlights on the key roles of the Amazon Basin in the Earth System and on the important ecosystem services it provides. It is evident that to avoid irreversible damage to this complex system we need a better understanding of the interactions between biosphere and atmosphere in this important region. While considerable knowledge has been gained from campaign-style studies, it is clear that the full picture will not emerge from these "snapshots," but rather that continuous, long-term studies are required at key locations (Hari et al., 2009; Zeri et al., 2014). This is true especially in view of the fact that the Amazon and its global environment are rapidly changing, and that continuing observations are essential to keep track of these changes. It is particularly urgent to obtain baseline data now, to document the present atmospheric and ecological conditions before upcoming changes, especially in the eastern part of the Basin, will forever change the face of Amazonia.

Observations from tall towers are especially useful for this purpose, because they allow measurements at several heights throughout the planetary boundary layer and thereby can reflect both local processes at the lower levels and regional influences at the upper levels (Bakwin et al., 1998; Andrews et al., 2014). The effects of emission and uptake by local vegetation and soil are much reduced at 300 m as compared to 50 m (Winderlich et al., 2010), and the analysis of the diurnal variation of the vertical concentration profile provides an estimate of the

Deleted: thrown

Deleted: highlights

Deleted: to avoid irreversible damage to this complex system

flux of trace gases such as CO_2 and CH_4 (Winderlich et al., 2014). The influence footprint of typical flux tower measurements made at a few tens of meters above the canopy is of the order of a few kilometers (e.g., de Araújo et al., 2002; Chen et al., 2012), whereas the concentration footprint of a tall tower is of the order of 1000 km, and measurements at the top of the tower are therefore representative of regional processes (Gloor et al., 2001; Heimann et al., 2014). For micrometeorological investigations, a tall tower provides the unique ability to obtain continuous measurements at a series of heights throughout the lower part of the planetary boundary layer. This makes possible investigations of phenomena such as the formation and dissolution of nocturnal stable boundary layers, the production and behavior of intermittent turbulent structures, gravity waves, boundary layer rolls, etc. A summary of the characteristics of the Amazon planetary boundary layer can be found in Fisch et al. (2004).

The need for tall tower observatories at mid-continental locations, especially in Eurasia, Africa, and South America, was recognized in the late 1990s (Gloor et al., 2000) and the establishment of sites in Siberia and Amazonia was proposed to the Max Planck Society. This lead to the construction of the Zotino Tall Tower Observatory (ZOTTO) as a joint Russian-German project, with measurements beginning in 2006 (Heimann et al., 2014), and to the concept of the Amazon Tall Tower Observatory (ATTO).

The ATTO project was initiated in 2008 as a Brazilian-German partnership. A site was selected 150 km northeast of Manaus which fulfilled the following criteria: 1) large fetch with minimal current human perturbation, but with potential future land use change at a large scale, 2) relatively flat topography with no large wetlands in the fetch region, 3) stable and protected land ownership and controlled access, and 4) the possibility to reach the site in a reasonable time to facilitate research and educational activities.

In order to characterize the site and begin research activities, the site was set up initially with two measurement towers of intermediate height (80 m). Atmospheric measurements from these towers and ecological studies of the surrounding forest ecosystems were initiated in 2012. The construction of the 325-m tall tower began in September 2014 and is currently nearing completion. The tall

Deleted: (Winderlich et al., 2010)(Winderlich et al., 2014)

Deleted: ¶

Deleted: ,

Deleted:

Deleted: ing

Deleted: .

Deleted: For this purpose, t

Deleted: Amazon Tall Tower Observatory (

Deleted:)

Deleted: has been established in the central Amazon Basin by

Deleted: present

Deleted: al

Deleted: T

Deleted: h

Deleted: been

Deleted: , and t

Deleted: a

Deleted: to perform chemical and meteorological measurements representing large footprints

tower will serve as a basis for continuous monitoring of long-lived biogeochemically important trace gases such as CO_2, CH_4, CO, and N_2O, and a multitude of reactive gases, including NO_x, O_3, and VOC, as well as a broad range of aerosol characteristics. The chemical measurements are complemented by a full suite of micrometeorological measurements. Furthermore, the observing system will also include a component directed at the underlying vegetation canopy, such as phenological observations from the tower by automated cameras, potentially a canopy lidar, as well as an array of in-situ sensors of critical physical and biological variables in the ecosystems near the tower and the ground.

The continuous long-term data collected at ATTO will also serve to evaluate airborne and satellite observations. Expected to operate for an indeterminate length of time, this unique observatory in South America will provide long-term observations of the tropical Amazonian ecosystem affected by climate change.

Specific research objectives at the ATTO observatory are:

1) To obtain regionally representative measurements of carbon gas concentrations (CO_2, CH_4, CO, and VOC), in order to improve our understanding of the carbon budget of the Amazonian rain forest under changing climate, land use, and other anthropogenic influences in the fetch region of ATTO.

2) To continuously observe anthropogenic and biogenic greenhouse gases in the lower troposphere, within the planetary boundary layer by day and outside it at night, in order to help constrain inverse methods for deriving continental source and sink strengths and their changes over time.

3) To continuously measure trace gases and aerosols for improvement of our understanding of atmospheric chemistry and physics in the Amazon, with emphasis on the atmospheric oxidant cycle and the life cycle of the Amazonian aerosol, and to identify the effects of anthropogenic perturbations, e.g., land use change and pollution, on these processes. Measurements of isotopic composition will be made to help distinguish anthropogenic and biogenic fluxes.

4) To determine vertical trace gas and aerosol fluxes and gradients from the tower top to the ground to estimate biosphere-atmosphere exchange rates.

Deleted: conditions

Deleted: within and outside the planetary boundary layer

Moved (insertion) [2]

Deleted: ally

Deleted: logically induced

Deleted: and further allow a continuous assessment of the effects of land use change on the atmosphere and climate.

Moved up [2]: Measurements of will be made to help distinguish anthropogenically and biologically induced fluxes. ¶
5) To investigate key atmospheric

Deleted: 4) To simultaneously measure anthropogenic and biogenic trace gases, contributing to our understanding of natural and anthropogenic effects on the atmosphere and climate. Measurements of isotopic composition will be made to help distinguish anthropogenically and biologically induced fluxes. ¶
5) To investigate key atmospheric ...

Deleted: 6

5) To study turbulence and transport processes in the lower atmospheric boundary layer, as well as to understand the extent and characteristics of the roughness sublayer over the forest.

6) To develop and validate dynamic vegetation models, atmospheric boundary layer models, and inverse models for the description of heat, moisture, aerosol, and trace gas fluxes.

7) To evaluate satellite estimates of greenhouse gas concentrations and temperature and humidity profiles by providing a ground truth site.

This paper is intended as an overview paper for a special issue on research at the ATTO observatory. Here we discuss the scientific background and context of the observatory and describe the site characteristics, infrastructure, and measurement methodologies. We present initial results from studies in the ecosystem surrounding ATTO and from measurements at the two 80-m towers. Future papers in the special issue will provide a detailed discussion of the tall tower and present the results of the various scientific investigations at ATTO.

2 Site description and infrastructure

2.1 Site characteristics

The ATTO site is located 150 km northeast of Manaus in the Uatumã Sustainable Development Reserve (USDR) in the Central Amazon (Fig. 1a). This conservation unit is under the control and administration of the Department of Environment and Sustainable Development of Amazonas State (SDS/CEUC). The USDR is bisected by the Uatumã River through its entire NE-SW extension. The climate is tropical humid, characterized by a pronounced rainy season from February to May and a drier season from June to October (IDESAM, 2009).

The tower site is located approximately 12 km NE of the Uatumã River (Fig. 1b). As is typical for this region in the central Amazon Basin, there is little large-scale relief, but at smaller scales a dense drainage network has produced a pattern of plateaus and valleys with a maximum relief height of about 100 m (Planalto Dissecado do Rio Trombetas - Rio Negro). The ATTO site is located at 120 m a.s.l. on a plateau that measures about 1.5 km in the NW-SE direction and

Deleted: 7

Deleted: 8

Deleted: 9

Deleted: In a workshop on 23 June 2009 in Manaus, Brazilian and German Scientists evaluated three potential sites in terms of logistical and scientific criteria and decided to establish ATTO in the USDR.

Deleted: with mean annual temperature of 28ºC and mean annual precipitation of 2,376 mm (IBGE, 2012). The region is

Deleted: ,

about 5 km along the NE-SW axis. The topography surrounding ATTO resembles that around the Manaus LBA site (ZF2, also referred to as k34 site) in the Cuieiras Reserve, where the influence of topography on the micrometeorology and the fluxes of CO_2 has been studied in detail by Tota et al. (2012). From the perspective of micrometeorological flux measurements, this is not an ideal type of terrain because it induces significant upslope and downslope circulations. The effects of local topography on the local flux measurements from the small towers are the subject of ongoing investigations.

It must be pointed out, however, that the main objective of the tall tower with respect to greenhouse gas and aerosol monitoring is the measurement of concentrations above the level of local circulations. For this purpose, measurements from tall towers, such as ATTO, have the advantage of being less influenced by the surface layer variability due to diurnal changes in photosynthesis and respiration, as well as by ecosystem and terrain heterogeneity. This results in smoothening of the large daily cycles of near-surface signals and efficient integration over daily cycles and small-scale heterogeneities, which facilitates the detection of long-term changes in the background atmospheric composition.

The plateaus in this region are covered by yellow clayey ferralsols (latosols, oxisols) overlying the Miocene sedimentary Barreiras formation (Chauvel et al., 1987). In the valleys, alisols and sandy podzols are the dominant soil types.

The USDR consists of several different forested ecosystems. Dense, non-flooded upland forests (terra firme) prevail on plateaus at a maximum altitude of approximately 130 m above sea level (asl). Seasonally flooded black-water (igapó) forest dominates along the main river channel, oxbow lakes, and the several smaller tributaries of the Uatumã River (approximately 25 m asl). Interspersed with these formations are non-flooded terra firme forests on ancient river terraces (35-45 m asl), and campinas (savanna on white-sand soils) and campinaranas (white-sand forest), which are predominantly located between the river terraces and the slope to the plateaus.

Upwind of the site in the main wind direction (northeast to east), large areas covered by mostly undisturbed terra firme forests extend over hundreds of kilometers. To the northeast, the nearest region with dense human activity is in the

Deleted: R

Deleted: ly

Deleted: es

Deleted: where dense, non-flooded upland forests (terra firme) prevail on plateaus at a maximum altitude of approximately 130 m above sea level (asl).

coastal regions of the Guyanas and of Amapá State, about 1100 km away. In the easterly direction, the main stem of the Amazon is in the fetch region of ATTO, with scattered smaller towns and the cities of Santarém and Belém at distances of about 500 and 900 km, respectively. To the southeast, the densely populated states of the Brazilian Nordeste lie at distances greater than 1000 km. Figure 2 presents on overview of the population density and the dominant land cover in northern South America.

The origins of the predominant airmasses at ATTO change throughout the year, as the Intertropical Convergence Zone (ITCZ) undergoes large seasonal shifts over the Amazon Basin, resulting in pronounced differences in meteorological conditions and atmospheric composition (Andreae et al., 2012). This is illustrated in Fig. 3, which shows monthly trajectory frequency plots for 9-day back-trajectories arriving at ATTO at an elevation of 1000 m. During boreal winter, the ITCZ can lie as far south as 20°S, so that a large part of the Basin, including ATTO, is in the meteorologically Northern Hemisphere (NH). Airmasses then arrive predominantly from the northeast over a clean fetch region covered with rain forest. During this period, long-range transport from the Atlantic and Africa brings episodes of marine aerosol, Saharan dust, smoke from fires in West Africa, and possibly even pollution from North America and Europe. This flow pattern shifts abruptly at the end of May, when the ITCZ moves to the north of ATTO. This shift marks the beginning of the dry season at ATTO, a period of time during which the site is exposed to airmasses from the easterly and southeasterly fetch regions, which receive considerable pollution from biomass burning and other human activities in northeastern Brazil. In July almost the entire Basin is south of the ITCZ, and thus lies in the meteorologically Southern Hemisphere (SH). The transition to the northeasterly flow pattern is more gradual, beginning in September and becoming complete only in March.

2.2 Access

The ATTO site is reached from Manaus by the paved highway BR-174 for 101 km northward, then 70 km to the E on highway AM-240 towards Balbina. From there, a 38 km dirt road along the Uatumã River, Ramal de Morena, leads to the small community of Porto Morena, where the road ends. After a 61 km motor-

Deleted: and

Deleted: both meteorologically and geographically

Deleted: following national

Deleted: to a junction south of Presidente Figuereido

Deleted: heading

Deleted: a paved side road,

Deleted: ,

Deleted: , then

Deleted: SE on the

Deleted: a

Deleted: along the Uatumã River

boat ride on the Rio Uatumã towards the SE one reaches the landing, Porto ATTO. The access road from the landing to the ATTO site on the plateau follows an old trail used in the 1980s to extract Pau Rosa wood from the forest. This trail was re-opened in 2010 and widened to an ATV and tractor trafficable path that was used during the initial years of the development of the ATTO site. In 2012/13 a 6 m wide dirt road was constructed between the Uatumã River and the ATTO tower site, which accommodates pickups and trucks. The overall distance along this road, Ramal ATTO, is 13.7 km, rising from 25 to 130 m a.s.l. Total travel time from Manaus to the site is about five hours. For the delivery of large and heavy equipment to Porto ATTO, fluvial transportation by ship or pontoon is possible from Manaus by going down the Amazonas River and up its tributary, Rio Uatumã, a distance of ca. 550 km and travel time of 2 days.

Deleted: River

Deleted: , is reached

Deleted: the government of the State of Amazonia, represented by the Secretaria de Estado de Infraestrutura, SEINFRA, financed and implemented

Deleted: During the years of the project development, the travel time from Manaus has been gradually reduced from a whole-day trip in 2009 to a 4.5 h ride in 2014

2.3 Camp

The base camp on the ATTO plateau was built in 2011/12 and has electrical power and water. Facilities include toilets and a dormitory with hammocks that can accommodate ca. 20 people. Another camp is planned by INPA at the Uatumã River landing, which will serve also as a base station for ecological research in the area. A helicopter landing site is intended adjacent to this camp.

Deleted: by a team of technicians from INPA/LBA and workers hired from the Uatumã Sustainable Development Reserve (USDR). The camp

Deleted: , and

Deleted: f

2.4 Towers

The measurement facilities on the ATTO plateau consist of two towers of ca. 80 m height, already implemented, and the 325-m tall tower, whose construction began in September 2014 and is now nearing completion. In 2010, an 81-m triangular mast was established for pilot measurements, which is currently used for a wide set of aerosol measurements, followed in 2011 by an 80-m heavy-duty guy-wired walk-up tower (Instant UpRight, Dublin, Ireland). The walk-up tower can carry a total payload of 900 kg, with outboard platforms on five levels. It is currently used for meteorological and trace gas measurements. The measurements at the top level, at 79.3 m, are the highest ground based measurements within the Amazonian rain forest performed so far. The tower coordinates (WGS 84) are given in Table 1. The measuring instruments are accommodated in three air-conditioned containers, the trace gas lab and the greenhouse gas lab at the base of

Deleted: ,

Deleted: , purchased from the Irish company UPRIGHT (formerly INSTANT)

Deleted: 5

the walk-up tower, and the aerosol lab at the base of the mast; each lab has inside dimensions of 292 x 420 x 200 cm (WxLxH) and is supplied by 230/135 V electrical power.

2.5 Communications

Since the end of 2013, the ATTO site has been connected to the internet by satellite. The uplink is realized by the mobile satellite terminal Cobham EXPLORER 700 using the INMARSAT / BGAN broadband network, providing a data bandwidth of up to 492 kbps. Operating in the L-Band, its active antenna performance allows up to 20 dB compensation of signal attenuation due to bad weather. The antenna is mounted at 50 m height on the walk-up tower, aligned by 43.9° elevation and 273.1° azimuth towards the geostationary satellite INMARSAT 4-F3 Americas.

A cluster of two redundant routers manages the internet traffic and provides direct access from the internet to the various computers and networkable instruments at the ATTO site. The routers provide additional features like centralized data storage, remote server access, optimized file transfer, monitoring systems, updating clients, VoIP telephony between the local infrastructure sites, etc. Internal data communication between the various sites on the ATTO plateau (towers, labs, camp) is realized via a wireless LAN bridge, operating in the 5 GHz mode, featured by access points with directed-beam antennas.

Data communication within each site occurs via wired LAN with data rates of up to 1000 kbps. In addition, at the camp there is WLAN available in the 2.4 GHz mode. The communication system allows monitoring and controlling of networkable instruments in all three lab containers, as well as internet e-mailing, locally and globally. For oral communication with the remote ATTO site and for safety matters, satellite phones (IsatPhonePro) are available operating in the INMARSAT net.

2.6 Electrical power supply

Electrical power is provided by a system of diesel generators. Currently, the scientific sites (lab containers and towers) are supplied by two 60 Hz genera-

Deleted: ,

Deleted: with

Deleted: are

Deleted: ing

Deleted: al

753 tors with 45 and 40 kVA, operating alternately by weekly switching. They are
754 located ca. 800 m downwind from the measuring sites to avoid contamination.
755 Due to the long distance between power generation and consumption, power is
756 transmitted via two 600 V transformers, using two parallel cables, each 3 x 16
757 mm^2. The voltage provided to the labs is 230 and 135 V, and UPSs are being used
758 to stabilize energy. Power to the camp is provided separately to avoid power fluc-
759 tuations at the measurement sites. When the tall tower is established, it is planned
760 to upgrade the power generation to a new system of 2 x 100 kVA generators at a
761 distance of 2-3 km downwind of the tower.

762 # 3 Measurement methods

763 ## 3.1 Ecological studies

764 ### 3.1.1 Floristic composition and biomass characterization

765 Forest plots of three ha each were inventoried in the igapó, the campinara-
766 na, the terra firme on ancient river terraces, and the terra firme on the plateau in
767 order to provide a preliminarily description of the floristic composition and turno-
768 ver as well as the aboveground wood biomass (AGWB). All trees with ≥ 10 cm
769 DBH (diameter at breast height) were numbered, tagged with aluminum plates,
770 and, when possible, identified in the field. Fertile and sterile vouchers were col-
771 lected for later identification in the INPA herbarium. The AGWB was estimated
772 by a pantropical allometric model (Feldpausch et al., 2012) considering DBH, tree
773 height, and wood specific gravity. We measured tree height with a trigonometric
774 measuring device (Blume-Leiss) and determined wood specific gravity by sam-
775 pling cores from the tree trunk and calculating the ratio between dry mass (after
776 drying the wood samples at 105 ºC for 72 hours) and fresh volume. Additionally
777 we used data from the Global Wood Density Database DRYAD (Chave et al.,
778 2009) for tree species in the terra firme forests and from Targhetta (2012) for tree
779 species in the campina and igapó forests.

780 ### 3.1.2 Leaf phenology

781 An RGB camera (Stardot Netcam XL 3MP) was installed in June 2013 at
782 the top of the walk-up tower. The wide-angle view with 2048 x 1536 pixel resolu-

Deleted: and

Deleted: ,

Deleted: in the different forested ecosystems near the tower site

Deleted: , Manaus

Deleted: without determined wood specific gravity

tion includes over 250 separable tree crowns within an area of ~4 ha of the forest plateau. The camera aim is steeply oblique and toward the west, so that the sun is behind the camera when images are recorded from mid-morning until noon. Illumination artifacts are minimized by selecting images with homogeneous overcast sky and a fixed narrow range of incident radiance, and by post-selection radiometric normalization. Leaf phenology change is most evident in individual crowns, so timelines of the green chromatic coordinate, g_c, (Richardson et al., 2007) were made for each crown. A steep and sustained increase in the g_c of a crown can only be caused by the flushing of a new leaf cohort. The number of crowns reaching a flush-caused peak of g_c in their individual timelines were counted each month.

Deleted: plateau

3.1.3 Soil characterization

Soil sampling was performed on the ancient terraces (old floodplains) and terra firme plateaus at the ATTO site according to a standard protocol (Quesada et al., 2010). Five samples up to 2 m in depth were taken in each forest plot and one 2 m depth pit was dug close to each plot. We used the World Reference Base for soil resources to classify soil types (IUSS (International Union of Soil Science) Working Group WRB, 2006). Soil exchangeable cations were determined with the silver thiourea method (Pleysier and Juo, 1980), and soil carbon and nitrogen were analyzed using an automated elemental analyzer (Pella, 1990; Nelson and Sommers, 1996). Particle size was analyzed using the pipette method (Gee and Bauder, 1986). Soil physical properties were calculated for each plot using the "Quesada Index" (Quesada et al., 2010). This index is based on measurements of effective soil depth, soil structure, topography, and anoxia. To investigate the current soil weathering levels, a chemically based weathering index, Total Reserve Bases (∑RB), was calculated. ∑RB is based on total soil cation concentration and is considered to give a chemical estimation of weatherable minerals (Quesada et al., 2010).

Deleted: in

3.2 Meteorology

The walk-up tower is equipped with a suite of standard meteorological sensors (Table 2). The following quantities are continuously recorded: (a) soil

Deleted: including vertical profiles, for details see

heat flux, soil moisture, and soil temperature (10 minutes time resolution), (b) incoming and outgoing short and long wave radiation, photosynthetic active radiation (PAR), net radiation, ultraviolet radiation, rainfall, relative humidity (RH), air temperature, atmospheric pressure, and wind speed and direction (1 minute time resolution). Data acquisition is performed by several data loggers (CR3000 and CR1000, Campbell Scientific Inc., USA). Visibility is measured with an optical fog sensor (OFS, Eigenbrodt GmbH, Königsmoor, Germany), which detects the backscattered light intensity from a 650 nm laser.

Deleted: realized

3.3 Turbulence and flux measurements

Turbulent exchange fluxes of H_2O and CO_2 as well as surface boundary layer stability are measured within and above the canopy using the eddy covariance (EC) technique. The method is well documented in the literature (e.g., Baldocchi, 2003; Foken et al., 2012) and will not be described here. Three-dimensional wind and temperature fluctuations were measured by sonic anemometers at 81, 46 and 1.0 m a.g.l. (see Table 2). CO_2 and H_2O fluctuations are detected by three fast response open-path CO_2/H_2O infrared gas analyzers installed at a lateral distance of about 10 cm from the sonic path. The high-frequency signals are recorded at 10 Hz by CR1000 data loggers. The raw data are processed applying state-of-the-art correction methods using the software Alteddy (version 3.9; www.climatexchange.nl/projects/alteddy/) based on Aubinet et al. (2000). Fluxes, means and variances are calculated for half-hourly intervals (de Araújo et al., 2002; de Araujo et al., 2008; de Araujo et al., 2010). Continuous micrometeorological measurements have been made since September 2012, with some interruptions due to technical problems. The raw data are archived and are made available under the LBA data policy (https://daac.ornl.gov/LBA/lba_data_policy.html).

Deleted: .0
Deleted: .0
Deleted: were
Deleted: were
Deleted: were
Deleted: Detailed information about this software is available in the internet (www.climatexchange.nl/projects/alteddy/).
Deleted: were

3.4 Vertical profiles of reactive trace gases and total OH reactivity

Ozone is measured by a UV-absorption technique (Thermo Scientific 49i, Franklin, MA, USA), using Nafion dryers to minimize the effects of changing water vapor concentrations (Wilson and Birks, 2006). Mixing ratios of CO_2 and H_2O are measured by non-dispersive infrared absorption techniques (Licor-7000, LI-COR, Lincoln, USA). The detection limits are 0.5 ppb for ozone, 1 ppm for

Deleted: with a Thermo Scientific 49i analyzer
Deleted: , as suggested by Wilson and Birks

CO_2 and 0.2 mmol mol^{-1} for H_2O. Instrumental noise for 60-s averages is 0.25 ppb for ozone, 6 ppb for CO_2 (at 370 ppm), and 0.4 ppm for H_2O (at 10 mmol mol^{-1}).

During intensive campaigns, measurements of mixing ratios of Volatile Organic Compounds (VOC), total OH reactivity, nitric oxide (NO), nitrogen dioxide (NO_2), ozone (O_3), and water vapor (H_2O) were carried out at 8 heights in and above the rain forest canopy, using a reactive trace gas profile system similar to that described by Rummel et al. (2007). The lower part of the vertical profile (0.05, 0.5, and 4 m above the forest floor) was set up at an undisturbed location near the walk-up tower (distance 12 m). The upper part of the vertical profile (12, 24, 38, 53, and 79 m above forest floor) was mounted on the north-west corner of the walk-up tower. Heated and insulated intake lines (PTFE) were fed to the analyzers, which were housed in the air conditioned lab container 10 m west of the walk-up tower.

The NO mixing ratio was determined by a gas-phase chemiluminescence technique (CLD TR-780, Ecophysics, Switzerland). NO_2 was determined by the same analyzer after specific conversion to NO by a photolytic converter (Solid-state Photolytic NO_2 Converter (BLC); DMT, Boulder/USA). Detection limits are 0.05 ppb for NO and 0.1 ppb for NO_2. The signal noise is <0.5% of signal, limited by the zero point noise.

Measurements of VOC were performed using a Proton Transfer Reaction Mass Spectrometer (PTR-MS, Ionicon, Austria) operated under standard conditions (2.2 hPa, 600 V, 127 Td; 1 Td = 10^{-21} V m^2.). The instrument is capable of continuously monitoring VOCs with proton affinities higher than water and at low mixing ratios (several ppt with a time resolution of about 1-20 s) (Lindinger et al., 1998). One entire VOC vertical profile (from 0.05 m to 80 m, 8 heights in total) can be determined every 16 minutes using the same inlet system as the NO, NO_2, O_3, and CO_2 instruments.

Calibration was performed using a gravimetrically prepared multicomponent standard (Ionimed, Apel&Riemer). Occasionally, samples were collected in absorbent packed tubes (130 mg of Carbograph 1 [90 m^2 g^{-1}] followed by 130 mg of Carbograph 5 [560 m^2 g^{-1}]; Lara s.r.l., Rome, Italy) (Kesselmeier et al., 2002) and analyzed by GC-FID in order to cross-validate the measurements by PTR-MS

Formatted: Subscript
Formatted: Superscript
Formatted: Subscript
Formatted: Subscript
Formatted: Subscript
Formatted: Superscript
Deleted: ,
Formatted: Right: 0 cm
Deleted: NO Chemiluminescence analyzer, model
Deleted: The mixing ratio of
Formatted: Not Highlight
Formatted: Not Highlight
Formatted: Not Highlight
Deleted: Volatile Organic Compounds (
Deleted:)
Deleted: . The proton transfer reaction is a soft chemical ionization technique, meaning that fractionation of compounds is low. More detailed information is provided elsewhere
Deleted: Protonated water molecules H_3O^+ are used to charge the compound of interest prior to separation and detection by a quadrupole mass spectrometer according to their mass to charge ratio.

and to determine the monoterpene speciation for the total OH reactivity measurement.

In addition to the measurement of individual reactive inorganic trace gases and the VOCs, the total OH reactivity was determined. Total OH reactivity is the summed loss rate of all OH-reactive molecules (mixing ratio × reaction rate coefficient) present in the atmosphere. Direct measurements of total OH reactivity were conducted by the Comparative Reactivity Method (Sinha et al., 2008) using a PTR-MS as a detector. The PTR-MS monitored the mixing ratio of a reagent (pyrrole) after mixing and reaction in a Teflon-coated glass reactor. Pyrrole alternatingly reacts with OH alone and with OH in the presence of ambient air containing many more OH reactive compounds. The competitive reactions of the reagent and the ambient OH reactive molecules cause a change in the detected levels of pyrrole. This can be equated to the atmospheric total OH reactivity provided the instrument is well calibrated and appropriate corrections are applied (Nölscher et al., 2012). The total OH reactivity instrument was regularly tested for linearity of response using an isoprene gas standard (Air Liquide). VOC and total OH reactivity measurements were performed simultaneously with two separate PTR-MS systems measuring from the same inlet, so that the results may be directly compared over time, height, and season. The CRM method was able to measure OH reactivity down to 3 s^{-1}, estimated by the minimum observable modulation above two times the standard deviation (σ) of the noise (measured in zero air). The overall uncertainty in the measurement was 16%, including errors in detector (5%), rate coefficient (14%), gas standard (5%) and flow dilution (2%).

Deleted: monitored

Deleted: Comparison of the directly measured total OH reactivity to the summed OH reactivity of the individually detected species allows quantification of the "missing or unmeasured" OH reactivity.

Deleted: first

Deleted: then

Formatted: Superscript

3.5 Vertical profiles of long-lived trace gases (CO, CO_2, and CH_4)

In March 2012, continuous and high precision CO_2/CH_4/CO measurements were established in an air-conditioned container at the foot of the 80 m-tall walk-up tower. The sample air inlets are installed at five levels: 79, 53, 38, 24, and 4 meters above ground. The inlet tubes are constantly flushed at a flow rate of several liters per minute to avoid wall interaction within the tubing. A portion of the sample air is sub-sampled from the high flow lines at a lower flow rate for analysis with instruments based on the cavity ring-down spectroscopy technique

Deleted: . The

(G1301 and G1302 analyzers [Picarro Inc., USA] for measuring CO_2/CH_4 and CO/CO_2, respectively).

The G1301 analyzer (Serial CFADS-109) provides data with a standard deviation of the raw data below 0.05 ppm for CO_2 and 0.5 ppb for CH_4, the long-term drift is below 2 ppm and 1 ppb per year for CO_2 and CH_4, respectively. For the G1302 (Serial CKADS-018), tests with a stable gas tank show a standard deviation of the raw data of 0.04 ppm for CO_2 and 7 ppb for CO. The long-term drift of the analyzer is below 2 ppm and 4 ppb per year for CO_2 and CO, respectively. Both analyzers agree well with a CO_2 difference below 0.02 ppm. When the G1301 analyzer broke down in 2012, it was replaced from December 2012 until October 2013 with a Fast Greenhouse Gas Analyzer (FGGA) based on Off-Axis Integrated Cavity Output Spectroscopy (OA-ICOS; Los Gatos Research Inc., USA) as an emergency solution. This $CO_2/CH_4/H_2O$ analyzer is designed for measuring at rates of ≥10 Hz and is primarily used for eddy covariance and chamber flux measurements, where a low drift rate is less vital than for highly precise and stable long-term measurements. The FGGA operates with a raw standard deviation of 0.6 ppm for CO_2 and 2 ppb for CH_4; the drift is quite large with 1 ppm and 3 ppb per day for CO_2 and CH_4, respectively. For the time when the FGGA was used, the calibration and drift correction routines were adopted accordingly. The detailed description of the whole measurement system, including measurement, calibration, and correction routines will be presented elsewhere.

3.6 Aerosol measurements

3.6.1 Size distributions and optical measurements

Aerosols are sampled above the canopy at 60 m height, without size cut-off, and transported in a laminar flow through a 2.5 cm diameter stainless steel tube into an air-conditioned container (aerosol lab at mast, see Sect. 2.4). The sample humidity is kept below 40% using silica diffusion driers. Since January 2015, the aerosol sample air is being dried using a fully automatic silica diffusion dryer, developed by the Institute for Tropospheric Research, Leipzig, Germany (Tuch et al., 2009). Aerosol size distributions at 60 m are currently measured from 10 nm up to 10 µm using three instruments: a Scanning Mobility Particle Sizer

Deleted: Picarro
Deleted: (
Deleted:)
Deleted: are used
Deleted: Although both analyzers also measure the H_2O concentration in air, these measurements are not calibrated and can therefore be regarded only as informative.
Deleted: by
Deleted:
Deleted:
Deleted: has been

(SMPS, TSI model 3080, St. Paul, MN, USA; size range: 10-430 nm), an Ultra-High Sensitivity Aerosol Spectrometer (UHSAS, DMT, Boulder, CO, USA; size range: 60-1000 nm), and an Optical Particle Sizer (OPS, TSI model 3330; size range: 0.3-10 µm). The SMPS provides an electromobility size distribution, whereas the UHSAS and OPS measure aerosol light scattering and derive the size distributions from the particle scattering intensity (Cai et al., 2008). In addition to these continuous above-canopy measurements, aerosol size distributions are measured with a Wide Range Aerosol Spectrometer (WRAS, Grimm Aerosol Technik, Ainring, Germany; size range: 6 nm - 32 µm) from a separate inlet line below the canopy at 3 m height. The WRAS provides electromobility size distributions in the size range of 6-350 nm and uses particle light scattering for the size range above 300 nm. Details of the instrumentation setup are given in Table 2.

For measuring aerosol light scattering, we use a three-wavelength integrating nephelometer (until Feb 2014: TSI model 3563, wavelengths 450, 550, and 700 nm; after Feb 2014: Ecotech Aurora 3000, wavelengths 450, 525, and 635 nm) (Anderson et al., 1996; Anderson and Ogren, 1998). Calibration is carried out using CO_2 as the high span gas and filtered air as the low span gas. The zero signals are measured once every twelve hours using filtered ambient air. For the 300-s averages applied here, the detection limits, defined as a signal to noise ratio of 2, for scattering coefficients are 0.45, 0.17, and 0.26 Mm^{-1} for 450, 550/525, and 700/635 nm, respectively. Since sub-micrometer particles predominate in the particle number size distribution at our remote continental site, the sub-micron corrections given in Table 4 of Anderson and Ogren (1998) were used for the truncation corrections. Bond et al. (2009) suggested that this correction is accurate to within 2% for a wide range of atmospheric particles, but that the error could be as high as 5% for highly absorbing particles.

A Multi-Angle Absorption Photometer (MAAP, Model 5012, Thermo Electron Group, USA, $\lambda = 670$ nm) and a 7-wavelength Aethalometer (until Jan 2015 model AE-31, since then model AE-33) (Magee Scientific Company, Berkeley, CA, USA, $\lambda = 370, 470, 520, 590, 660, 880$, and 950 nm) are used for measuring the light absorption by particles. The MAAP and aethalometer have been deployed at ATTO since March 2012. In the MAAP instrument, the optical ab-

Deleted: estimate

Deleted: size

Deleted: the

Deleted: Argon

Deleted: Noise level and detection limits for the TSI 3563 have been investigated by Anderson et al. (1996). At low particle concentrations and/or short sampling times, random noise dominates the nephelometer uncertainties.

Deleted: -

Deleted: (as opposed to super-micron correction or an average of the two) corrections

Deleted: Carusso /

Deleted: MAAP

Deleted: 615,

sorption coefficient of aerosol collected on a filter is determined by radiative transfer calculations, which include multiple scattering effects and absorption enhancement due to reflections from the filter. A mass absorption efficiency (α_{abs}) of 6.6 m^2 g^{-1} was used to convert the MAAP absorption data to equivalent BC (BC_e). For the Aethalometer, an empirical correction method described by Rizzo et al. (2011) was used to correct the data for the scattering artifact.

Refractory black carbon (rBC) is measured by a 4-channel Single Particle Soot Photometer (SP2). The instrument is calibrated every 6 months using monodisperse fullerene aerosol particles for rBC calibration, and polystyrene latex (PSL) spheres for scattering calibration. The instrument is sensitive to rBC in the size range between 70 and 280 nm. A recent instrumental upgrade provides a broader rBC dynamic range (70 - 480 nm).

Regular quality checks are performed with all aerosol sizing instruments and CPCs, including flow checks, zero tests, and intercomparisons with ambient aerosol and monodisperse PSL cells. Exemplary plots are already included in the manuscript (Fig. 26). The MAAP and aethalometer are subject to frequent intercomparisons with the other optical instruments. For example, two aethalometers and the MAAP were operated side-by-side during an intensive campaign in Nov/Dec 2014. The BC_e concentrations from the individual instruments agreed well. The SP2 instrument was carefully intercalibrated with another SP2 during the GoAmazon-2014 campaign.

Fluorescent biological aerosol particles (FBAP) are measured with the Wideband Integrated Bioaerosol Spectrometer (WIBS-4A, DMT). The WIBS utilizes light-induced fluorescence technology to detect biological materials in real-time based on the presence of fluorophores in the ambient particles (Kaye et al., 2005). A 2x2 excitation (280 nm and 370 nm) - emission (310-400 nm and 420-650 nm) matrix is recorded along with the particle optical size and shape factor. The FBAP concentrations reported in this study correspond to the FL3 channel (excitation at 370 nm and emission in the waveband of 420-650 nm) of the WIBS instrument (Healy et al., 2014).

Deleted: B

3.6.2 Chemical measurements and hygroscopicity

The submicron non-refractory aerosol composition at a height of 60 m is measured using an Aerosol Chemical Speciation Monitor (ACSM, Aerodyne, USA) as described by Ng et al. (2011). The ACSM samples aerosol particles in the 75-650 nm size range. The non-refractory fraction flash vaporizes on a hot surface (600 °C), the evaporated gas phase compounds are ionized by 70 eV electron impact, and their spectra determined using a quadrupole mass spectrometer. The chemical speciation is determined via deconvolution of the mass spectra according to Allan et al. (2004). Mass concentrations of particulate organics, sulfate, nitrate, ammonium, and chloride are obtained with detection limits <0.2 µg m^{-3} for 30 min of signal averaging. Mass calibration of the system is performed using size-selected ammonium nitrate and ammonium sulfate aerosol following the procedure described by Ng et al. (2011). A collection efficiency (CE) of 1.0 is applied (similar to Chen et al., 2015), yielding good agreement with other instruments.

PM2.5 sampling was carried out from 7 March to 21 April 2012 on Nuclepore® polycarbonate filters at 80 m on the walk-up tower using a Harvard Impactor; samples were collected over 48 hour periods. They were analyzed by Energy-Dispersive X-ray Fluorescence (EDXRF) (MiniPal 4, PANalytical) at 1 mA and 9 kV for low-Z (Na to Cl) elements, and 0.3 mA, 30 kV, and internal Al filter for the other elements. Soluble species were determined by Ion Chromatography (Dionex, ICS-5000) using conductivity detection for cations and anions and UV-VIS for soluble transition metals. For cation separation, a capillary column CS12A was used, for anions, an AS19 column, and for transition metals, a CS5A column (calibrated to quantify traces of Fe^{2+} and Fe^{3+}).

Size-resolved cloud condensation nuclei (CCN) measurements are performed using a continuous-flow streamwise thermal gradient CCN counter (CCNC; model CCN-100, DMT, Boulder, CO, USA), a differential mobility analyzer (DMA, Grimm Aerosol Technik, Ainring, Germany) and a condensation particle counter (CPC model 5412, Grimm Aerosol Technik). By changing the temperature gradient, the supersaturation of the CCNC is set to values between 0.1% and 1.1%. The completion of a full measurement cycle comprising CCN

Deleted: The instrument is a compact version of the widely used Aerodyne Aerosol Mass Spectrometer (Jayne et al., 2000).

Deleted: efficiently

Deleted: through an aerodynamic lens

Deleted: and characterizes the mass and chemical composition of the non-refractory species

Deleted: focused particle beam is transmitted into a detection chamber where the

Deleted: typically at

Deleted: . Subsequently,

Deleted: PANanytical

Deleted: , MiniPal4

Deleted: the

Deleted:), commercially available from Droplet Measurement Technologies, Inc. (

Deleted: Particles with a critical supersaturation equal to or smaller than the prescribed supersaturation (S_{presc}) are activated and form water droplets.

efficiency spectra at 10 different supersaturation levels takes ~ 4 h. The CCNC is calibrated frequently as part of the maintenance routines with size selected monodisperse ammonium sulfate particles (Rose et al., 2008; Gunthe et al., 2009).

3.6.3 Microspectroscopic analysis of single aerosol particles

Aerosol samples for Scanning Electron Microscopy with Electron Probe Micro-analysis (EPMA) were collected on top of the 80 m tower in April 2012. For the collection of size-segregated samples for single particle analysis, we used a Battelle impactor with aerodynamic diameter cut-offs at 4, 2, 1 and 0.5 µm. The particles were collected on TEM grids covered with a thin carbon film (15–25 nm). Aerosol samples for x-ray microspectroscopy were collected using a single stage impactor, operated at a flow rate of 1-1.5 L min^{-1} and a corresponding 50% size cut-off of about 500 nm. Particles below this nominal cut-off are not deposited quantitatively; however, a certain fraction is still collected via diffusive deposition. Aerosol particles were collected onto silicon nitride substrates (membrane width 500 µm, membrane thickness 100 nm, Silson Ltd., Northhampton, UK) for short sampling periods (~ 20 min), which ensures an thin particle coverage on the substrate appropriate for single particle analysis.

Scanning Transmission X-ray Microscopy with Near-Edge X-ray Absorption Fine Structure Analysis (STXM-NEXAFS) measurements were made at the Advanced Light Source (ALS, Berkeley, CA, USA) and the Berliner Elektronenspeicherring-Gesellschaft für Synchrotronstrahlung (BESSY II, Helmholtz-Zentrum Berlin für Materialien und Energie (HZB), Germany). A detailed description of the instrumentation and techniques can be found elsewhere (Kilcoyne et al., 2003; Follath et al., 2010; Pöhlker et al., 2012; Pöhlker et al., 2014). Scanning Electron Microscopy with Energy Dispersive X-ray spectroscopy (SEM/EDX) analysis was carried out using a Jeol JSM-6390 SEM equipped with an Oxford Link SATW ultrathin window EDX detector. For EPMA, quantitative and qualitative calculations of the particle composition were performed using iterative Monte Carlo simulations and hierarchical cluster analysis (Ro et al., 2003) to obtain average relative concentrations for each different cluster of similar particle types.

Moved down [5]: The measurement period already covers 12 months and is being continued. The long-term data set provides unique information on the size dependent hygroscopicity of Amazonian aerosol particles throughout the seasons. The results will complement and extend the results from previous campaigns (e.g., Gunthe et al., 2009; Rose et al., 2011; Levin et al., 2014).

Deleted: Complementary to the online long-term aerosol measurements, modern offline techniques were applied to aerosol samples collected at the ATTO site. In particular, microspectroscopic techniques, such as Scanning Transmission X-ray Microscopy with Near-Edge X-ray Absorption Fine Structure Analysis (STXM-NEXAFS) and Scanning Electron Microscopy with Energy Dispersive X-ray spectroscopy (SEM-EDX), were utilized to shed light on the morphology and composition of single aerosol particles with nanometer resolution.¶

Formatted: No widow/orphan control, Don't adjust space between Latin and Asian text, Don't adjust space between Asian text and numbers

Deleted: at the ATTO site

Deleted: (i.e., EPMA)

Deleted: ¶

Deleted: homemade

Deleted: which was

Deleted: and therefore available for the STXM analysis

Deleted: Si_3N_4,

Deleted: appropriately

Deleted: . Detailed information can be found in (Pöhlker et al., 2012; 2014)

Deleted: is a synchrotron-based technique and

Deleted: In the soft X-ray regime, STXM-NEXAFS is a powerful microscopic tool with high spectroscopic sensitivity for the light elements carbon (C), nitrogen (N) and oxygen (O) as well as a variety of other atmospherically relevant elements (e.g., K, Ca, Fe, S, Na). The technique allows analyzing the microstructure, mixing state, as well as the chemical composition of individual aerosol particles. ¶
The

3.6.4 Chemical composition of secondary organic aerosol

Filter sampling for Secondary Organic Aerosol (SOA) analysis was performed on the walk-up tower at a height of 42 m above ground level. Fine aerosol (PM 2.5) was sampled at a flow rate of 2.3 m^3 h^{-1} on TFE-coated borosilicate glass fiber filters (PALLFLEX, T60A20, Pall Life Science, USA). The sampling times were 6, 12, or 24 hours. After sampling the filters were stored at 255 K until extraction.

The extraction of the filters was performed with acetonitrile (≥ 99.9%; Sigma Aldrich) in a sonication bath at room temperature. The filter extracts were evaporated with a gentle nitrogen flow at room temperature in an evaporation unit (Reacti Vap 1; Fisher Scientific), and the residue was re-dissolved in 100 µL HPLC grade water (Milli-Q water system, Millipore, Bedford, USA) / acetonitrile (≥ 99.9%; Sigma Aldrich) mixture (8:2).

The separation and analysis was performed with an UHPLC-system (Dionex UltiMate 3000) coupled to a Q Exactive electrospray ionization Orbitrap mass spectrometer (Thermo Scientific). A Hypersil Gold column (50 mm x 2.1 mm, 1.9 µm particle size, 175 Å pore size; Thermo Scientific) was used. The eluents were HPLC grade water (Milli-Q water system, Millipore, Bedford, USA) with 0.01% formic acid and 2% acetonitrile (eluent A) and acetonitrile with 2% HPLC grade water (eluent B). The flow rate of the mobile phase was 0.5 mL min^{-1}. The column was held at a constant temperature of 298 K in the column oven. The MS was operated with an auxiliary gas flow rate of 15 (instrument specific arbitrary units, AU), a sheath gas flow rate of 30 AU, a capillary temperature of 623 K, and a spray voltage of 3000 V. The MS was operated in the negative ion mode, the resolution was 70000, and the measured mass range was m/z 80-350.

Deleted:

Deleted: series, auto sampler, gradient pump and degasser

Deleted: -

4 Ongoing Research and Initial Results

Deleted: Results and Discussion

4.1 Ecological studies

4.1.1 Tree species richness, composition, turnover, and aboveground wood biomass

In total, 7293 trees ≥ 10 cm DBH were recorded in the 12 1-ha inventoried plots, which included 60 families, 206 genera, and 417 species. Tree species richness was highest in the terra firme forest on the plateau, followed by the terra firme forest on the fluvial terrace, the campinarana, and the seasonally flooded igapó (Table 3). Floristic similarity (Bray-Curtis index) within plots of the same forest types ranged from 45-65%, but was highly variable between different forest types (2-54%). Accordingly, the species turnover across the investigated forest types was high, especially when seasonally inundated forest plots were compared to their non-flooded counterparts (Fig. 4). AGWB varied considerably between the studied forest ecosystems as a result of varying tree heights, DBH, and basal area (Table 3). Carbon stocks in the AGWB increased from 74±12 Mg ha^{-1} in the igapó forest to 79±26 Mg ha^{-1} in the campina/campinarana, and 101±13 Mg ha^{-1}on the ancient fluvial terrace, reaching maximum values of 170±13 Mg ha^{-1} in the terra firme forests. Tree species richness correlated significantly with carbon stocks in AGWB (n=12; $r^2 = 0.61$; $p<0.01$).

Deleted: inventoried

The floristic data indicate that the rain forests at the ATTO site combine high alpha diversity with high beta diversity at a small geographic scale, where tree species segregate mainly due to contrasting local edaphic conditions (e.g., Tuomisto et al., 2003; ter Steege et al., 2013; Wittmann et al., 2013). Biomass and carbon stocks vary considerably between habitats, and show low values on flooded and nutrient-poor soils and high values on well-drained upland soils, as previously reported elsewhere for other Amazonian regions (e.g., Chave et al., 2005; Malhi et al., 2006; Schöngart et al., 2010).

Deleted: C-

Deleted: up

Deleted: up

4.1.2 Cryptogamic covers

We are investigating the potential of cryptogamic covers to serve as a source of bioaerosol particles and chemical compounds. Cryptogamic covers

Deleted: e

comprise photoautotrophic communities of cyanobacteria, algae, lichens, and bryophytes in varying proportions, which may also host fungi, other bacteria, and archaea (Elbert et al., 2012). A common feature of all these organism groups is their poikilohydric nature, meaning that their moisture status follows the external water conditions. Thus the organisms dry out under dry conditions, being reactivated again upon rain, fog, or condensation.

Since September 2014, we have been conducting long-term measurements to monitor the activity patterns of cryptogamic covers at four different canopy heights at 10-min intervals, during which we measure temperature and water content within and light intensities directly on top of bio-crusts growing on the trunk of a tree. First analyses of the microclimate data indicate that microorganisms in the upper stem region of the trees are activated by fog or dewfall in the early morning hours, often coinciding with an aerosol particle burst in the accumulation mode. Particle measurements conducted on isolated organisms also show a significant release of accumulation mode particles by wet and thus active organisms, e.g., fungi belonging to the phylum of Basidiomycota. Thus, we have the first clear indications that cryptogamic covers may play a key role in the enigmatic bioaerosol occurrence frequently observed at the ATTO site.

Deleted: Starting in

Deleted: have

Deleted: are

Deleted: ed

Deleted: in

4.1.3 Upper Canopy Leaf Phenology

Formatted: Heading 3, Right: 0 cm

A single annual leaf flush was seen in most upper canopy crowns, concentrated in the five driest months (July to November) (Fig. 5). Consequently, mature leaves with high light-use efficiency will be most abundant in the late dry season and early wet season. Massive leaf renewal in the dry season on the ATTO plateau may drive seasonality of photosynthesis and of photosynthetic capacity at the landscape scale, as has been indicated at the Santarém and the LBA km34 eddy flux tower sites in the Central Amazon (Doughty and Goulden, 2008; Restrepo-Coupe et al., 2013).

Formatted: Indent: First line: 1.25 cm, Right: -0 cm

The lack of a near-infrared (NIR) band in our camera precludes the direct measurement of leaf amount, but the RGB band space discriminates crown phenostages whose relative NIR reflectances are known. Gradual leaf attrition over the wet season, when leaf replacement is low, followed by early dry season preflush abscission and the emergence of young unexpanded leaves, should all lead

to a lower landscape-scale amount of fully expanded leaves around June or July. Completion of leaf flushing in most crowns by the late dry season should lead to a maximum amount of fully expanded leaves in the late dry and early wet seasons. This is consistent with the seasonal pattern of Central Amazon leaf amount detected with the Enhanced Vegetation Index from the MODIS orbital sensor (e.g., Huete et al., 2006) and counters recent critiques of detectability of seasonal change in Amazon forest greenness (Galvão et al., 2011; Morton et al., 2014).

4.1.4 Soil Characterization

Soils in the terra firme plateaus were classified as Ferralsol, which are ancient, highly weathered, and well-drained soils frequently occurring in geologically ancient surfaces (Chauvel et al., 1987). Soils at the fluvial terraces were classified as Alisol, which show a more recent pedogenetic status when compared to the highly weathered Ferralsols at the plateaus. Due to their lower weathering degree, soils from the terrace have a greater capacity to supply nutrients, with higher total P and higher total reserve bases. The soil carbon stocks varied from 129±7 Mg ha^{-1} on the terrace to 164±7 Mg ha^{-1} on the plateau, indicating that belowground C stocks are of similar magnitude to the aboveground carbon stocks in the forest (Table 4). Differences of belowground carbon stocks between terrace and plateau are mainly associated with a higher clay content of the plateau soils.

Soil physical constraints are more frequent on the terraces, which show higher bulk density values (Fig. 6) and therefore increased soil compaction. Some of these terrace soils also show signs of anoxia (mottling) in deeper layers. Such impeditive conditions may have an influence on forest structure (Quesada et al., 2012; Emilio et al., 2014) and dynamics (Cintra et al., 2013), thereby possibly restricting tree height or even tree individual biomass storage (Martins et al., 2015).

4.2 Meteorological conditions and fluxes

An overview of the climatic characteristics of the Amazon Basin has been presented by Nobre et al. (2009). The meteorological setting of the ATTO site has been described in Section 2.1, and the basic meteorological measurements (wind, temperature, humidity, radiation, etc.) at the site reflect the regional climate and

Formatted: Heading 3, Indent: First line: 0 cm

Deleted: <#>The activation patterns of cryptogamic covers upon dewfall will be of particular interest to check for correlation with patterns of particle release. In on-site measurements cryptogamic covers are analyzed for their release of biogenic aerosols (e.g., spores). These particles will be investigated and compared with results from offline and online aerosol measurements at the ATTO site.¶

micrometeorological conditions influenced by local topography and vegetation. In the following sections we present overviews of meteorological observations that characterize the site and initial results of micrometeorological investigations at ATTO. Since the quantification of the exchange of trace gases and aerosols between the rain forest and the atmosphere is a key objective of the ATTO program, the study of the structure and behavior of the atmospheric boundary layer is a central focus here.

Deleted: the

4.2.1 Wind speed and direction above the forest canopy

The wind roses for the dry season (15 June - 30 Nov) and the wet season (1 Dec - 14 June) (based on half-hourly averages of wind speed and direction measured at 81 m a.g.l. for the period from 18 Oct 2012 to 23 July 2014; Fig. 7) indicate the dominance of easterly trade wind flows at the measurement site. A slight shift of the major wind direction towards ENE is observed during the wet season, whereas flows are mainly from the east during the dry season. This seasonality can be explained by the inter-annual north-south migration of the Intertropical Convergence Zone (ITCZ), which also governs the amount of rainfall (see Poveda et al., 2006). The wind roses show a slight diurnal variation with small contributions from the north, west and south during nighttime, when the nocturnal boundary layer is decoupled, in both seasons. In contrast, during daytime the wind blows nearly all the time from the east (dry season) and northeast (wet season), with much higher wind speeds. Maximal wind speeds observed at the site are about 9 m s^{-1}. The influence of river and/or lake breeze systems caused by the Rio Uatumã (~12 km distance) is of minor importance and an effect from Lake Balbina (~50 km distance) or other thermally driven mesoscale circulations could not be detected. This shows that the sampled air masses mainly have their origin within the fetch of the green ocean extending several hundred kilometers to the east of the site.

Deleted: 5

Deleted: while

Deleted: variation of the wind roses between daytime and nighttime was insignificant.

Deleted: or

Deleted: and

Deleted: is of minor importance

4.2.2 Temperature, precipitation, and radiation

As is typical for the central Amazon Basin, the mean air temperature does not show strong variations at seasonal timescales due to the high incident solar radiation throughout the year (Nobre et al., 2009). Climatologically in the Manaus

region, the highest temperatures are observed during the dry season, with a September monthly mean of 27.5 °C, whereas the lowest temperatures prevail in the rainy season, with a monthly mean of 25.9 °C in March.

Vertical profiles of temperature show clear diurnal cycles driven by radiative heating of the canopy during the day and cooling of the canopy and the forest floor during the night (Fig. 8). Therefore, both temperature minima and maxima are observed at the canopy top during both seasons. A second temperature minimum during night can be observed at the forest floor during the dry and wet season. During the day warm air from above the canopy is transported into the forest. Minimum temperatures at the canopy top are around 22.5 °C during both seasons, whereas daytime maxima are around 28 °C during the wet season and may reach slightly above 30 °C in the dry season.

Deleted: radiative

Deleted: 6

Rainfall in the Manaus region shows a pronounced seasonal variation, reaching the highest amounts in March (335.4 mm) and the lowest amounts in August (47.3 mm), for an average annual total of 2307.4 mm at the INMET station in Manaus for the standard reference period 1961 to 1990 (www.inmet.gov.br). Precipitation at the ATTO site follows this seasonal cycle with maximum values around March and minimum values in August and September (Fig. 9). The interannual variability appears to be high at all times of the year, but especially in the transition to the rainy season, a fact that has also been evident in the data from the years 1981 to 2010 at the Manaus station (Fernandes, 2014). Therefore, the large deviations from the regional mean during October to January and also in April, when the ATTO values from the years 2012-2014 differ substantially from the long term mean of Manaus, are likely the result of interannual variability.

Deleted: 7

Overall, however, the precipitation patterns at the ATTO site are in good agreement with its position in the Central Amazon, where the months between February and May are the wettest ones. In this period, the ITCZ reaches its southernmost position and acts as a strong driver of convective cloud formation at the equatorial trough. Due to the interaction of trade winds and sea breeze at the northeast Brazilian coastline, the ITCZ also takes part in the formation of instability lines that enter the continent and regenerate during their westerly propagation

Deleted: in

(Greco et al., 1990). In this way, they account for substantial amounts of precipitation. After this period, the ITCZ shifts to the northern hemisphere, accompanying the movement of the zenith position of the sun. This leads to less precipitation at the ATTO site, with the driest months being between July and September, when precipitation is formed mostly by local convection. In the following months, the amount of precipitation increases again, which coincides with the formation of a cloud band in a NW/SE direction that is linked to convection in the Amazon due to the South Atlantic Convergence Zone (SACZ) (Figueroa and Nobre, 1990; Rocha et al., 2009; Santos and Buchmann, 2010).

The radiation balance at ATTO as well as the albedo presents a clear difference between the wet and the dry seasons. Some episodes when the incident solar radiation exceeds the top-of-atmosphere radiation have been observed for the ATTO data. They were more frequent during the wet season, probably due to the effect of cloud gap modulation that intensifies the radiation received at the surface by reflection and scattering.

Deleted:

Deleted:

Deleted: s

Deleted: y

4.2.3 Roughness sublayer measurements

The measurement of turbulent fluxes over tall forest canopies very often implies that these measurements are made in the so-called *roughness sublayer* (RSL). It is usually assumed that the RSL extends to 2 or 3 times the height of the roughness obstacles, h_0 (Williams et al., 2007). The roughness sublayer is considered to be a part of the surface sublayer of the atmospheric boundary layer, but it is too close to the roughness elements for Monin-Obukhov Similarity Theory (MOST) to hold. Some progress in the parameterization of the RSL has been made in terms of applying correction factors to the traditional similarity functions of the surface layer (see for example, Mölder et al., 1999, and references therein). However, the universality of such procedures remains unknown.

Deleted:

In this section, we briefly show strong evidence that a simple adjustment factor that depends on the factor z/z_* (where z is the height of measurement and z_* is the height of the RSL), as employed by Mölder et al. (1999), is not able to collapse the "variance method" dimensionless variables

$$\phi_w(\zeta) \equiv \frac{\sigma_w}{u_*} \quad (1)$$

and

$$\phi_a(\zeta) \equiv \frac{\sigma_a}{a_*}, \quad (2)$$

where σ_w is the standard deviation of the vertical velocity, u_* is the friction velocity, σ_a is the standard deviation of a scalar, and a_* is its turbulent scale (see (3) and (4) below). In (1) and (2), ζ is the Obukhov length with a zero-plane displacement height calculated as $d_0 = 2h_0/3$, $h_0 = 40$ m.

We analyzed measurements collected during April 2012 at the 39.5 m level, which is right at the height of the tree tops, in terms of the turbulent scales

$$\overline{u'w'} \equiv -u_*^2 \quad (3)$$

and

$$|\overline{w'a'}| \equiv u_* a_*. \quad (4)$$

We only analyzed measurements under unstable conditions, and considered only cases where the sensible and latent heat fluxes are both positive (directed upwards) and the CO_2 flux is negative (directed downwards). In (4), the absolute value is used, so that a_* is always positive. The scalar a represents virtual temperature θ_v (measured by the sonic anemometer), specific humidity q, and CO_2 mixing ratio c.

The analysis is made in terms of the dimensionless standard deviation functions, $\phi_w(\zeta)$ and $\phi_a(\zeta)$, defined above. The overall results for vertical velocity, virtual temperature, and CO_2 concentration are shown in Fig. 10. The solid lines in the figure give representative functions found in the literature for the surface layer well above the roughness sublayer (see, for example, Dias et al., 2009).

Similar figures were drawn for specific times of day, namely 0700-0900, 0900-1100, 1100-1300, 1300-1500 and 1500-1700 LT, in an attempt to identify periods of the day when better agreement (or even a systematic departure, for example by a constant vertical shift) with the surface-layer curves could be identified. Temperature and humidity are somewhat better behaved in this case, but not CO_2, for reasons that are not clear. Because no conclusive explanation can be found, we do not show these analyses here.

Deleted: heat flux is positive (directed upwards),

Deleted: the

Deleted: is

Deleted: O

Deleted: s

Deleted: 8-

Deleted: s

Finally, we tried to apply some concepts recently developed by Cancelli et al. (2012) to relate the applicability of MOST to the strength of the surface forcing. Cancelli et al. (2012) found that the applicability of MOST can be well predicted by their "surface flux number",

$$\mathrm{Sf}_a = \frac{|\overline{w'a'}|(z-d_0)}{\nu_a \Delta\overline{a}}, \quad (5)$$

where ν_a is the molecular diffusivity of scalar a in the air, and $\Delta\overline{a}$ is the gradient of its mean concentration between the surface and the measurement height.

In our case, there is no easy way to obtain $\Delta\overline{a}$, so instead we use

$$\mathrm{Sf}_a = \frac{|\overline{w'a'}|(z-d_0)}{\nu_a \sigma_a}. \quad (6)$$

As a measure of the applicability of MOST, we use the absolute value of the difference between the observed value of $\phi_a(\zeta)$ and its reference value for the surface layer, as used by Dias et al. (2009), and shown by the solid lines in Fig. 10. The results are shown in Fig. 11. A relatively stronger forcing is clearly related to a behavior that is closer to that expected by MOST for both temperature and humidity, *but not for CO_2*. This suggests that CO_2 presents even greater challenges for our proper understanding of its turbulent transport in the roughness sublayer over the Amazon Forest.

Ultimately, the lack of conformity to MOST found in these investigations (a fact that has been generally observed in the roughness sublayer over other forests) implies that scalar fluxes over the Amazon forest derived from standard models, which use MOST, are bound to have larger errors here than over lower vegetation, such as grass or crops. We can expect this to affect any chemical species, and therefore the implications for ATTO are quite wide-ranging. On the other hand, once the 325-m tall tower is instrumented and operational, a much better picture will emerge on the extent of the roughness sublayer and the best strategies to model scalar fluxes over the forest.

Deleted: s

Deleted: 8-

Deleted: Monin-Obukhov Similarity Theory

4.2.4 Nighttime vertical coupling mechanisms between the canopy and the atmosphere

During daytime, intense turbulent activity provides an effective and vigorous coupling between the canopy layer and the atmosphere above it. As a consequence, vertical profiles of chemical species do not commonly show abrupt variations induced by episodes of intense vertical flux divergence. Accordingly, scalar fluxes between the canopy and the atmosphere are relatively well-behaved during daytime, so that their inference from the vertical profiles of mean quantities can be achieved using established similarity relationships. At night, on the other hand, the reduced turbulence intensity often causes the canopy to decouple from the air above it (Fitzjarrald and Moore, 1990; Betts et al., 2009; van Gorsel et al., 2011; Oliveira et al., 2013). In these circumstances, vertical fluxes converge to shallow layers in which the scalars may accumulate intensely over short time periods. In the absence of convective turbulence, which is the main factor for daytime transport, other physical processes become relevant in the stable boundary layer (SBL), such as drainage flow (Sun et al., 2004), vertical divergence of radiation (Drüe and Heinemann, 2007; Hoch et al., 2007), global intermittency (Mahrt, 1999), atmosphere-surface interactions (Steeneveld et al., 2008), and gravity waves (Nappo, 1991; Brown and Wood, 2003; Zeri and Sa, 2011).

In this section, we discuss the role of intermittent turbulent events of variable intensity and periodicity, which provide episodic connection between the canopy and the atmosphere and can induce oscillatory behavior in the nocturnal boundary layer (Van de Wiel et al., 2002). They are characterized by brief episodes of turbulence with intervening periods of relatively weak or unmeasurably small fluctuations (Mahrt, 1999). In some cases, such events may comprise almost the entirety of the scalar fluxes during a given night. The effects of gravity waves are discussed in the next section.

Nocturnal decoupling occurs rather frequently at the ATTO site, usually punctuated by intermittent mixing episodes, in agreement with previous studies made over the Amazon forest (Fitzjarrald and Moore, 1990; Ramos et al., 2004). During a typical decoupled, intermittent night, the horizontal wind components are weak in magnitude and highly variable temporally, often switching signs in an

Moved (insertion) [4]

Moved (insertion) [3]

Deleted: While

Deleted: , this driving mechanism decays after nightfall. As a result

Field Code Changed

Deleted: GWs

Field Code Changed

Moved up [4]: In these circumvertical fluxes converge to shallow layers in which the scalars may accumulate intensely over short time periods.

Deleted: In these circumstances, vertical fluxes converge to shallow layers in which the scalars may accumulate intensely over short time periods. FurthermoreIn these circumstar…

unpredictable manner (Fig. 12). As a consequence, it is common that winds from all possible directions occur in such a night. The example from the ATTO site indicates that despite such a large variability, both horizontal wind components are generally in phase above the canopy, from the 42-m to the 80-m level. Vertical velocity at the 42-m level is highly intermittent, with various turbulent events of variable intensity scattered throughout the night. While being less turbulent, the 80-m level is also less intermittent, presenting a more continuous behavior. The relevance of the intermittent events to characterize canopy-atmosphere exchange becomes clear when one looks at the fluxes of the scalars, such as CO_2 (Fig. 12, bottom panel). During this night, the majority of the exchange just above the canopy (42 m) happened during two specific events, at around 02:00 and 03:30 LT.

A proper understanding of nocturnal vertical profiles and fluxes of scalars above any forest canopy depends, therefore, on explaining the atmospheric controls on intermittent turbulence at canopy level. In the Amazon forest, this necessity is enhanced, as there are indications that turbulence is more intermittent here, possibly as a consequence of flow instabilities generated by the wind profile at canopy level (Ramos et al., 2004). This is corroborated by early observations at the ATTO site, which indicated decoupling and intermittency occurring during more than half of the nights.

Deleted: t

Deleted: the

It is not yet clear what triggers these intermittent events. In general, previous studies indicate that the more intense events are generated above the nocturnal boundary layer, propagating from above (Sun et al., 2002; Sun et al., 2004). On the other hand, less intense events that occur in the decoupled state have been characterized as natural modes of turbulence variability generated near the surface (Costa et al., 2011). At ATTO, the occurrence of the highest intensity at 42 m indicates that intermittency is generated at the canopy level. Is it possible, then, to identify the mechanisms that trigger their occurrence?

Some evidence can be gathered from a spectral decomposition of the turbulent flow at the different observation levels. Although the horizontal velocities in Fig. 12 are highly in phase between 42 and 80 m, it is clear from this plot that the wind speed is generally higher at 80 m, while there are more turbulent fluctuations at 42 m. When these signals are decomposed in terms of their time scale to

provide a turbulent kinetic energy (TKE) spectrum (Acevedo et al., 2014), the more intense turbulence at 42 m appears as a peak at time scales just greater than 10 s (Fig. 13). At longer time scales, on the other hand, there is a sharp energy increase at 80 m, making this the most energetic level for scales larger than 100 s. This low-frequency flow at 80 m is characterized by the large wind direction variability apparent in Fig. 12. These are non-turbulent flow patterns that have been recently classified as "submeso" (Mahrt, 2009). Submeso flow has low intensity, with large and apparently unpredictable temporal variability. It is usually present in the atmospheric boundary layer, becoming dominant in conditions when the turbulent scales are highly reduced, such as in the decoupled nocturnal boundary layer.

Evidence from ATTO indicates that it is possible to associate the intermittent events at canopy level with the mean wind shear above the canopy. In Figure 14, it is evident that the two intense events at 42 m, around 21:30 and 02:00 LT, are triggered by episodes of intense wind shear between 42 and 80 m. In conditions where the 80-m wind field is dominated by submeso processes, such as in the examples in Figs. 12 and 14, it is this portion of the flow that determines the occurrence of intense wind shear episodes. Furthermore, it is clear from these examples that flow patterns at levels as high as 80 m exert important controls on the exchange of scalars at canopy level. Questions such as the height variation of submeso flow have yet to be answered. Tall tower observations, such as those planned to be carried on at ATTO, are very important to provide the data for this kind of analysis and to deepen the understanding of exchange processes between the canopy and the atmosphere during the calm nights that are common in the Amazon forest.

4.2.5 Orographically induced gravity waves in the stable boundary layer above the Amazon forest

Gravity waves (GWs) may occur in the forest boundary layer during relatively calm nights. Depending on the magnitude of the turbulent drag, they influence the exchange processes that take place in the stable boundary layer of the atmosphere (Steeneveld et al., 2009). Internal gravity waves can be generated by several forcing mechanisms, including sudden changes of surface roughness, to-

Deleted:

Deleted: Such a

Deleted: at

Moved up [3]: While convective turbulence is the main factor for daytime transport, this driving mechanism decays after nightfall. As a result, other physical processes become relevant in the stable boundary layer (SBL), such as drainage flow (Sun et al., 2004), vertical divergence of radiation (Drüe and Heinemann, 2007; Hoch et al., 2007), global intermittency (Mahrt, 1999), atmosphere-surface interactions (Steeneveld et al., 2008), and GWs (Nappo, 1991; Brown and Wood, 2003; Zeri and Sa, 2011).

pography, convection, terrain undulations, etc. (Nappo, 2002). These features can reallocate energy and momentum and are significant in determining atmospheric vertical structure and the coupling of mesoscale to microscale phenomena (Steeneveld et al., 2008; Steeneveld et al., 2009). Chimonas and Nappo (1989) showed that under typical conditions of the planetary boundary layer, GWs can interact with the mean flow resulting in turbulence at unexpected altitudes.

Fast response data of vertical wind velocity, w, and temperature, T, measured in the nocturnal boundary layer (NBL) at the ATTO site were analyzed to detect the occurrence of GWs, and to identify under which situations they would be generated by terrain undulations, using the methodology proposed by Steeneveld et al. (2009). One of the goals of this study is to investigate the structure of turbulence associated with the conditions under which GWs would be forced by ground undulations (class I) in contrast to those under which GWs would be expected to be forced by other mechanisms (class II). To reach this goal, the methodology of Steeneveld et al. (2009), based on Chimonas and Nappo (1989), has been used to define whether a specific measurement belongs to class I or class II, based on the condition:

$$L_S^2 = N^2/U^2 - U''/U > k^2 \quad (7)$$

where k is the wave number associated with the ground undulations, L is the Scorer parameter, U is the mean wind speed, and U" is second derivative of the wind speed in relation to the height, z, computed as

$$U'' = \partial^2 U / \partial z^2 \quad (8)$$

N is the Brunt-Väisälä frequency, defined as:

$$N = \sqrt{g \Delta_z \theta / \theta} \quad (9)$$

where g is the gravity acceleration and $\Delta_z \theta / \theta$ is the dimensionless gradient of the virtual potential temperature.

Two kinds of data were used: topographic and meteorological. A digital topographic image of the region surrounding the experimental site (Fig. 15a) was used to analyze the features of surface undulations and their scales of occurrence, as well as the space-scale analysis by complex Morlet wavelet transforms (Farge,

Deleted: gravity waves (

Deleted:)

Deleted: and

1992; Thomas and Foken, 2005). Local geomorphometric variables were derived from the Shuttle Radar Topographic Mission (SRTM) data (Valeriano, 2008). These data were refined to 1 arcsecond (~30 m) from the original spatial resolution of 3 arcsecond (~90 m) and are available on the site www.dsr.inpe.br/topodata/dados.php.

Time series of the vertical wind velocity and of the fast response temperature data provided by a sonic anemometer and thermometer were used to detect GW events at a height of 81 m above the ground. The sampling rate of the measured turbulence data was 10 Hz. Wind speed and temperature vertical profiles were provided by cup anemometer and thermometer measurements, respectively, with a sampling rate of 60 Hz for both, making it possible to compute the Brunt–Väisälä frequency, the vertical gradients of wind velocity, and the Scorer parameter for GW classification (Steeneveld et al., 2009). Data from five nights were analyzed, consisting of 120 files of 30 minutes each between Julian days 42 and 46 of the year 2012, representing the first observational data available from the ATTO site. The analyses were carried out for the time between 18:00 and 06:00 LT for each night with available data (Fig. 15).

The black points on the arrows in Fig. 15b represent the GW events that were induced by the topography of the terrain, whereas the gray points represent GW events that were not generated by terrain orography. The results show that a considerable fraction of the analyzed situations represent GWs induced by terrain undulations. This finding is very important for the environmental studies that are being carried out at the ATTO site, as it indicates that some mixing characteristics of the nocturnal boundary layer depend on the characteristics of terrain undulations and therefore change with the wind direction.

4.2.6 Coherent structure time scale above the ATTO site

Coherent structures (CSs) are a ubiquitous phenomenon in the turbulent atmospheric flow, particularly over forests (Hussain, 1986). They occur in the roughness sub-layer immediately above the plant canopy, where the CSs of the scalar signals show a "ramp-like" shape associated with the two-phase movement of sweep and ejection of the flow interacting with the canopy. Coherent structures play an important role in biosphere-atmosphere exchange processes (Gao and Li,

Deleted: SRTM (
Deleted:)
Deleted:
Deleted: s
Deleted: have been
Deleted: number
Deleted: (local time)
Deleted: ,
Deleted: Figure 15a shows a topographic image of the experimental site with colors ranging from blue to red representing the altimetry values in meters above sea level.
Deleted: axes
Deleted: have been
Deleted: have
Deleted: been
Deleted: s
Deleted: Uatumã

1993; Serafimovich et al., 2011). There is some consensus that CSs are associated with turbulent flows, although there is no full agreement on the percentage of the turbulent fluxes associated with them (Lu and Fitzjarrald, 1994; Thomas and Foken, 2007; Foken et al., 2012). There has been much research on the dominant scale of occurrence of CSs (Collineau and Brunet, 1993; Thomas and Foken, 2005) and the physical mechanisms responsible for their generation (Paw U et al., 1992; Raupach et al., 1996; McNaughton and Brunet, 2002; Campanharo et al., 2008; Dias Júnior et al., 2013). Considerable research has also been devoted to the detection of CSs (Collineau and Brunet, 1993; Krusche and Oliveira, 2004) and the dissimilarity between CSs associated with the transport of momentum and scalars (Li and Bou-Zeid, 2011). However, many aspects of their occurrence are still poorly known, particularly: i) their vertical variability (Lohou et al., 2000); ii) the manifestations of their interaction with gravity waves (Sorbjan and Czerwinska, 2013); iii) the influence of surface heterogeneity on their features; iv) aspects of their numerical simulation (Patton, 1997; Bou-Zeid et al., 2004; Dupont and Brunet, 2009; Wan and Porte-Agel, 2011), particularly in the nocturnal boundary layer (Durden et al., 2013; Zilitinkevich et al., 2013), and v) implications of the existence of CSs for the chemistry of the atmosphere (Steiner et al., 2011; Foken et al., 2012).

Deleted:

Deleted: among

A study on the structure of atmospheric turbulence was performed at the ATTO site under daytime conditions, with the aim of contributing to the detection of CSs and developing a better understanding of their vertical and temporal variability over a very uneven terrain covered by primary forest in central Amazonia. Wind, temperature, and humidity data were obtained using sonic anemometers and gas analyzers, installed at 42 m and 81 m above ground, as specified in the methods section. The scales of coherent structures were determined following the methodology proposed by Thomas and Foken (2005). Figure 16 shows the average duration of CSs for horizontal and vertical wind velocities (u, w), temperature (T), and humidity (q). For the data at 81 m height, the CS of u and w exhibit temporal scales around 46 s and 29 s, respectively. For the two scalars, T and q, the time scales of the CS are about 44 s and 55 s, respectively. For the height of 42 m the coherent structure time scales of u, w, T, and q were approximately equal to 33 s, 26 s, 30 s, and 31 s, respectively.

The results revealed that the CS time scale of the vertical wind velocity is often smaller than the scales of the horizontal velocity and the scalar properties, for both levels. This can be explained by the fact that the scalar spectra exhibit greater similarity to the spectra of the horizontal velocity than to the vertical velocity for low frequencies. Another interesting feature is that the temporal scale of the CSs for both the wind velocity and scalars are considerably shorter for the data measured at 81 m ~~compared with those at 42 m, i.e., the region immediately above~~ the forest canopy appears to be under the influence of a high-pass filter that removes the lower frequency oscillations of the turbulent signals (Krusche and Oliveira, 2004; Thomas and Foken, 2005).

4.2.7 Characteristics of the nocturnal boundary layer

The characteristics of the nocturnal boundary layer (NBL) at the ATTO site near the Uatumã River were analyzed for the wet and the dry seasons, based on two methodologies: i) the thermodynamic classes of the NBL proposed by Cava et al. (2004) and ii) the turbulence regimes proposed by Sun et al. (2012).

Cava et al.'s (2004) classification of nocturnal time series is based on the existence of a dominant pattern in scalar data, such as CO_2 concentration, temperature, or specific humidity. It also takes into account the variability of nocturnal net radiation (R_n), measured at a sufficiently high sampling rate, which allows cloud detection (with passage of clouds being identified by rapid R_n changes greater than 10 W m^{-2}). Classes (I), (II), (III), are defined by atmospheric conditions free of the influence of clouds, which can disturb the stable boundary layer above the forest. The classes are defined as followed by Cava et al. (2004): (I) the occurrence of coherent structures in the form of "ramps" in scalar time series; (II) the presence of sinusoidal signals ("ripples") that simultaneously occur in the time series of scalars above the canopy, and that are typical for gravity waves; (III) the existence of turbulence fine structure (i.e., according to Cava et al. (2004), "periods that lack any geometric structure or periodicity in the time series data"). The last two categories, (IV) and (V), of Cava et al.'s classification refer to the simultaneous occurrence of clouds and organized movements with variations in R_n >10 W m^{-2}. They are: (IV) cases where the net radiation induces organized move-

Deleted: are

Formatted: Subscript

Formatted: Subscript

Deleted: ,

Deleted: which

Formatted: Subscript

ments, and (V) those where the change in net radiation is not correlated with changes in organized movements.

The search of parameters to characterize the turbulent regimes of the nocturnal boundary layer is based on Sun et al. (2012). The three turbulent regimes in the NBL are defined as follows: Regime 1 shows weak turbulence generated by local shear instability and modulated by the vertical gradient of potential temperature. Regime 2 shows strong turbulence and wind speed exceeding a threshold value (V_λ), above which turbulence increases systematically with increasing wind speed. This describes the turbulence generated by bulk shear instability, defined as the mean wind speed divided by the measuring height. In Regime 3, the turbulence occurs at wind speeds lower than V_λ, but is associated with occasional bursts of top-down turbulence. In Regimes 1 and 2 the scale of turbulent velocity (V_{TKE}) is related to the mean wind velocity, V. The turbulent velocity, V_{TKE}, is defined as:

$$V_{TKE} = \left[(1/2)\left(\sigma_u^2 + \sigma_v^2 + \sigma_w^2\right)\right]^{1/2} \quad (10)$$

where u, v, and w are the components of the zonal, meridional and vertical winds, respectively, and σ represents the standard deviation of each variable.

We analyzed 53 data files from the wet season and 79 data files collected during the dry season at the ATTO site. Our results show that the prevailing conditions in the NBL are represented by Cava's classes I, II, and V for both wet and dry seasons (Table 5). Furthermore, during the wet season the classes I and V show their highest percentage of occurrence associated with turbulent Regime 3. Class IV is more frequent when turbulence Regime 1 prevails. For the dry season we observe that turbulent classes I, IV and V occur most frequently in situations associated with Regime 1 (Table 6).

Deleted: 4

Deleted: 5

4.3 Measurements of atmospheric composition

In March 2012, a basic set of measurements (CO, CO_2, CH_4, and equivalent black carbon, BC_e) was initiated at the site, which has been running almost continuously up to the present. As CO_2 and BC_e were measured with multiple instruments in parallel (see Table 2) an almost complete time series since March 2012 is available for these quantities. In November 2012, the long-term measure-

ment setup was upgraded to include measurements of ozone, aerosol scattering, aerosol size distribution, and aerosol number concentration. Due to the complex logistics at this remote site, there are a few large data gaps in some of these time series, but the datasets are almost complete from the middle of May 2013 to November 2013 and from February 2014 to now. Continuous measurements of aerosol chemical composition by an aerosol mass spectrometer were also initiated in February 2014. Furthermore, several intensive campaigns were conducted with additional measurements of aerosol properties, VOC, OH reactivity, and NO_x.

4.3.1 CO_2, CH_4, and CO

Figures 17a-c show the diurnal cycles of the vertical distributions of CO_2, CH_4, and CO at the ATTO site. CO_2 and CO show a nighttime accumulation in the sub-canopy space and a corresponding steepening of the vertical concentration gradient, which is greatly reduced during daytime due to the enhanced vertical mixing throughout the canopy. In addition, CO_2 exhibits a clear minimum during daytime at mid-canopy level induced by photosynthesis. Interestingly, the build-up of the nighttime maximum of CH_4 proceeds from above the canopy (Fig. 17b). The origin of this behavior, which seems to be linked to multiple processes, is under investigation. During daytime, CO_2, CH_4, and CO still exhibit a small vertical gradient below the canopy, indicating a local source near the ground.

Additional evidence for local surface sources are sporadic concurrent increases of CH_4 and CO, predominantly at the lowest measurement level. Examples are shown in Fig. 18. The origin of this local CH_4 and CO source is not known. A remote source (e.g., from the large water reservoir behind the Balbina Dam, 60 km northwest of ATTO) seems unlikely, as such a signal would be vertically diluted before reaching the ATTO site. A combustion source also appears unlikely, as the observed CH_4/CO ratios are several orders of magnitude higher than the values typical of combustion emissions.

Apart from these CH_4 and CO peaks, we occasionally observe, mostly during nighttime, short CH_4 peaks of up to more than 100 ppb amplitude. These peaks last a few hours, they do not always concur with increases in CO concentrations, and often coincide with “bursts” of particles with a diameter of a few tens of nanometers.

Deleted: its current status,
Deleted: ing
Deleted: r
Deleted: -19
Deleted: the concentrations of
Deleted: 8
Deleted: a
Deleted: on
Deleted: 20
Deleted: -
Deleted: /

Figure 19 shows the statistics of monthly daytime (defined as between 1300-1600 LT, or 1700-2000 UT) 30-min measurements of CO_2 from three levels (4 m, 38 m, and 79 m). The values at the 4-m level are consistently higher than at the upper levels, while the 38-m level consistently shows lower values during daytime than the top level (79 m). This indicates that photosynthesis is active throughout the year. The record is still too short to reveal a clear seasonality. Nevertheless, it appears that CO_2 from June to August is about 5 ppm above the values during the months from December to February.

Statistics of monthly daytime 30-min measurements of CH_4 and CO are shown in Fig. 20 (from the 79-m level only). Because of a large data gap due to a malfunctioning of the analyzer, a seasonal cycle is not discernible in the present CH_4 record. CO does show a seasonal cycle at ATTO with concentrations higher by about 50 ppb during the dry months with a significant fraction of air coming from the south-east (see Fig. 3), where vegetation fires are very active at this time.

Monthly daytime concentrations of CO_2, CH_4, and CO are compared in Fig. 21 with measurements upstream of ATTO: Cape Verde (green symbols) reflecting the subtropics of the northern hemisphere, and Ascension Island (brown symbols) representing conditions in the southern hemisphere. At least during the period of July to December, CO_2 concentrations clearly reach lower values than at both upstream locations, reflecting the regional carbon sink in the Amazon domain. In contrast, CH_4 levels at ATTO lie almost on northern hemisphere levels throughout the year, even when the ITCZ is north of ATTO in austral winter and the site is in the atmospheric southern hemisphere with its lower background CH_4 concentrations. This suggests the presence of regional CH_4 emissions in the airshed of ATTO. The CO concentrations at ATTO during the wet season are close to those at Cape Verde, reflecting the absence of significant combustion sources in the South American part of the fetch during this season. In contrast, dry season CO mixing ratios at ATTO are about 80 ppb higher than those at Ascension Island, reflecting biomass burning emissions in the southeastern Amazon (Andreae et al., 2012).

Deleted: 21

Deleted: respectively

Deleted: measurements

Deleted: 2

Deleted: 3

Deleted: southern end

Deleted: Likewise

4.3.2 Biogenic volatile organic compounds and OH reactivity

The first successful vertical gradients of biogenic VOCs and total OH reactivity were measured in November 2012 at the walk-up tower using the gradient system as described in Section 3.4. Diurnal fluctuations of isoprene are apparent at all heights (Fig. 22). Under daylight conditions, isoprene mixing ratios were always highest at the 24 m level, reaching up to 19.9±2.0 ppb (average ± standard deviation) and indicating a source at the canopy top. During nighttime, the light-driven emissions of isoprene cease and the in-canopy mixing ratio fell to 1.1±0.5 ppb, which was lower than observed above the forest at 79 m (2.3±0.3 ppb). Measurements in the canopy (24 m) vary by a factor of ten from day to night, while measurements close to the ground (0.05 m) vary only by a factor of two. This clearly demonstrates a canopy emission of isoprene, with a peak around noon, when light and temperature are at their maximum. Isoprene mixing ratios at the ground level were always the lowest, indicating a potential sink at the soil/litter level or relatively slow downward mixing. A detailed discussion of measurements of isoprene and other biogenic VOC at ATTO was published recently (Yañez-Serrano et al., 2015).

In November 2012, the high levels of isoprene measured above the canopy contributed significantly (on average about 85%) to the total OH reactivity. From Fig. 23, it can be seen that median isoprene mixing ratios of between 0.5 ppb at 6:00 LT and 8 ppb in the late afternoon above the canopy give an OH reactivity of about 1-20 s^{-1}. The gap between the two curves is the fraction of total OH reactivity that is not due to isoprene. For most of the time this gap is small and within the uncertainty of the measurements. On two occasions, however, the total OH reactivity was significantly higher than the isoprene contribution, these being in the early morning (0900 LT) coincident with a drop in light levels, and in the afternoon just after sunset (1700 LT). For all other times in the course of the day, isoprene was the major sink for OH above the canopy. Overall, a distinct diel variability in total OH reactivity can be observed, similar to that of its major contributor, isoprene. The median lifetime of OH radicals during the dry-to-wet transition season above the forest canopy at 80 m varied from about 50 ms by day to 100 ms

Deleted: INSTANT

Deleted: 4

Deleted: 80

Deleted: 5

Deleted: within this dataset from November 2012

at night. Ongoing measurements will determine the seasonal variability in total OH reactivity and the relative contribution of isoprene.

4.3.3 Ozone profiles

The O_3 mixing ratios (Fig. 24) show typical diurnal cycles for both seasons, with values increasing from the morning to the afternoon and subsequently decreasing due to deposition and chemical reactions. The afternoon O_3 maxima at the uppermost height (79 m) are about a factor of 1.4 higher during the dry season than during the wet season, averaging about ~11 ppb and ~8 ppb, respectively. As found in previous studies, its deposition to surfaces causes O_3 to exhibit pronounced vertical gradients (Fig. 24), which makes a direct intercomparison to measurements at other sites difficult. However, the mixing ratios above the canopy from different studies in the Amazonian rain forest during the wet season are within a narrow range of 7 to 12 ppb, and the value measured at ATTO falls near the lower end of this range (Kirchhoff et al., 1990; Andreae et al., 2002; Rummel et al., 2007; Artaxo et al., 2013). A budget study by Jacob and Wofsy (1990) revealed that downward transport of O_3 mainly controlled the losses near the surface, with only a minor contribution from photochemical formation above the canopy. This may explain the similar mixing ratios in the different studies. Furthermore, only small O_3 differences were measured between 38 m (just above the canopy) and the top of the tower at 79 m during the wet season.

A different picture is observed during the dry season, with much higher O_3 mixing ratios at more polluted sites (~40 ppb in Rondônia: Kirchhoff et al., 1989; Andreae et al., 2002; Rummel et al., 2007; Artaxo et al., 2013), which can be related to biomass burning emissions causing photochemical O_3 formation (Crutzen and Andreae, 1990). A site comparable to the ATTO site is the ZF2 site, located about 60 km north-west of Manaus, which has been used extensively in the past (Artaxo et al., 2013), but which is occasionally affected by the Manaus urban plume (Kuhn et al., 2010; Trebs et al., 2012). At the ZF2 site, mean maximum O_3 mixing ratios measured at 39 m from 2009-2012 (Artaxo et al., 2013) match exactly those measured at the ATTO site for the wet season, but are about a factor of 1.5 higher during the dry season. This may be attributed to the more pristine character of the ATTO site, but could also be related to the different measurement

Deleted: by

Deleted: 6

Deleted: distinct

Deleted: profiles

Deleted: 6

Deleted: other

Deleted: during the wet season

Deleted: mixing ratios

periods or different biogenic emissions at the sites. In order to distinguish these different influences, high-quality long-term measurements are required, which are now being generated within the ATTO project.

During the wet season, the amplitude of the mean diurnal cycle at 79 m is only about 2 ppb, whereas it is 3-4 ppb during the dry season. The highest amplitudes are observed within the canopy and the understory with up to 5 ppb (24 m) in the dry season. These variations can be attributed to downward mixing of O_3, which is "stored" within the canopy (so called storage flux, see Rummel et al., 2007). It is subsequently depleted by chemical reactions, mostly with soil biogenic NO, and deposition after the forest canopy becomes decoupled from the atmosphere above at nighttime. During the wet season, the largest decrease in O_3 mixing ratios occurs at the canopy top. This might be attributed to a lower canopy resistance to O_3 deposition due to enhanced stomatal aperture during the wet season as proposed by Rummel et al. (2007) and will be the subject of future work. Further investigations will also focus on the interactions between turbulence (supply of O_3) and trace gases that react with O_3, especially nitric oxide (NO).

Deleted: ,

Deleted: for

4.3.4 Aerosol optical properties

The aerosol optical properties measured at the ATTO site are shown as a time series in Fig. 25 and summarized in Table 7. The averages were calculated for the dry season, August-October, and the wet season, February-May (2012-13 for the absorption measurements and 2013 for the scattering measurements). The transition periods between these two seasons are not included in the summary, in order to show the contrast between the cleanest and "more polluted" periods. The scattering coefficients are similar to those reported by Rizzo et al. (2013) from measurements performed at the ZF2 site (60 km N of Manaus). The regional transport of biomass burning emissions and fossil-fuel derived pollution is the main source of particles during the dry season. Its influence is pronounced, as can be seen by comparing the scattering and absorption coefficients from both seasons, which average about 3-6 times higher during the dry than during the wet season. During the wet season, ATTO is meteorologically located in the NH and the scattering and absorption coefficients reach their minimum values; however,

Deleted: 7

Deleted: 6

Deleted: significant

Deleted: ,

episodes of long-range transport of aerosols from the Atlantic Ocean and Africa still lead to episodically elevated values.

The contrast between the wet and dry seasons can be attributed to a combination of higher removal rates by wet deposition during the wet season and the dominant influence from biomass burning and fossil fuel emissions during the dry season, which are the main sources of submicron particles at that time. The scattering Ångström exponent ($å_s$) averages 1.25 during the wet season, lower than the 1.62 obtained for the dry season. This behavior results from the high relative proportion of larger particles (mostly primary biogenic particles, but also dust and seaspray) during the wet season, because in contrast to the large seasonal variability of the submicron particles, the supermicron fraction shows less intense seasonal changes.

The seasonality of the absorption coefficient, σ_a, is comparable to that of the scattering coefficient. The regional transport of biomass burning emissions, most important between August and October, produces a rise in the σ_a values, reaching an average of 3.46 Mm^{-1} during this period. In contrast, during the wet season, σ_a is very low, around 0.52 Mm^{-1} on average.

The absorption Ångström exponent ($å_a$) is often used to estimate the composition of light absorbing aerosols. An $å_a \sim 1$ indicates the aerosol is in the Rayleigh regime, and the absorption is dominated by soot-like carbon and is therefore wavelength independent (Moosmüller et al., 2011). Higher $å_a$ values indicate the presence of additional light absorbing material, like brown carbon (BrC) (Andreae and Gelencsér, 2006). This kind of yellowish or brown organic material, abundant in biomass burning aerosols, usually has an $å_a \sim 2.0$ or greater (Bond et al., 1999). Our measurements show only relatively minor seasonal differences in $å_a$, with somewhat higher values during the wet season (1.53) than in the dry season (1.40), suggesting that soot carbon is the most important contributor to aerosol light absorption throughout the year. The contribution of the different light absorbing components of the aerosol to the total observed aerosol absorption is currently being investigated.

We conducted the first long-term refractory black carbon (rBC) measurements by an SP2 instrument at a remote Amazonian site. The mass absorption

Deleted: some

Deleted: o

Deleted: an important

cross section (α_a) has been calculated by applying an orthogonal regression to the MAAP absorption coefficient measurements at 637 nm vs. rBC mass concentrations measured by the SP2. The average α_a obtained for the 2013-2014 wet season measurements was 13.5 m^2 g^{-1}, which is much higher than the 4.7 m^2 g^{-1} reported previously for another Amazonian forest site (Gilardoni et al., 2011), who used a thermal-optical method to determine the apparent elemental carbon content. The high apparent α_a could be partly explained by the fact that the SP2 size dynamic range was 70-280 nm and thus the technique did not account for rBC particles larger than 280 nm. However, it is also likely related to an enhancement of light absorption by coatings on the rBC particles, or to the presence of additional light-absorbing substances besides rBC (Bueno et al., 2011; McMeeking et al., 2014). Single-particle studies (Section 4.3.7) on aerosols from the ATTO site consistently show thick coatings on the soot carbon particles. Our preliminary results indicate that the constant α_a (6.6 m^2 g^{-1}), implemented by the MAAP in order to retrieve the BC mass concentration, is not representative of the true optical properties of Amazonian aerosol particles.

Deleted: the refractive BC (

Deleted:)

Deleted: an

Deleted: measured also during the wet season.

4.3.5 Aerosol number concentrations and size distributions

Continuous measurements of aerosol particle size and concentration have been conducted at the ATTO site since March 2012. Over the last years, the extent of the sizing instrumentation has been increased stepwise to provide uninterrupted and redundant aerosol size and concentration time series. Figure 26 shows one of the frequent instrument intercomparisons, including four different instruments that are based on optical and electromobility sizing. It confirms the overall consistency and comparability of the different sizing techniques. Integrated particle number concentrations agree within 15% with measurements of total particle number concentrations by a CPC. The sample air for this intercomparison was collected through the main aerosol inlet at 60 m height, which is also used for instruments measuring aerosol scattering, absorptivity, hygroscopicity, and chemical composition.

Deleted: 8

Deleted: of

Deleted: the backup

Deleted: within 15%

Deleted: has been

At the ATTO site, the atmospheric aerosol burden shows remarkable differences in terms of size distribution and concentration depending on the seasons. Figure 27 displays the average particle number and volume size distributions for

Deleted: 9

typical wet (6-13 May 2014) and dry season (13-20 Sep 2014) conditions, covering an aerosol size range from 10 nm to 10 µm. The wet season is characterized by clean air masses from NE directions (Fig. 3), which result in a near-pristine atmospheric state at the ATTO site. Total particle concentrations typically range from 100-400 cm^{-3} and aerosol size spectra reveal the characteristic "wet season shape". A representative example is shown in Fig. 27. The size spectrum is characterized by a 3-modal shape with pronounced Aitken and accumulation modes as well as a noticeable coarse mode. Aitken (maximum at ~70 nm) and accumulation (maximum at ~150 nm) modes are separated by the so called Hoppel minimum (at ~110 nm), which is thought to be caused by cloud processing (e.g., Zhou et al., 2002; Rissler et al., 2004; Artaxo et al., 2013).

The near-pristine conditions that prevail at the ATTO site during the wet season, when the aerosol concentrations are remarkably low and dominated by local and/or regional biogenic sources, are episodically interrupted by long-range transport of sea spray, Saharan dust, and/or African biomass burning and fossil fuel combustion aerosol (e.g., Talbot et al., 1990; Martin et al., 2010a; Martin et al., 2010b; Baars et al., 2011). Figure 28 displays characteristic changes in the wet season size distribution during selected episodes with long-range transport intrusions. Typically, the aerosol abundance in the accumulation and coarse mode size range is substantially increased and the Hoppel minimum almost completely disappears. The aerosol volume distribution clearly indicates a pronounced enhancement of coarse particles, which increases the integrated particle volume concentration by almost one order of magnitude (Fig.28b).

During the dry season, the dominant wind direction is E to SE (Fig. 3), which brings polluted air from urban sources and deforestation and pasture fires in in the southeastern Amazon and the Brazilian Nordeste to the ATTO site. Dry season aerosol number concentrations typically range from 500-2000 cm^{-3}. A characteristic dry season size spectrum is illustrated in Fig. 27, which shows increased particle concentrations across the entire size range. Typically, the accumulation mode (maximum at ~140 nm) shows the highest relative increase and therefore partly 'swamps' the Aitken mode (shoulder at ~70 nm).

Deleted: . The comparison focusses on SMPS and OPS measurements

Deleted: ¶

Deleted: 9

Deleted: maximum

Deleted: controlled

Deleted: 30

Deleted: large

Deleted: 30

Deleted: SE Brazil

Deleted: 9

Besides the Aitken and accumulation modes, which dominate the total aerosol number concentration, a persistent coarse mode is observed at about 3 µm, which accounts for a significant fraction of the total aerosol mass (Fig. 27). The coarse mode peak occurs throughout the year, with higher abundance in the dry season. In the absence of long-range transport, primary biological aerosol particles (PBAP) are assumed to dominate the coarse mode (Pöschl et al., 2010; Huffman et al., 2012).

Autofluorescence-based techniques such as the Wideband Integrated Bioaerosol Sensor, WIBS-4A) are an efficient approach to probe fluorescent biological aerosol particles (FBAP) in online measurements (Kaye et al., 2005; Healy et al., 2014). Figure 29 shows the first measurements of the FBAP number and volume size distributions from the WIBS instrument at the ATTO site. The FBAP size distributions are dominated in number by a narrow peak at 2.7 µm and in volume by a broad peak from 2 to 5 µm (Fig. 29). For particles larger than 1 µm, the mean integral FBAP number concentration is 0.22 cm^{-3} (40% of the concentration of supermicron particles), and the corresponding volume concentration is calculated to be 3.0 μm^3 cm^{-3} (62%). The ratio of FBAP to total particles (number concentration) shows a clear size dependence, starting from 10% at 1 µm and rising to a peak value ~70-80% in the size range of 3-10 µm. These observations are consistent with FBAP measurements made with an alternative instrument (UVAPS) during the AMAZE-08 campaign at the ZF2 rainforest site north of Manaus (Pöschl et al., 2010; Huffman et al., 2012).

CCN size/supersaturation spectra have been measured since 2014 and are being continued. The long-term data set provides unique information on the size dependent hygroscopicity of Amazonian aerosol particles throughout the seasons. The results will complement and extend the results from previous campaigns (e.g., Gunthe et al., 2009; Rose et al., 2011; Levin et al., 2014). The measurements of CCN and other aerosol properties at the ATTO site will also be an important reference for the analysis of the results from the ACRIDICON-CHUVA aircraft campaign, which took place in central Amazonia in September 2014 (Wendisch et al., 2015).

Deleted: 9

Deleted: (Fig. 29)

Deleted:

Deleted: (e.g.,

Deleted: have become an established

Deleted: 31

Deleted: the

Deleted: operation

Deleted: at the ATTO site

Deleted: , which are in good agreement with the OPS measurements.

Deleted: 31

Moved (insertion) [5]

Deleted: The

Deleted: are

Deleted: being

Deleted: measurement period already covers 12 months and is

Field Code Changed

4.3.6 Aerosol chemical composition

For the continuous determination of aerosol composition, an Aerosol Chemical Speciation Monitor (ACSM) was installed at the ATTO site in February 2014 with the objective of making long-term measurements. The data reported here summarize the annual cycle of aerosol concentrations and composition from May 2014 to April 2015 (Fig. 30).

During the middle of the rainy season (March to May), the aerosol concentrations at ATTO reach their annual minimum and are in relatively good agreement with previous wet season studies, including those conducted at the ZF2 site, ca. 140 km SW of ATTO (Chen et al., 2009; Pöschl et al., 2010; Artaxo et al., 2013). With the onset of the dry season, the shift of airmass origins to the southeast, and the transition of ATTO into the atmospheric southern hemisphere (Fig. 3), aerosol concentrations increase sharply and remain high until the end of December, well into the rainy season. Trajectory analyses suggest that burning in Africa may contribute significantly to pollution levels at ATTO during this part of the year. Only when the rainy conditions in the Amazon combine again with dominant airmass origins in the tropical and subtropical North Atlantic and with the waning of biomass burning in West Africa can aerosol concentrations at ATTO drop again to their seasonal lows.

The composition of the aerosol at ATTO shows surprisingly little variation throughout the year in spite of the huge change in total concentrations between seasons. Organic aerosol is always the dominant mass fraction at about 70%, sulfate comprises about 10-15%, followed by BC_e (5-11%), ammonium (~5%), nitrate (~4%) and chloride. Elevated concentrations of chloride were observed during a few episodes, when this species represented up to 13% of the total submicron particulate mass, which is consistent with earlier observations of long-range transport of sea salt, going back to the ABLE-2B campaign (Talbot et al., 1990).

The ionic mass balance indicates that the aerosol was approximately acid-base neutral. While sulfate is mostly in the form of ammonium sulfate, there is some indication that part of the nitrate could be present in the form of organic nitrate. This is because the ratio between the fragments NO^+ and NO_2^+ (main nitrate fragments measured by the ACSM at mass-to-charge ratios 30 and 46) is

Deleted: , a sample air stream is taken from the shared aerosol inlet (60 m) and the non-refractory submicrometer aerosol composition is determined using

Deleted: that

Deleted: were taken during the early wet season transition from 1 to 31 Mar 2015

Deleted: The time series of aerosol concentrations and the average chemical speciation are given in Fig. 32.

Deleted: T

Deleted: average

Deleted: of non-refractory aerosols, as well as the chemical speciation

Deleted: is

Deleted: during AMAZE-08 (

Deleted:),

Deleted: with organic matter dominating (78%) the aerosol composition and inorganic ions making relatively minor contributions

Deleted: Sulfate

Deleted: d

Deleted: 12

Deleted: of the mass concentration

Deleted: measured by the ACSM

Formatted: Subscript

Deleted: (2%)

Moved (insertion) [6]

Deleted: d

Deleted: mostly

Deleted: ized

expected to be large (~10) when this ion is in organic forms, and low (2-3) when in inorganic forms, such as ammonium nitrate (Alfarra et al., 2006; Fry et al., 2009). Large values for this ratio were often observed during this period and may indicate the presence of organic nitrate.

The bulk composition of $PM_{2.5}$ was measured for up to 10 elements by EDXRF analysis on a set of samples obtained in March/April 2012. The analysis showed a high abundance of crustal elements, illustrating one exemplary episode of long-range dust transport from Africa (Fig. 31). Back trajectories indicate that this period was indeed influenced by dust transport from Africa, which is a phenomenon observed annually and particularly pronounced in February, March, and April (Prospero et al., 1981; Swap et al., 1992; Ben-Ami et al., 2012). Local sources of mineral dust aerosol can be excluded, especially during the wet season, because of the wetness of the soils. The prevalence of mineral dust aerosols during the wet season, when airmass trajectories reach from the North African deserts to the Amazon Basin, in combination with observations of transatlantic dust plumes by lidar, is strong evidence for the long-range origin of the observed crustal elements.

To explore the bioavailability of important trace elements, the oxidation state and solubility of iron (Fe) in the $PM_{2.5}$ aerosols were analyzed. The soluble (and therefore bioavailable) fraction of Fe is an important parameter in the overall biogeochemical cycles, with impact on the phosphorus cycle and biomass production (Liptzin and Silver, 2009). A soluble fraction of only 1.5% (1.8 ng m^{-3} Fe(III) of 120 ng m^{-3} of total Fe) was found, suggesting that aeolian transport of Fe is not likely to make a significant contribution of bioavailable Fe to the ecosystem at ATTO.

The extended measurements of aerosol composition at the ATTO site, now reaching well over a full year, suggest the need for a reassessment of the relative contributions of biogenic and anthropogenic sources even in this very remote region. Black carbon, a unique tracer of combustion, is present in a roughly equal fraction throughout the year. Sulfate, which has a more complex mixture of sources, also contributes a fairly constant fraction. In the rainy season, much of this sulfate could come from biogenic or marine sources (Andreae et al., 1990),

Moved up [6]: Elevated concentrations of chloride were observed during a few episodes, when this species represented up to 13% of the total submicron particulate mass, which is consistent with earlier observations of long-range transport of sea salt, going back to the ABLE-2B campaign (Talbot et al., 1990).

Deleted: Because quantification of this species still requires further analysis, the results are not shown here.

Deleted: 3

Moved down [7]: A soluble fraction of only 1.5% (1.8 ng m^{-3} Fe(III) of 120 ng m^{-3} of total Fe) was found.

Moved (insertion) [7]

but the high concentrations during the August to December period suggest substantial contributions from fossil fuel burning. Periods with aerosol compositions suggesting pristine conditions (low BC_e and sulfate, dominant organic matter) occur more as episodes at ATTO than as seasonal characteristics, similar to what is observed at the remote ZOTTO site in Siberia (Chi et al., 2013).

4.3.7 Microspectroscopic analysis of single aerosol particles

The microspectroscopic analysis of aerosol samples can be seen as a 'snapshot' of the aerosol population at a given time. In combination with the long-term aerosol measurements at the ATTO site, single particle characterization provides detailed insights into the highly variable aerosol cycling in the rain forest ecosystem. In the soft X-ray regime, STXM-NEXAFS is a powerful microscopic tool with high spectroscopic sensitivity for the light elements carbon (C), nitrogen (N), and oxygen (O) as well as a variety of other atmospherically relevant elements (e.g., K, Ca, Fe, S, and Na). The technique allows analyzing the microstructure, mixing state, and the chemical composition of individual aerosol particles. As an example, Fig. 32 displays the STXM-NEXAFS analysis of an aerosol sample with substantial anthropogenic pollution, collected at the ATTO site during the dry season. X-ray microspectroscopy reveals a substantial fraction of internally mixed particles with soot cores (strong π-bond signals) and organic coatings of variable thickness. The spectral signature of the organic coating is characteristic for secondary organic material (SOM) (Pöhlker et al., 2014). These observations underline the dominance of aged pyrogenic aerosols at the ATTO site during the dry season. During the rainy season, when biomass burning is absent and undisturbed biosphere-atmosphere interactions prevail in the region, the aerosol population is dominated by biogenic aerosol, such as primary biological aerosol particles (PBAP), biogenic SOA, and biogenic salts (Pöhlker et al., 2012). Figure 33 displays STXM elemental maps of this typical rainy season aerosol population.

As mentioned in the previous section, the biogenic background aerosol in the wet season (i.e., February to April) is episodically superimposed by transatlantic dust and smoke events. Statistical analysis of the electron microscope (EPMA) results by hierarchical clustering reveals the abundance of the various particle types observed at the ATTO tower in this season (Table 8). In order to determine

Formatted: Subscript

Deleted: 4

Deleted: 5

Deleted: 7

the sources and possible chemical interactions, particles were classified into representative groups according to their chemical composition. They are classified as "mineral" when Al, Si, O, and Ca are dominant, and also contain minor elements like K, Na, Mg, and Fe. Particles are identified as being "organic", when the concentrations of C and O in the particles are similar and when they also contain some P and S (<10 weight %). "Biogenic" particles occur in the larger size classes; they have smooth boundaries and always contain C, O, S, N, P, and K. Irregular crystallized particles with Na, Mg, S, O and C are classified as "salt" particles. Soot particles can be distinguished by their morphology, and always contain the elements C and O.

With single particle analysis, important information was obtained concerning the contribution from organic aerosol particles and the agglomeration of various types of particles. The majority of particles in the fine fraction consist of organic matter with traces of S and K. This observation corroborates that small biogenic potassium and sulfur-containing particles from primary emissions can act as seeds for the condensation of organic material (Pöhlker et al., 2012).

4.3.8 Chemical composition of secondary organic aerosol

Measurements of the organic chemical composition of the aerosol over the Amazon rainforest are rare. Levoglucosan, several mono- di- and polycarboxylic acids, as well as isoprene tracer compounds have been identified in the aerosol phase (Mayol-Bracero et al., 2002; Claeys et al., 2004; Schkolnik et al., 2005; Claeys et al., 2010), whereas the contribution of highly reactive compounds, such as monoterpenes and sesquiterpenes, to SOA in this region is still largely unknown.

The concentrations of monoterpene and sesquiterpene oxidation products in ambient aerosol collected in November 2012 at the ATTO research site are shown in Fig. 34. A median concentration of 102 ng m^{-3} was measured for the sum of terpene oxidation products in the aerosol sampled over the Amazon rain forest. As can be seen in Fig. 34, monoterpene oxidation products accounted for the major part of the terpene oxidation products. Their concentration showed a high variance during November ranging between 23 and 146 ng m^{-3}. The oxida-

Formatted: Superscript

tion products derived from the pinene skeleton (α- and ß-pinene) were most abundant in the sampled aerosols, followed by limonene oxidation products. Among the pinene derived oxidation products, MBTCA (3-methyl-1,2,3-butanetricarboxylic acid) was observed to be the most abundant individual monoterpene oxidation product, with concentrations of up to 73 ng m^{-3}, followed by pinonic acid with a maximum concentration of 46 ng m^{-3} (van Eijck, 2013). Interestingly, these concentrations are in the same range as monoterpene oxidation products measured during summertime in boreal forest environments (Vestenius et al., 2014), ecosystems which are known to strongly emit monoterpenes. However, these observations of high monoterpene product concentrations match with the high monoterpene mixing ratios measured at the same site (Yañez-Serrano et al., 2015).

The products from sesquiterpene oxidation showed much lower concentrations (Fig. 34). On average the sesquiterpene oxidation products reached about 10% of the monoterpene oxidation product concentration; however, on some days they were as high as 26% of the total monoterpene oxidation product concentration. Overall, twenty-three individual oxidation products of sesquiterpenes were identified in the aerosol collected in the Amazonian rainforest. The total concentration of these sesquiterpene oxidation products ranged from 6 to 12 ng m^{-3}. The oxidation products could be assigned to four sesquiterpene precursors: β-caryophyllene, aromadendrene, cedrene, and isolongifolene. Among them, the products from the oxidation of β-caryophyllene were the most abundant (van Eijck, 2013). Very few measurements exist of sesquiterpene oxidation product concentrations and actually none in tropical forests, which complicates a comparison. Measurements in boreal ecosystems (Vestenius et al., 2014) showed mean summertime concentrations of caryophyllinic acid (one of the β-caryophyllene oxidation products) of about 8 ng m^{-3}, which is a high concentration for a single compound compared to the concentrations measured at ATTO, where the measured concentration range of caryophyllinic acid is 0.26 – 1.38 ng m^{-3}.

In summary, the contribution of monoterpene oxidation products to SOA at ATTO is relatively high and essentially comparable with their contribution to

boreal forest SOA, whereas the contribution of sesquiterpene products is much less (about one tenth) than in boreal forest ecosystems.

5 Summary and Future Outlook

Our initial ecological studies have shown the ATTO site to be located in an area of high biodiversity, containing forest and wetland ecosystems that are representative of many regions in the central Amazon Basin. The meteorological measurements reflect rainfall, temperature, and wind conditions typical of the region, with pronounced seasonality in rainfall and airmass origins, but they also show substantial interannual variability. Early micrometeorological studies have characterized the nocturnal boundary layer and its coupling with the overlying atmosphere, the properties of turbulence structures in the boundary layer, and the formation of orographically induced gravity waves.

Continuous measurements of the carbon gases CO_2, CO, and CH_4 at five heights reveal the effects of photosynthesis and respiration on the vertical distribution of CO_2, the presence of a source of CO at the forest floor, and yet unidentified intensive and episodic sources of CH_4. Ozone, VOC, and OH reactivity measurements indicate an active photochemical cycle in the tropical boundary layer and a strong forest sink for ozone.

The Amazonian aerosol is strongly influenced by seasonal variations in airmass origins. In the rainy season, when airmasses come from the northeast across almost undisturbed rain forest, there are long periods when natural, biogenic aerosols prevail, characterized by low particle number concentrations and a very large fraction of organic matter. In spite of considerable research efforts, the mode of formation of these aerosols remains enigmatic. Nucleation and new particle formation events are almost never observed in clean air over Amazonia. The deployment of instrumentation that explores the size range at the border between gases and particles, and the measurement of species that are involved in the formation and growth of aerosol particles, such as H_2SO_4, extremely low volatility organic compounds (ELVOCs), ammonia, and amines may shed light on the processes responsible for the formation of biogenic aerosols over the tropical forest (Kulmala et al., 2014).

Deleted: A median concentration of 102 ng m^{-3} was measured for terpene oxidation products in the aerosol sampled over the Amazon rain forest. The concentration of monoterpene and sesquiterpene oxidation products in ambient aerosol collected in November 2012 is shown in Fig. 36. Monoterpene oxidation products accounted for the major part of the terpene oxidation products, whereas the sesquiterpene oxidation products showed much lower concentrations. On average the sesquiterpene oxidation products reached about 10% of the monoterpene oxidation product concentration, however, on some days they were even as high as 26% of the total monoterpene oxidation product concentration. The monoterpene oxidation products showed a high variance during November ranging between 23 and 146 ng m^{-3}, whereas the concentration of sesquiterpene oxidation products stayed quite constant around a median concentration of 8 ng m^{-3}.¶

Deleted: Conclusions

Deleted: which are

During the rainy season, the biogenic aerosol over Amazonia is overprinted periodically by episodes of intense transatlantic transport, which bring Saharan dust, smoke from fires in West Africa, Atlantic marine aerosols, and possibly pollution from fossil fuel burning in Africa, Europe, and North America to the site. In contrast, during the dry season the dominant airmass source regions lie to the east and southeast, where biomass and fossil fuel combustion result in persistent and substantial production of pollution aerosols.

Overall, our measurements at ATTO support the view that there is no longer any place on Earth that can be considered truly pristine. Even at this remote site, trace gas and aerosol concentrations show the impact of anthropogenic emissions. For long-lived species, like CO_2 and CH_4, this reflects the secular increase in concentrations as a result of global emissions. For shorter-lived trace gases and aerosols, the effects of regional sources and long range transport can be detected almost at all times, even though they may be very small during the cleanest periods.

During 2015, we expect that many measurements will be relocated from the 80-m towers to the 325-m tall tower. This will significantly enlarge the footprint of the measurements of long-lived trace gases, especially CO_2. Integration of ATTO into networks for the study of carbon cycling, such as the proposed long-term, pantropical network that assesses NPP using multiple approaches (Cleveland et al., 2015) could significantly increase the knowledge that can be gained from this site. The challenge for the future will be to maintain these measurements over the coming decades, so that they can reveal secular trends in atmospheric composition and the health of the Amazonian ecosystem.

Acknowledgements

We thank the Max Planck Society and the Instituto Nacional de Pesquisas da Amazonia for continuous support. We acknowledge the support by the German Federal Ministry of Education and Research (BMBF contract 01LB1001A) and the Brazilian Ministério da Ciência, Tecnologia e Inovação (MCTI/FINEP contract 01.11.01248.00) as well as the Amazon State University (UEA), FAPEAM, LBA/INPA and SDS/CEUC/RDS-Uatumã. Leonardo Sá thanks CNPq for his

Deleted: Also in this season

Deleted: by

Deleted: and

Deleted: D

Deleted: ,

Deleted: t

Formatted: Right: 0 cm

Productivity in Research Grant, Process 303728/2010-8. Cléo Dias-Júnior thanks CAPES for his Ph.D. grant. Maria Teresa F. Piedade thanks CNPq and FAPEAM for research grants (PELD-Project, Process 403792/2012-6). The ALS is supported by the Director, Office of Science, Office of Basic Energy Sciences, of the US Department of Energy under Contract DE-AC02-05CH11231. We thank the Helmholtz-Zentrum Berlin for the allocation of synchrotron radiation beamtime at BESSY II. We also thank M. Weigand, M. Bechtel, and A. L. D. Kilcoyne for their constant support during the beamtime sessions. We would like to especially thank all the people involved in the technical and logistical support of the ATTO project, in particular Thomas Disper, Andrew Crozier, Uwe Schulz, Steffen Schmidt, Alcides Camargo Ribeiro, Hermes Braga Xavier, Elton Mendes da Silva, Nagib Alberto de Castro Souza, Adir Vasconcelos Brandão, Amauri Rodrigues Perreira, Thiago de Lima Xavier, Josué Ferreira de Souza, Roberta Pereira de Souza, and Wallace Rabelo Costa. We acknowledge the micrometeorological group of INPA/LBA for their collaboration concerning the meteorological parameters, with special thanks to Antonio Huxley Melo Nascimento and Leonardo Ramos de Oliveira. The aerosol team thanks Isabella Hrabe de Angelis and Sachin S. Gunthe for their help with instrument maintenance and I. Lieberwirth and G. Glaßer (Max Planck Institute for Polymer Research, Mainz, Germany) for kind support with SEM imaging. We thank Tracey W. Andreae for help with copyediting the manuscript. This paper contains results of research conducted under the Technical/Scientific Cooperation Agreement between the National Institute for Amazonian Research, the State University of Amazonas, and the Max-Planck-Gesellschaft e.V.; the opinions expressed are the entire responsibility of the authors and not of the participating institutions.

Deleted: and

Deleted: the

Deleted: Antonio Huxley

Deleted: Leonardo Oliveira

Deleted: -

Deleted: -

Figure captions

Figure 1: (a) Location of the ATTO site. The main map shows the access to the site via the road and riverboat connections (background map from Google Earth). (b) Topography in the region around the ATTO site. The Balbina Reservoir is in the northwestern corner of the map.

Figure 2: Land cover and population density map of northern South America. The land cover map (GlobCover 2009, downloaded from: http://www.esa-landcover-cci.org/, 11/07/14, ESA and UCLouvain) highlights vegetated areas in green tones (deciduous forest, broadleaf forest, evergreen forest, and mixed broadleaf and needleleaf forest) and water bodies in blue tones (regularly flooded and permanently flooded areas). Populated areas (given as population density map) span a range from 1 (light red) to 1000+ (dark red) persons per km^2 (from: Gridded Population of the World, Version 3 (GPWv3) provided by the Center for International Earth Science Information Network (CIESIN), Columbia University). The ATTO site is marked by a star.

Figure 3: Back trajectory frequency plots and satellite fire maps for the ATTO site in 2014. Back trajectories (9 days) have been calculated with HYSPLIT (NOAA-ARL, GDAS1, start height 1000 m) (Draxler and Rolph, 2015). Four back trajectories have been initiated per day (0:00, 06:00, 12:00, 18:00 UTC) – frequency plots are based on monthly trajectory ensembles. Color coding of frequency plots: >10% (green), >1% (blue), >0.1% (cyan). Monthly fire map derived from GFAS (Global Fire Assimilation System) and averaged to 1 degree grid resolution (Kaiser et al., 2012).

Figure 4: Species turnover of the four inventoried forest types at the ATTO site. Turnover is expressed as Shmida & Wilson's (1985) index: SMI = (g+l) / (a+b); where g and l are gained and lost species from site 1 to site 2; a and b are the numbers of species in site 1 and site 2. TF = terra firme forest upon plateau, Terr = terra firme forest upon fluvial terrace, Camp = campinarana, and IG = seasonally flooded black-water forest (igapó).

Figure 5: Portion of camera view, contrast enhanced. Spatial and temporal crown color differences are most evident in the five driest months (July to November) when crowns present rapidly changing phenostages associated with leaf flush -- briefly deciduous pre-flush abscission, young red unexpanded leaves, or bright green recently expanded leaves.

Figure 6: Plot of bulk density (g cm^{-3}) and carbon stocks (Mg ha^{-1}) against soil depth. Pronounced differences of belowground carbon stocks between terrace and plateau occur in deeper layers (Depth > 100 cm).

Figure 7: Wind roses for (a) dry season (15 June - 30 Nov) and (b) wet season (1 Dec - 14 June) based on half-hourly averages of wind speed and direction measured at 81 m a.g.l. for the period from 18 Oct 2012 to 23 July 2014.

Figure 8: Diurnal profiles of temperature for a) wet season (March 2014) and b) dry season (September 2013). Contour plots interpolate from measurements at 0.4 m, 1.5 m, 4 m, 12 m, 26 m, 36 m, 40 m, 55 m, 73 m, and 81 m.

Deleted: .
Deleted: B
Deleted: .
Deleted: one
Formatted: Superscript
Formatted: Superscript
Deleted: 5
Deleted: 6

Figure 9: Monthly sums of precipitation at the ATTO site for the years 2012 to 2014. For comparison the data from the Manaus INMET-station (www.inmet.gov.br) ~~for the standard reference period (1961-1990) are~~ shown.

Figure 10: The dimensionless standard deviation function for a) vertical velocity $\phi_w(\zeta)$, b) virtual temperature $\phi_{\theta_v}(\zeta)$, and c) CO_2 concentration $\phi_c(\zeta)$ for the ATTO site from measurements at 39.5 m.

Figure 11: From top to bottom, the departure of the dimensionless standard deviation function, $\phi_a(\zeta)$, from its surface-layer behavior for θ_v, q, and c, respectively.

Figure 12: Upper panels: Temporal evolution of the three wind components for the night of 27 April 2012 at each of the ATTO observation levels. The lower panel shows the corresponding eddy covariance CO_2 fluxes.

Figure 13: Mean multi-resolution turbulent kinetic energy (TKE) spectra at the three observation levels.

Figure 14: Upper panel: Multi-resolution 42-m vertical velocity spectra for the night of 04 May 2012 (colors and contours), and mean wind difference between the 80-m and 42-m levels (red line, scale at the right side). Lower panel: temporal evolution of vertical velocity at the 42-m level for the same night.

Figure 15: (a) Area of approximately 900 km^2 surrounding the ATTO site. The axes represent the directions (0°, 5°, 10°, 15°, ..., 175°, 180°) from the ATTO tower. The color scale represents terrain elevation in meters above sea level. (b) Schematic with axes corresponding to (a); the black dots indicate gravity wave events induced by terrain undulations and the gray points represent gravity wave events not induced by terrain effects.

Figure 16: Coherent structures time scale of w, u, T, and q, recorded at heights of 42 m and 81 m at the ATTO site.

Figure 17: Diurnal cycle of a) CO_2 , b) CH_4, and c) CO. The CO_2 plot is computed from the measurements in January 2013, the CH_4 and CO plots from all available measurements until the end of 2014. Time is given in UT, with the first 12 hours repeated for clarity. The white vertical lines indicate the times of local sunrise (10 UT) and sunset (22 UT), respectively. Black dashed horizontal lines show the heights of the 5 inlets.

Figure 18: Examples of sporadic concurrent increases in CH_4 and CO recorded at the lowermost (4 m) inlet in 2012.

Figure 19: Statistics of monthly daytime (1700-2000 UT) 30-min measurements of CO_2 at the 80-m walk-up tower. Shown are whisker plots indicating min/max and quartiles of the monthly measurements. The white line in the box indicates the median. Brown: 4-m level, green: 38-m level, blue: 79-m level.

Figure 20: Statistics of monthly daytime (1700-2000 UT) 30-min measurements of CH_4 and CO at the 79-m level of the 80-m walk-up tower. Shown are

Deleted: 7

Deleted: of

Deleted: 8

Deleted: ,

Deleted: Figure 9: The dimensionless standard deviation function for virtual temperature, $\phi_{\theta_v}(\zeta)$, for the ATTO site from measurements at 39.5m.¶
Figure 10: The dimensionless standard deviation function for CO_2 concentration, $\phi_c(\zeta)$, for the ATTO site from measurements at 39.5m.¶

Deleted: TKE

Deleted: in the Uatumã Sustainable Development Reserve

Deleted: C

Deleted: GW

Deleted: GW

Deleted: above

Deleted: computed from the measurements in January 2013

Deleted: Figure 18: Same as Figure 17, but for CH_4 (computed by pooling all available CH_4 measurements until the end of 2014). ¶
Figure 19: Same as Figure 17, but for CO (computed by pooling all available measurements until the end of 2014). ¶

Deleted: 20

Deleted: 21

Deleted: 22

whisker plots indicating min/max and quartiles of the monthly measurements. The white line in the box indicates the median.

Figure 21: Monthly averaged daytime (1700-2000 UT) measurements of CO_2, CH_4 and CO at the 79 m level of the ATTO tower (blue line, standard deviation indicated by shading) in comparison with monthly averaged concentration measurements from Ascension Island (brown; data for 2014 are preliminary; Dlugokencky et al., 2014; Novelli and Masarie, 2014) and Cape Verde (green: Carpenter et al., 2010, updated).

Figure 22: Profiles of isoprene derived from measurements at three different heights (0.05 m, 24 m, and 79.3 m) below, within, and above the canopy,respectively, in November 2012 (transition period from dry to wet season).

Figure 23: Isoprene and total OH reactivity measurements during November 2012 at the highest point above the canopy (79 m), binned as 60 minute medians for all periods when both data were available (about 4 days). The isoprene mixing ratio scale (left axis) was set to match its contribution to the total OH reactivity (1 ppb isoprene = 2.46 s^{-1} isoprene OH reactivity), which is presented on the right axis. The upper panel shows the diel variation of temperature (measured at 81 m) and the net radiation.

Figure 24: Mean diurnal profiles of O_3 mixing ratios measured on the walk-up tower during the dry season (left panel, 15 August to 14 September 2013) and the wet season (right panel, 1 February to 3 March 2014).

Figure 25: Time series of scattering and absorption coefficients and particle number concentration (diameter > 80 nm).

Figure 26: Intercomparison of the median particle number size distributions from the SMPS, OPS, WRAS, and UHSAS instruments. Instruments were operated for 6 h using the same inlet line during clean rainy-season conditions (26 Jan 2015).

Figure 27: Median particle number (a) and volume (b) size distributions from the SMPS and OPS instruments, representative for conditions during the wet (dashed lines) and dry (solid lines) seasons. Plotted data sets comprise continuous SMPS and OPS data covering 7-day periods for wet (06-13 May 2014) and dry (13-20 Sep 2014) season conditions. Integrated number and volume concentrations for the selected wet season period: $N_{Ait,wet}$ = 141 cm^{-3}, $N_{Acc,wet}$ = 130 cm^{-3}, $N_{Total,wet}$ = 282 cm^{-3}; $V_{sub\text{-}\mu,wet}$ = 0.5 μm^3 cm^{-3}, $V_{super\text{-}\mu,wet}$ = 1.5 μm^3 cm^{-3}, $V_{Total,wet}$ = 2.0 μm^3 cm^{-3}. Integrated number and volume concentrations for the selected dry season period: $N_{Ait,dry}$ = 395 cm^{-3}, $N_{Acc,dry}$ = 967 cm^{-3}, $N_{Total,dry}$ = 1398 cm^{-3}; $V_{sub\text{-}\mu,dry}$ = 4.0 μm^3 cm^{-3}, $V_{super\text{-}\mu,dry}$ = 3.5 μm^3 cm^{-3}, $V_{Total,dry}$ = 7.5 μm^3 cm^{-3}.

Figure 28: Median particle number (a) and volume (b) size distributions from the SMPS and OPS instruments, showing the contrast between pristine wet season conditions and episodes with long-range transport influence (i.e., Saharan dust, African biomass burning, and sea salt). Wet season number and volume size spectra are taken from Fig. 27. The long-range transport size spectrum is averaged from three selected episodes in Feb and Mar

Deleted: 23

Deleted: 24

Deleted: 25

Deleted: 26

Deleted: 27

Deleted: 28

Deleted: 29

Formatted: Don't hyphenate

Deleted: -

Deleted: -

Deleted: 30

Deleted: 9

2014. Integrated number and volume concentrations for the long-range transport episodes: $N_{Ait,long}$ = 80 cm^{-3}, $N_{Acc,long}$ = 308 cm^{-3}, $N_{Total,long}$ = 409 cm^{-3}; $V_{sub-\mu,long}$ = 2.3 μm^3 cm^{-3}, $V_{super-\mu,long}$ = 12.7 μm^3 cm^{-3}, $V_{Total,long}$ = 15.0 μm^3 cm^{-3}.

Figure 29: Average number (a) and volume (b) size distributions of the total and fluorescent aerosol particles measured by WIBS. Orange lines refer to the size-resolved fraction of FBAP.

Figure 30: Time series of monthly mean aerosol mass concentrations and chemical speciation at the ATTO site, measured by ACSM from May 2014 to April 2015.

Figure 31: Average bulk elemental concentrations (in weight-percent) of PM 2.5 aerosols collected at 80 m height between 7 March and 21 April 2012.

Figure 32: STXM images and elemental maps with corresponding NEXAFS spectra of aerosol particles collected at the ATTO site during a period with anthropogenic pollution. (a) Carbon post-edge image (293 eV) of a characteristic region showing internally mixed droplet-like particles with cores (black arrows) and coatings of variable thickness (green boxes). (a) Carbon elemental map (pre-edge 280 eV, post-edge 293 eV) showing the distribution of carbonaceous material. (a) NEXAFS spectra showing high abundance of pi- (C=C) and keto (O=C) functional groups in cores. Coating reveals high abundance of carboxylic acid groups (CCOH) and weaker signals for keto and pi groups.

Figure 33: Microscopic images of aerosol particles during rainy season. (a) SEM images of representative region. (b) STXM carbon post-edge image (293 eV) and (c-f) STXM elemental maps of same region. The particle types are indicated in panel (b): primary biological aerosol particles (region i), droplet-like SOA particles (region ii), and potassium-rich biogenic salts (region iii).

Figure 34: Concentration of monoterpene and sesquiterpene oxidation products in ambient aerosol collected in November 2012 over the Amazon rain forest.

Deleted: 31

Deleted: 32

Deleted: Time series of aerosol concentration and average chemical speciation at the ATTO site, measured by ACSM during the early wet season from 1 to 31 March 2015.

Deleted: 33

Deleted: 34

Deleted: A

Deleted: B

Deleted: C

Deleted: 35

Deleted: A

Deleted: B

Deleted: C-F

Deleted: Region shows

Deleted: 36

References

Abril, G., Martinez, J. M., Artigas, L. F., Moreira-Turcq, P., Benedetti, M. F., Vidal, L., Meziane, T., Kim, J. H., Bernardes, M. C., Savoye, N., Deborde, J., Souza, E. L., Alberic, P., de Souza, M. F. L., and Roland, F., Amazon River carbon dioxide outgassing fuelled by wetlands: Nature, 505, 395-398, doi:10.1038/nature12797, 2014.

Acevedo, O. C., Costa, F. D., Oliveira, P. E. S., Puhales, F. S., Degrazia, G. A., and Roberti, D. R., The influence of submeso processes on stable boundary layer similarity relationships: J. Atmos. Sci., 71, 207-225, doi:10.1175/jas-d-13-0131.1, 2014.

Alfarra, M. R., Paulsen, D., Gysel, M., Garforth, A. A., Dommen, J., Prevot, A. S. H., Worsnop, D. R., Baltensperger, U., and Coe, H., A mass spectrometric study of secondary organic aerosols formed from the photooxidation of anthropogenic and biogenic precursors in a reaction chamber: Atmos. Chem. Phys., 6, 5279-5293, 2006.

Allan, J. D., Delia, A. E., Coe, H., Bower, K. N., Alfarra, M. R., Jimenez, J. L., Middlebrook, A. M., Drewnick, F., Onasch, T. B., Canagaratna, M. R., Jayne, J. T., and Worsnop, D. R., A generalised method for the extraction of chemically resolved mass spectra from aerodyne aerosol mass spectrometer data: J. Aerosol Sci., 35, 909-922, doi:10.1016/j.jaerosci.2004.02.007, 2004.

Anderson, T. L., Covert, D. S., Marshall, S. F., Laucks, M. L., Charlson, R. J., Waggoner, A. P., Ogren, J. A., Caldow, R., Holm, R. L., Quant, F. R., Sem, G. J., Wiedensohler, A., Ahlquist, N. A., and Bates, T. S., Performance characteristics of a high-sensitivity, three- wavelength, total scatter/backscatter nephelometer: J. Atmos. Ocean. Technol., 13, 967-986, 1996.

Anderson, T. L., and Ogren, J. A., Determining aerosol radiative properties using the TSI 3563 integrating nephelometer: Aerosol Sci. Tech., 29, 57-69, 1998.

Andreae, M. O., Berresheim, H., Bingemer, H., Jacob, D. J., Lewis, B. L., Li, S.-M., and Talbot, R. W., The atmospheric sulfur cycle over the Amazon Basin, 2. Wet Season: J. Geophys. Res., 95, 16,813-16,824, 1990.

Andreae, M. O., The Biosphere: Pilot or Passenger on Spaceship Earth?, in *Contributions to Global Change Research*, edited by D. Heinen, S. Hoch, T. Krafft, C. Moss, P. Scheidt, & A. Welschhoff, pp. 59-66, German National Committee on Global Change Research, Bonn, 2001.

Andreae, M. O., Artaxo, P., Brandão, C., Carswell, F. E., Ciccioli, P., da Costa, A. L., Culf, A. D., Esteves, J. L., Gash, J. H. C., Grace, J., Kabat, P., Lelieveld, J., Malhi, Y., Manzi, A. O., Meixner, F. X., Nobre, A. D., Nobre, C., Ruivo, M. d. L. P., Silva-Dias, M. A., Stefani, P., Valentini, R., von Jouanne, J., and Waterloo, M. J., Biogeochemical cycling of carbon, water, energy, trace gases and aerosols in Amazonia: The LBA-

2852 EUSTACH experiments: J. Geophys. Res., 107, 8066,
2853 doi:10.1029/2001JD000524, 2002.

2854 Andreae, M. O., Rosenfeld, D., Artaxo, P., Costa, A. A., Frank, G. P., Longo, K.
2855 M., and Silva-Dias, M. A. F., Smoking rain clouds over the Amazon:
2856 Science, 303, 1337-1342, 2004.

2857 Andreae, M. O., and Gelencsér, A., Black carbon or brown carbon? The nature of
2858 light-absorbing carbonaceous aerosols: Atmos. Chem. Phys., 6, 3131-
2859 3148, 2006.

2860 Andreae, M. O., Correlation between cloud condensation nuclei concentration and
2861 aerosol optical thickness in remote and polluted regions: Atmos. Chem.
2862 Phys., 9, 543–556, 2009.

2863 Andreae, M. O., Artaxo, P., Beck, V., M. Bela, Gerbig, C., Longo, K., Munger, J.
2864 W., Wiedemann, K. T., and Wofsy, S. C., Carbon monoxide and related
2865 trace gases and aerosols over the Amazon Basin during the wet and dry
2866 seasons: Atmos. Chem. Phys., 12, 6041–6065, 2012.

2867 Andrews, A. E., Kofler, J. D., Trudeau, M. E., Williams, J. C., Neff, D. H.,
2868 Masarie, K. A., Chao, D. Y., Kitzis, D. R., Novelli, P. C., Zhao, C. L.,
2869 Dlugokencky, E. J., Lang, P. M., Crotwell, M. J., Fischer, M. L., Parker,
2870 M. J., Lee, J. T., Baumann, D. D., Desai, A. R., Stanier, C. O., De Wekker,
2871 S. F. J., Wolfe, D. E., Munger, J. W., and Tans, P. P., CO_2, CO, and CH_4
2872 measurements from tall towers in the NOAA Earth System Research
2873 Laboratory's Global Greenhouse Gas Reference Network: instrumentation,
2874 uncertainty analysis, and recommendations for future high-accuracy
2875 greenhouse gas monitoring efforts: Atmos. Meas. Tech., 7, 647-687,
2876 doi:10.5194/amt-7-647-2014, 2014.

2877 Ansmann, A., Baars, H., Tesche, M., Muller, D., Althausen, D., Engelmann, R.,
2878 Pauliquevis, T., and Artaxo, P., Dust and smoke transport from Africa to
2879 South America: Lidar profiling over Cape Verde and the Amazon
2880 rainforest: Geophys. Res. Lett., 36, L11802, doi:10.1029/2009GL037923,
2881 2009.

2882 Artaxo, P., Martins, J. V., Yamasoe, M. A., Procópio, A. S., Pauliquevis, T. M.,
2883 Andreae, M. O., Guyon, P., Gatti, L. V., and Leal, A. M. C., Physical and
2884 chemical properties of aerosols in the wet and dry season in Rondonia,
2885 Amazonia: J. Geophys. Res., 107, 8081, doi:10.1029/2001JD000666,
2886 2002.

2887 Artaxo, P., Rizzo, L. V., Brito, J. F., Barbosa, H. M. J., Arana, A., Sena, E. T.,
2888 Cirino, G. G., Bastos, W., Martin, S. T., and Andreae, M. O., Atmospheric
2889 aerosols in Amazonia and land use change: from natural biogenic to
2890 biomass burning conditions: Faraday Discussions, 165, 203-235,
2891 doi:10.1039/C3FD00052D, 2013.

2892 Baars, H., Ansmann, A., Althausen, D., Engelmann, R., Artaxo, P., Pauliquevis,
2893 T., and Souza, R., Further evidence for significant smoke transport from
2894 Africa to Amazonia: Geophys. Res. Lett., 38, L20802,
2895 doi:10.1029/2011GL049200, 2011.

2896 Baccini, A., Goetz, S. J., Walker, W. S., Laporte, N. T., Sun, M., Sulla-Menashe,
2897 D., Hackler, J., Beck, P. S. A., Dubayah, R., Friedl, M. A., Samanta, S.,
2898 and Houghton, R. A., Estimated carbon dioxide emissions from tropical
2899 deforestation improved by carbon-density maps: Nature Climate Change,
2900 2, 182-185, doi:10.1038/nclimate1354, 2012.

2901 Bakwin, P. S., Tans, P. P., Hurst, D. F., and Zhao, C. L., Measurements of carbon
2902 dioxide on very tall towers: results of the NOAA/CMDL program: Tellus
2903 Series B-Chemical and Physical Meteorology, 50, 401-415, 1998.

2904 Balch, J. K., Drought and fire change sink to source: Nature, 506, 41-42,
2905 doi:10.1038/506041a, 2014.

2906 Beck, V., Chen, H., Gerbig, C., Bergamaschi, P., Bruhwiler, L., Houweling, S.,
2907 Röckmann, T., Kolle, O., Steinbach, J., Koch, T., Sapart, C. J., van der
2908 Veen, C., Frankenberg, C., Andreae, M. O., Artaxo, P., Longo, K. M., and
2909 Wofsy, S. C., Methane airborne measurements and comparison to global
2910 models during BARCA: J. Geophys. Res., 117, D15310,
2911 doi:10.1029/2011JD017345, 2012.

2912 Ben-Ami, Y., Koren, I., Rudich, Y., Artaxo, P., Martin, S. T., and Andreae, M. O.,
2913 Transport of Saharan dust from the Bodélé Depression to the Amazon
2914 Basin: a case study: Atmos. Chem. Phys., 10, 7533–7544, 2010.

2915 Ben-Ami, Y., Koren, I., Altaratz, O., Kostinski, A., and Lehahn, Y., Discernible
2916 rhythm in the spatio/temporal distributions of transatlantic dust: Atmos.
2917 Chem. Phys., 12, 2253-2262, doi:10.5194/acp-12-2253-2012, 2012.

2918 Betts, A. K., Fisch, G., von Randow, C., Dias, M. A. F. S., Cohen, J. C. P., da
2919 Silva, R., and Fitzjarrald, D. R., The Amazonian boundary layer and
2920 mesoscale circulations, in *Amazonia and Global Change*, edited by M.
2921 Keller, M. Bustamante, J. Gash, & P. Dias, pp. 163-181, American
2922 Geophysical Union, Washington, DC, 2009.

2923 Bevan, S. L., North, P. R. J., Grey, W. M. F., Los, S. O., and Plummer, S. E.,
2924 Impact of atmospheric aerosol from biomass burning on Amazon dry-
2925 season drought: J. Geophys. Res., 114, D09204,
2926 doi:10.1029/2008jd011112, 2009.

2927 Bond, T. C., Bussemer, M., Wehner, B., Keller, S., Charlson, R. J., and
2928 Heintzenberg, J., Light absorption by primary particle emissions from a
2929 lignite burning plant: Environ. Sci. Technol., 33, 3887-3891, 1999.

2930 Bond, T. C., Covert, D. S., and Müller, T., Truncation and angular-scattering
2931 corrections for absorbing aerosol in the TSI 3563 nephelometer: Aerosol
2932 Sci. Tech., 43, 866-871, doi:10.1080/02786820902998373, 2009.

2933 Bou-Zeid, E., Meneveau, C., and Parlange, M. B., Large-eddy simulation of
2934 neutral atmospheric boundary layer flow over heterogeneous surfaces:
2935 Blending height and effective surface roughness: Water Resources
2936 Research, 40, W02505, doi:10.1029/2003wr002475, 2004.

2937 Brienen, R. J. W., Phillips, O. L., Feldpausch, T. R., Gloor, E., Baker, T. R.,
2938 Lloyd, J., Lopez-Gonzalez, G., Monteagudo-Mendoza, A., Malhi, Y.,
2939 Lewis, S. L., Vasquez Martinez, R., Alexiades, M., Alvarez Davila, E.,

Alvarez-Loayza, P., Andrade, A., Aragao, L. E. O. C., Araujo-Murakami, A., Arets, E. J. M. M., Arroyo, L., Aymard C., G. A., Banki, O. S., Baraloto, C., Barroso, J., Bonal, D., Boot, R. G. A., Camargo, J. L. C., Castilho, C. V., Chama, V., Chao, K. J., Chave, J., Comiskey, J. A., Cornejo Valverde, F., da Costa, L., de Oliveira, E. A., Di Fiore, A., Erwin, T. L., Fauset, S., Forsthofer, M., Galbraith, D. R., Grahame, E. S., Groot, N., Herault, B., Higuchi, N., Honorio Coronado, E. N., Keeling, H., Killeen, T. J., Laurance, W. F., Laurance, S., Licona, J., Magnussen, W. E., Marimon, B. S., Marimon-Junior, B. H., Mendoza, C., Neill, D. A., Nogueira, E. M., Nunez, P., Pallqui Camacho, N. C., Parada, A., Pardo-Molina, G., Peacock, J., Pena-Claros, M., Pickavance, G. C., Pitman, N. C. A., Poorter, L., Prieto, A., Quesada, C. A., Ramirez, F., Ramirez-Angulo, H., Restrepo, Z., Roopsind, A., Rudas, A., Salomao, R. P., Schwarz, M., Silva, N., Silva-Espejo, J. E., Silveira, M., Stropp, J., Talbot, J., ter Steege, H., Teran-Aguilar, J., Terborgh, J., Thomas-Caesar, R., Toledo, M., Torello-Raventos, M., Umetsu, R. K., van der Heijden, G. M. F., van der Hout, P., Guimaraes Vieira, I. C., Vieira, S. A., Vilanova, E., Vos, V. A., and Zagt, R. J., Long-term decline of the Amazon carbon sink: Nature, 519, 344-348, doi:10.1038/nature14283, 2015.

Brown, A. R., and Wood, N., Properties and parameterization of the stable boundary layer over moderate topography: J. Atmos. Sci., 60, 2797-2808, 2003.

Bueno, P. A., Havey, D. K., Mulholland, G. W., Hodges, J. T., Gillis, K. A., Dickerson, R. R., and Zachariah, M. R., Photoacoustic measurements of amplification of the absorption cross section for coated soot aerosols: Aerosol Sci. Tech., 45, 1217-1230, doi:10.1080/02786826.2011.587477, 2011.

Cai, Y., Montague, D. C., Mooiweer-Bryan, W., and Deshler, T., Performance characteristics of the ultra high sensitivity aerosol spectrometer for particles between 55 and 800 nm: Laboratory and field studies: J. Aerosol Sci., 39, 759-769, doi:10.1016/j.jaerosci.2008.04.007, 2008.

Campanharo, A., Ramos, F. M., Macau, E. E. N., Rosa, R. R., Bolzan, M. J. A., and Sa, L. D. A., Searching chaos and coherent structures in the atmospheric turbulence above the Amazon forest: Phil. Trans. R. Soc. A, 366, 579-589, doi:10.1098/rsta.2007.2118, 2008.

Camponogara, G., Silva Dias, M. A. F., and Carrió, G. G., Relationship between Amazon biomass burning aerosols and rainfall over the La Plata Basin: Atmos. Chem. Phys., 14, 4397-4407, doi:10.5194/acp-14-4397-2014, 2014.

Cancelli, D. M., Dias, N. L., and Chamecki, M., Dimensionless criteria for the production-dissipation equilibrium of scalar fluctuations and their implications for scalar similarity: Water Resources Research, 48, W10522, doi:10.1029/2012wr012127, 2012.

Carpenter, L. J., Fleming, Z. L., Read, K. A., Lee, J. D., Moller, S. J., Hopkins, J. R., Purvis, R. M., Lewis, A. C., Mueller, K., Heinold, B., Herrmann, H., Fomba, K. W., van Pinxteren, D., Mueller, C., Tegen, I., Wiedensohler,

2986 A., Mueller, T., Niedermeier, N., Achterberg, E. P., Patey, M. D.,
2987 Kozlova, E. A., Heimann, M., Heard, D. E., Plane, J. M. C., Mahajan, A.,
2988 Oetjen, H., Ingham, T., Stone, D., Whalley, L. K., Evans, M. J., Pilling, M.
2989 J., Leigh, R. J., Monks, P. S., Karunaharan, A., Vaughan, S., Arnold, S. R.,
2990 Tschritter, J., Poehler, D., Friess, U., Holla, R., Mendes, L. M., Lopez, H.,
2991 Faria, B., Manning, A. J., and Wallace, D. W. R., Seasonal characteristics
2992 of tropical marine boundary layer air measured at the Cape Verde
2993 Atmospheric Observatory: J. Atmos. Chem., 67, 87-140,
2994 doi:10.1007/s10874-011-9206-1, 2010.

2995 Carswell, F. E., Costa, A. L., Palheta, M., Malhi, Y., Meir, P., Costa, J. d. P. R.,
2996 Ruivo, M. d. L., Leal, L. d. S. M., Costa, J. M. N., Clement, R. J., and
2997 Grace, J., Seasonality in CO_2 and H_2O flux at an eastern Amazonian rain
2998 forest: J. Geophys. Res., 107, LBA 43-1-LBA 43-15,
2999 doi:10.1029/2000JD000284, 2002.

3000 Cava, D., Giostra, U., Siqueira, M., and Katul, G., Organised motion and radiative
3001 perturbations in the nocturnal canopy sublayer above an even-aged pine
3002 forest: Boundary-Layer Meteorology, 112, 129-157,
3003 doi:10.1023/B:BOUN.0000020160.28184.a0, 2004.

3004 Chambers, J. Q., Negron-Juarez, R. I., Marra, D. M., Di Vittorio, A., Tews, J.,
3005 Roberts, D., Ribeiro, G. H. P. M., Trumbore, S. E., and Higuchi, N., The
3006 steady-state mosaic of disturbance and succession across an old-growth
3007 Central Amazon forest landscape: Proc. Natl. Acad. Sci., 110, 3949-3954,
3008 doi:10.1073/pnas.1202894110, 2013.

3009 Chauvel, A., Lucas, Y., and Boulet, R., On the genesis of the soil mantle of the
3010 region of Manaus, Central Amazonia, Brazil: Experientia, 43, 234-241,
3011 doi:10.1007/bf01945546, 1987.

3012 Chave, J., Andalo, C., Brown, S., Cairns, M. A., Chambers, J. Q., Eamus, D.,
3013 Folster, H., Fromard, F., Higuchi, N., Kira, T., Lescure, J. P., Nelson, B.
3014 W., Ogawa, H., Puig, H., Riera, B., and Yamakura, T., Tree allometry and
3015 improved estimation of carbon stocks and balance in tropical forests:
3016 Oecologia, 145, 87-99, doi:10.1007/s00442-005-0100-x, 2005.

3017 Chave, J., Coomes, D., Jansen, S., Lewis, S. L., Swenson, N. G., and Zanne, A.
3018 E., Towards a worldwide wood economics spectrum: Ecology Letters, 12,
3019 351-366, doi:10.1111/j.1461-0248.2009.01285.x, 2009.

3020 Chen, B., Coops, N. C., Fu, D., Margolis, H. A., Amiro, B. D., Black, T. A.,
3021 Arain, M. A., Barr, A. G., Bourque, C. P. A., Flanagan, L. B., Lafleur, P.
3022 M., McCaughey, J. H., and Wofsy, S. C., Characterizing spatial
3023 representativeness of flux tower eddy-covariance measurements across the
3024 Canadian Carbon Program Network using remote sensing and footprint
3025 analysis: Remote Sens. Environ., 124, 742-755,
3026 doi:http://dx.doi.org/10.1016/j.rse.2012.06.007, 2012.

3027 Chen, Q., Farmer, D. K., Schneider, J., Zorn, S. R., Heald, C. L., Karl, T.,
3028 Guenther, A., Allan, J. D., Robinson, N., Coe, H., Kimmel, J. R.,
3029 Pauliquevis, T., Borrmann, S., Pöschl, U., Andreae, M. O., Artaxo, P.,
3030 Jimenez, J. L., and Martin, S. T., Mass spectral characterization of

submicron biogenic organic particles in the Amazon Basin: Geophys. Res. Lett., 36, L20806, doi:10.1029/2009GL039880, 2009.

Chen, Q., Farmer, D. K., Rizzo, L. V., Pauliquevis, T., Kuwata, M., Karl, T. G., Guenther, A., Allan, J. D., Coe, H., Andreae, M. O., Pöschl, U., Jimenez, J. L., Artaxo, P., and Martin, S. T., Submicron particle mass concentrations and sources in the Amazonian wet season (AMAZE-08): Atmos. Chem. Phys., 15, 3687-3701, doi:10.5194/acp-15-3687-2015, 2015.

Chi, X., Winderlich, J., Mayer, J.-C., Panov, A. V., Heimann, M., Birmili, W., Heintzenberg, J., Cheng, Y., and Andreae, M. O., Long-term measurements of aerosols and carbon monoxide at the ZOTTO tall tower to characterize polluted and pristine air in the Siberian Taiga: Atmos. Chem. Phys., 13, 12,271-12,298, doi:10.5194/acp-13-12271-2013, 2013.

Chimonas, G., and Nappo, C. J., Wave drag in the planetary boundary layer over complex terrain: Boundary-Layer Meteorology, 47, 217-232, doi:10.1007/bf00122330, 1989.

Chou, W. W., Wofsy, S. C., Harriss, R. C., Lin, J. C., Gerbig, C., and Sachse, G. W., Net fluxes of CO_2 in Amazonia derived from aircraft observations: J. Geophys. Res., 107, 4614, doi:10.1029/2001JD001295, 2002.

Ciais, P., Sabine, C., Bala, G., Bopp, L., Brovkin, V., Canadell, J., Chhabra, A., DeFries, R., Galloway, J., Heimann, M., Jones, C., Quéré, C. L., Myneni, R. B., Piao, S., and Thornton, P., Chapter 6: Carbon and Other Biogeochemical Cycles, in *IPCC, Climate Change 2013: The Physical Science Basis. Contribution of Working Group I to the Fifth Assessment Report of the Intergovernmental Panel on Climate Change*, edited by T. F. Stocker, D. Qin, G.-K. Plattner, M. Tignor, S. K. Allen, J. Boschung, A. Nauels, Y. Xia, V. Bex, & P. M. Midgley, pp. 465-570, Cambridge University Press, Cambridge, United Kingdom and New York, NY, USA, 2013.

Cintra, B. B. L., Schietti, J., Emillio, T., Martins, D., Moulatlet, G., Souza, P., Levis, C., Quesada, C. A., and Schöngart, J., Soil physical restrictions and hydrology regulate stand age and wood biomass turnover rates of Purus-Madeira interfluvial wetlands in Amazonia: Biogeosciences, 10, 7759-7774, doi:10.5194/bg-10-7759-2013, 2013.

Cirino, G. G., Souza, R. A. F., Adams, D. K., and Artaxo, P., The effect of atmospheric aerosol particles and clouds on net ecosystem exchange in the Amazon: Atmos. Chem. Phys., 14, 6523-6543, doi:10.5194/acp-14-6523-2014, 2014.

Claeys, M., Graham, B., Vas, G., Wang, W., Vermeylen, R., Pashynska, V., Cafmeyer, J., Guyon, P., Andreae, M. O., Artaxo, P., and Maenhaut, W., Formation of secondary organic aerosols through photooxidation of isoprene: Science, 303, 1173-1176, 2004.

Claeys, M., Kourtchev, I., Pashynska, V., Vas, G., Vermeylen, R., Wang, W., Cafmeyer, J., Chi, X., Artaxo, P., Andreae, M. O., and Maenhaut, W., Polar organic marker compounds in atmospheric aerosols during the LBA-

SMOCC 2002 biomass burning experiment in Rondônia, Brazil: sources and source processes, time series, diel variations and size distributions: Atmos. Chem. Phys., 10, 9319–9331, doi:10.5194/acp-10-9319-2010, 2010.

Clark, D. A., Brown, S., Kicklighter, D. W., Chambers, J. Q., Thomlinson, J. R., Ni, J., and Holland, E. A., Net primary production in tropical forests: An evaluation and synthesis of existing field data: Ecol. Appl., 11, 371-384, doi:10.2307/3060895, 2001.

Cleveland, C. C., Taylor, P., Chadwick, K. D., Dahlin, K., Doughty, C. E., Malhi, Y., Smith, W. K., Sullivan, B. W., Wieder, W. R., and Townsend, A. R., A comparison of plot-based satellite and Earth system model estimates of tropical forest net primary production: Global Biogeochemical Cycles, 29, 626-644, doi:10.1002/2014GB005022, 2015.

Coe, M. T., Costa, M. H., and Soares-Filhoc, B. S., The influence of historical and potential future deforestation on the stream flow of the Amazon River - Land surface processes and atmospheric feedbacks: Journal of Hydrology, 369, 165-174, doi:10.1016/j.jhydrol.2009.02.043, 2009.

Collineau, S., and Brunet, Y., Detection of turbulent coherent motions in a forest canopy. 2. Time-scales and conditional averages: Boundary-Layer Meteorology, 66, 49-73, doi:10.1007/bf00705459, 1993.

Costa, F. D., Acevedo, O. C., Mombach, J. C. M., and Degrazia, G. A., A simplified model for intermittent turbulence in the nocturnal boundary layer: J. Atmos. Sci., 68, 1714-1729, doi:10.1175/2011jas3655.1, 2011.

Crutzen, P. J., The role of the tropics in atmospheric chemistry, in *The Geophysiology of Amazonia*, edited by R. E. Dickinson, pp. 107-130, John Wiley, New York, 1987.

Crutzen, P. J., and Andreae, M. O., Biomass burning in the tropics: Impact on atmospheric chemistry and biogeochemical cycles: Science, 250, 1669-1678, 1990.

D'Amelio, M. T. S., Gatti, L. V., Miller, J. B., and Tans, P., Regional N_2O fluxes in Amazonia derived from aircraft vertical profiles: Atmos. Chem. Phys., 9, 8785-8797, 2009.

Da Silva, J. M. C., Rylands, A. B., and Da Fonseca, G. A. B., The fate of the Amazonian areas of endemism: Conservation Biology, 19, 689-694, doi:10.1111/j.1523-1739.2005.00705.x, 2005.

Davidson, E. A., de Araujo, A. C., Artaxo, P., Balch, J. K., Brown, I. F., Bustamante, M. M. C., Coe, M. T., DeFries, R. S., Keller, M., Longo, M., Munger, J. W., Schroeder, W., Soares, B. S., Souza, C. M., and Wofsy, S. C., The Amazon basin in transition: Nature, 481, 321-328, doi:10.1038/nature10717, 2012.

de Araujo, A. C., Kruijt, B., Nobre, A. D., Dolman, A. J., Waterloo, M. J., Moors, E. J., and de Souza, J. S., Nocturnal accumulation of CO(2) underneath a tropical forest canopy along a topographical gradient: Ecol. Appl., 18, 1406-1419, 2008.

de Araujo, A. C., Dolman, A. J., Waterloo, M. J., Gash, J. H. C., Kruijt, B., Zanchi, F. B., de Lange, J. M. E., Stoevelaar, R., Manzi, A. O., Nobre, A. D., Lootens, R. N., and Backer, J., The spatial variability of CO_2 storage and the interpretation of eddy covariance fluxes in central Amazonia: Agricultural and Forest Meteorology, 150, 226-237, doi:10.1016/j.agrformet.2009.11.005, 2010.

de Araújo, A. C., Nobre, A. D., Kruijt, B., Elbers, J. A., Dallarosa, R., Stefani, P., von Randow, C., Manzi, A. O., Culf, A. D., Gash, J. H. C., Valentini, R., and Kabat, P., Comparative measurements of carbon dioxide fluxes from two nearby towers in a central Amazonian rainforest: The Manaus LBA site: J. Geophys. Res., 107, 8090, doi:10.1029/2001JD000676, 2002.

Dias Júnior, C. Q., Sa, L. D. A., Pacheco, V. B., and de Souza, C. M., Coherent structures detected in the unstable atmospheric surface layer above the Amazon forest: Journal of Wind Engineering and Industrial Aerodynamics, 115, 1-8, doi:10.1016/j.jweia.2012.12.019, 2013.

Dias, N. L., Hong, J., Leclerc, M. Y., Black, T. A., Nesic, Z., and Krishnan, P., A simple method of estimating scalar fluxes over forests: Boundary-Layer Meteorology, 132, 401-414, doi:10.1007/s10546-009-9408-0, 2009.

Dlugokencky, E. J., Lang, P. M., Masarie, K. A., Crotwell, A. M., and Crotwell, M. J., Atmospheric Carbon Dioxide Dry Air Mole Fractions from the NOAA ESRL Carbon Cycle Cooperative Global Air Sampling Network, 1968-2013, Version: 2014-06-27, ftp://aftp.cmdl.noaa.gov/data/trace_gases/co2/flask/surface/ (2014).

Doughty, C. E., and Goulden, M. L., Seasonal patterns of tropical forest leaf area index and CO2 exchange: Journal of Geophysical Research-Biogeosciences, 113, G00B06, doi:10.1029/2007jg000590, 2008.

Doughty, C. E., Metcalfe, D. B., Girardin, C. A. J., Amezquita, F. F., Cabrera, D. G., Huasco, W. H., Silva-Espejo, J. E., Araujo-Murakami, A., da Costa, M. C., Rocha, W., Feldpausch, T. R., Mendoza, A. L. M., da Costa, A. C. L., Meir, P., Phillips, O. L., and Malhi, Y., Drought impact on forest carbon dynamics and fluxes in Amazonia: Nature, 519, 78-82, doi:10.1038/nature14213, 2015.

Draxler, R. R., and Rolph, G. D., HYSPLIT (HYbrid Single-Particle Lagrangian Integrated Trajectory) Model access via NOAA ARL READY Website (http://www.arl.noaa.gov/ready/hysplit4.html). NOAA Air Resources Laboratory, Silver Spring, MD. (2015).

Drüe, C., and Heinemann, G., Characteristics of intermittent turbulence in the upper stable boundary layer over Greenland: Boundary-Layer Meteorology, 124, 361-381, doi:10.1007/s10546-007-9175-8, 2007.

Dupont, S., and Brunet, Y., Coherent structures in canopy edge flow: a large-eddy simulation study: Journal of Fluid Mechanics, 630, 93-128, doi:10.1017/s0022112009006739, 2009.

Durden, D. J., Nappo, C. J., Leclerc, M. Y., Duarte, H. F., Zhang, G., Parker, M. J., and Kurzeja, R. J., On the impact of wave-like disturbances on turbulent fluxes and turbulence statistics in nighttime conditions: a case

study: Biogeosciences, 10, 8433-8443, doi:10.5194/bg-10-8433-2013, 2013.

Eck, T. F., Holben, B. N., Reid, J. S., O'Neill, N. T., Schafer, J. S., Dubovik, O., Smirnov, A., Yamasoe, M. A., and Artaxo, P., High aerosol optical depth biomass burning events: A comparison of optical properties for different source regions: Geophys. Res. Lett., 30, 2035, doi:10.1029/2003GL017861, 2003.

Elbert, W., Weber, B., Burrows, S., Steinkamp, J., Büdel, B., Andreae, M. O., and Pöschl, U., Contribution of cryptogamic covers to the global cycles of carbon and nitrogen: Nature Geoscience, 5, 459-462, 2012.

Emilio, T., Quesada, C. A., Costa, F. R. C., Magnusson, W. E., Schietti, J., Feldpausch, T. R., Brienen, R. J. W., Baker, T. R., Chave, J., Alvarez, E., Araujo, A., Banki, O., Castilho, C. V., Honorio C., E. N., Killeen, T. J., Malhi, Y., Mendoza, E. M. O., Monteagudo, A., Neill, D., Alexander Parada, G., Pena-Cruz, A., Ramirez-Angulo, H., Schwarz, M., Silveira, M., ter Steege, H., Terborgh, J. W., Thomas, R., Torres-Lezama, A., Vilanova, E., and Phillips, O. L., Soil physical conditions limit palm and tree basal area in Amazonian forests: Plant Ecology & Diversity, 7, 215-229, doi:10.1080/17550874.2013.772257, 2014.

Farge, M., Wavelet transforms and their applications to turbulence: Annual Review of Fluid Mechanics, 24, 395-457, doi:10.1146/annurev.fluid.24.1.395, 1992.

Feldpausch, T. R., Lloyd, J., Lewis, S. L., Brienen, R. J. W., Gloor, M., Mendoza, A. M., Lopez-Gonzalez, G., Banin, L., Abu Salim, K., Affum-Baffoe, K., Alexiades, M., Almeida, S., Amaral, I., Andrade, A., Aragao, L., Murakami, A. A., Arets, E., Arroyo, L., Aymard, G. A., Baker, T. R., Banki, O. S., Berry, N. J., Cardozo, N., Chave, J., Comiskey, J. A., Alvarez, E., de Oliveira, A., Di Fiore, A., Djagbletey, G., Domingues, T. F., Erwin, T. L., Fearnside, P. M., Franca, M. B., Freitas, M. A., Higuchi, N., Honorio, E., Iida, Y., Jimenez, E., Kassim, A. R., Killeen, T. J., Laurance, W. F., Lovett, J. C., Malhi, Y., Marimon, B. S., Marimon, B. H., Lenza, E., Marshall, A. R., Mendoza, C., Metcalfe, D. J., Mitchard, E. T. A., Neill, D. A., Nelson, B. W., Nilus, R., Nogueira, E. M., Parada, A., Peh, K. S. H., Cruz, A. P., Penuela, M. C., Pitman, N. C. A., Prieto, A., Quesada, C. A., Ramirez, F., Ramirez-Angulo, H., Reitsma, J. M., Rudas, A., Saiz, G., Salomao, R. P., Schwarz, M., Silva, N., Silva-Espejo, J. E., Silveira, M., Sonke, B., Stropp, J., Taedoumg, H. E., Tan, S., ter Steege, H., Terborgh, J., Torello-Raventos, M., van der Heijden, G. M. F., Vasquez, R., Vilanova, E., Vos, V. A., White, L., Willcock, S., Woell, H., and Phillips, O. L., Tree height integrated into pantropical forest biomass estimates: Biogeosciences, 9, 3381-3403, doi:10.5194/bg-9-3381-2012, 2012.

Fernandes, M. J. S., Índice de erosividade da chuva média anual para Manaus/AM de 1981 a 2010: Revista Geonorte, 10, 46- 49, 2014.

Figueroa, S. N., and Nobre, C. A., Precipitions distribution over Central and Western Tropical South America: Climanálise, 5, 36-44, 1990.

Fisch, G., Tota, J., Machado, L. A. T., Dias, M., Lyra, R. F. D., Nobre, C. A., Dolman, A. J., and Gash, J. H. C., The convective boundary layer over pasture and forest in Amazonia: Theoretical and Applied Climatology, 78, 47-59, 2004.

Fitzjarrald, D. R., and Moore, K. E., Mechanisms of nocturnal exchange between the rain-forest and the atmosphere: J. Geophys. Res., 95, 16,839-16,850, doi:10.1029/JD095iD10p16839, 1990.

Foken, T., Meixner, F. X., Falge, E., Zetzsch, C., Serafimovich, A., Bargsten, A., Behrendt, T., Biermann, T., Breuninger, C., Dix, S., Gerken, T., Hunner, M., Lehmann-Pape, L., Hens, K., Jocher, G., Kesselmeier, J., Luers, J., Mayer, J. C., Moravek, A., Plake, D., Riederer, M., Rutz, F., Scheibe, M., Siebicke, L., Sorgel, M., Staudt, K., Trebs, I., Tsokankunku, A., Welling, M., Wolff, V., and Zhu, Z., Coupling processes and exchange of energy and reactive and non-reactive trace gases at a forest site - results of the EGER experiment: Atmos. Chem. Phys., 12, 1923-1950, doi:10.5194/acp-12-1923-2012, 2012.

Follath, R., Schmidt, J. S., Weigand, M., and Fauth, K., The Xray microscopy beamline UE46-PGM2 at BESSY: AIP Conf. Proc., 1234, 323-326, doi:10.1063/1.3463201, 2010.

Formenti, P., Andreae, M. O., Lange, L., Roberts, G., Cafmeyer, J., Rajta, I., Maenhaut, W., Holben, B. N., Artaxo, P., and Lelieveld, J., Saharan dust in Brazil and Suriname during the Large-Scale Biosphere-Atmosphere Experiment in Amazonia (LBA)- Cooperative LBA Regional Experiment (CLAIRE) in March 1998: J. Geophys. Res., 106, 14,919-14,934, 2001.

Fraser, B., Carving up the Amazon: Nature, 509, 418-419, 2014.

Freud, E., Rosenfeld, D., Andreae, M. O., Costa, A. A., and Artaxo, P., Robust relations between CCN and the vertical evolution of cloud drop size distribution in deep convective clouds: Atmos. Chem. Phys., 8, 1661–1675, 2008.

Fry, J. L., Kiendler-Scharr, A., Rollins, A. W., Wooldridge, P. J., Brown, S. S., Fuchs, H., Dube, W., Mensah, A., dal Maso, M., Tillmann, R., Dorn, H. P., Brauers, T., and Cohen, R. C., Organic nitrate and secondary organic aerosol yield from NO_3 oxidation of beta-pinene evaluated using a gas-phase kinetics/aerosol partitioning model: Atmos. Chem. Phys., 9, 1431-1449, 2009.

Galvão, L. S., dos Santos, J. R., Roberts, D. A., Breunig, F. M., Toomey, M., and de Moura, Y. M., On intra-annual EVI variability in the dry season of tropical forest: A case study with MODIS and hyperspectral data: Remote Sens. Environ., 115, 2350-2359, doi:10.1016/j.rse.2011.04.035, 2011.

Gao, W., and Li, B. L., Wavelet analysis of coherent structures at the atmosphere forest interface: J. Appl. Meteor., 32, 1717-1725, 1993.

Gatti, L. V., Miller, J. B., D'Amelio, M. T. S., Martinewski, A., Basso, L. S., Gloor, M. E., Wofsy, S., and Tans, P., Vertical profiles of CO_2 above eastern Amazonia suggest a net carbon flux to the atmosphere and balanced biosphere between 2000 and 2009: Tellus Series B-Chemical and

Physical Meteorology, 62, 581-594, doi:10.1111/j.1600-0889.2010.00484.x, 2010.

Gatti, L. V., Gloor, M., Miller, J. B., Doughty, C. E., Malhi, Y., Domingues, L. G., Basso, L. S., Martinewski, A., Correia, C. S. C., Borges, V. F., Freitas, S., Braz, R., Anderson, L. O., Rocha, H., Grace, J., Phillips, O. L., and Lloyd, J., Drought sensitivity of Amazonian carbon balance revealed by atmospheric measurements: Nature, 506, 76-80, doi:10.1038/nature12957, 2014.

Gee, G. W., and Bauder, J. W., Particle size analysis, in *Methods in Soil Analysis, Part 1. Physical and Mineralogical Methods*, edited by A. Klute, pp. 383-409, American Society of Agronomy and Soil Science Society of America, Madison, Wisconsin, USA, 1986.

Gilardoni, S., Vignati, E., Marmer, E., Cavalli, F., Belis, C., Gianelle, V., Loureiro, A., and Artaxo, P., Sources of carbonaceous aerosol in the Amazon basin: Atmos. Chem. Phys., 11, 2747-2764, 2011.

Gimeno, L., Stohl, A., Trigo, R. M., Dominguez, F., Yoshimura, K., Yu, L. S., Drumond, A., Duran-Quesada, A. M., and Nieto, R., Oceanic and terrestrial sources of continental precipitation: Rev. Geophys., 50, RG4003, doi:10.1029/2012rg000389, 2012.

Gloor, M., Fan, S. M., Pacala, S., and Sarmiento, J., Optimal sampling of the atmosphere for purpose of inverse modeling: A model study: Global Biogeochemical Cycles, 14, 407-428, 2000.

Gloor, M., Bakwin, P., Hurst, D., Lock, L., Draxler, R., and Tans, P., What is the concentration footprint of a tall tower?: J. Geophys. Res., 106, 17,831-17,840, 2001.

Gloor, M., Gatti, L., Brienen, R., Feldpausch, T. R., Phillips, O. L., Miller, J., Ometto, J. P., Rocha, H., Baker, T., de Jong, B., Houghton, R. A., Malhi, Y., Aragao, L., Guyot, J. L., Zhao, K., Jackson, R., Peylin, P., Sitch, S., Poulter, B., Lomas, M., Zaehle, S., Huntingford, C., Levy, P., and Lloyd, J., The carbon balance of South America: a review of the status, decadal trends and main determinants: Biogeosciences, 9, 5407-5430, doi:10.5194/bg-9-5407-2012, 2012.

Gloor, M., Brienen, R. J. W., Galbraith, D., Feldpausch, T. R., Schöngart, J., Guyot, J. L., Espinoza, J. C., Lloyd, J., and Phillips, O. L., Intensification of the Amazon hydrological cycle over the last two decades: Geophys. Res. Lett., 40, 1729-1733, doi:10.1002/grl.50377, 2013.

Goulding, M., Barthem, R. B., and Duenas, R., The Smithsonian Atlas of the Amazon. Washington, D.C.: Smithsonian Books, 253 p, 2003.

Grace, J., Lloyd, J., McIntyre, J., Miranda, A. C., Meir, P., Miranda, H. S., Nobre, C., Moncrieff, J., Massheder, J., Malhi, Y., Wright, I., and Gash, J., Carbon dioxide uptake by an undisturbed tropical rain forest in southwest Amazonia, 1992 to 1993: Science, 270, 778-780, 1995.

Greco, S., Swap, R., Garstang, M., Ulanski, S., Shipman, M., Harriss, R. C., Talbot, R., Andreae, M. O., and Artaxo, P., Rainfall and surface kinematic

conditions over Central Amazonia during ABLE 2B: J. Geophys. Res., 95, 17,001-17,014, 1990.

Gunthe, S. S., King, S. M., Rose, D., Chen, Q., Roldin, P., Farmer, D. K., Jimenez, J. L., Artaxo, P., Andreae, M. O., Martin, S. T., and Pöschl, U., Cloud condensation nuclei in pristine tropical rainforest air of Amazonia: size-resolved measurements and modeling of atmospheric aerosol composition and CCN activity: Atmos. Chem. Phys., 9, 7551–7575, 2009.

Hari, P., Andreae, M. O., Kabat, P., and Kulmala, M., A comprehensive network of measuring stations to monitor climate change: Boreal Environment Research, 14, 442-446, 2009.

Healy, D. A., Huffman, J. A., O'Connor, D. J., Pöhlker, C., Pöschl, U., and Sodeau, J. R., Ambient measurements of biological aerosol particles near Killarney, Ireland: a comparison between real-time fluorescence and microscopy techniques: Atmos. Chem. Phys., 14, 8055-8069, doi:10.5194/acp-14-8055-2014, 2014.

Heiblum, R. H., Koren, I., and Feingold, G., On the link between Amazonian forest properties and shallow cumulus cloud fields: Atmos. Chem. Phys., 14, 6063-6074, doi:10.5194/acp-14-6063-2014, 2014.

Heimann, M., Schulze, E.-D., Winderlich, J., Andreae, M. O., Chi, X., Gerbig, C., Kolle, O., Kübler, K., Lavric, J., Mikhailov, E., Panov, A., Park, S., Rödenbeck, C., and Skorochod, A., The Zotino Tall Tower Observatory (ZOTTO): Quantifying large scale biogeochemical changes in Central Siberia: Nova Acta Leopoldina, 117, 51-64, 2014.

Hoch, S. W., Calanca, P., Philipona, R., and Ohmura, A., Year-round observation of longwave radiative flux divergence in Greenland: Journal of Applied Meteorology and Climatology, 46, 1469-1479, doi:10.1175/jam2542.1, 2007.

Hoorn, C., Wesselingh, F. P., ter Steege, H., Bermudez, M. A., Mora, A., Sevink, J., Sanmartin, I., Sanchez-Meseguer, A., Anderson, C. L., Figueiredo, J. P., Jaramillo, C., Riff, D., Negri, F. R., Hooghiemstra, H., Lundberg, J., Stadler, T., Sarkinen, T., and Antonelli, A., Amazonia through time: Andean uplift, climate change, landscape evolution, and biodiversity: Science, 330, 927-931, doi:10.1126/science.1194585, 2010.

Huete, A. R., Didan, K., Shimabukuro, Y. E., Ratana, P., Saleska, S. R., Hutyra, L. R., Yang, W. Z., Nemani, R. R., and Myneni, R., Amazon rainforests green-up with sunlight in dry season: Geophys. Res. Lett., 33, L06405, doi:10.1029/2005GL025583, 2006.

Huffman, J. A., Sinha, B., Garland, R. M., Snee-Pollmann, A., Gunthe, S. S., Artaxo, P., Martin, S. T., Andreae, M. O., and Pöschl, U., Size distributions and temporal variations of biological aerosol particles in the Amazon rainforest characterized by microscopy and real-time UV-APS fluorescence techniques during AMAZE-08: Atmos. Chem. Phys., 12, 11,997–12,019, 2012.

Hussain, A. K. M. F., Coherent structures and turbulence: Journal of Fluid Mechanics, 173, 303-356, doi:10.1017/s0022112086001192, 1986.

IDESAM, Plano de Gestão da Reserva de Desenvolvimento Sustentável do Uatumã. Versão para consulta pública. Instituto de Conservação e Desenvolvimento Sustentável do Amazonas, Manaus. (2009).

IUSS (International Union of Soil Science) Working Group WRB, World reference base for soil resources 2006: A framework for international classification, correlation and communication, World Soil Resources Report 103. FAO, Rome, 145 p. (2006).

Jacob, D. J., and Wofsy, S. C., Budgets of reactive nitrogen, hydrocarbons, and ozone over the Amazon forest during the wet season: J. Geophys. Res., 95, 16,737-16,754, 1990.

Kaiser, J. W., Heil, A., Andreae, M. O., Benedetti, A., Chubarova, N., Jones, L., Morcrette, J.-J., Razinger, M., Schultz, M. G., Suttie, M., and van der Werf, G. R., Biomass burning emissions estimated with a global fire assimilation system based on observations of fire radiative power: Biogeosciences, 9, 527-554, doi:10.5194/bg-9-527-2012, 2012.

Kaye, P. H., Stanley, W. R., Hirst, E., Foot, E. V., Baxter, K. L., and Barrington, S. J., Single particle multichannel bio-aerosol fluorescence sensor: Optics Express, 13, 3583-3593, doi:10.1364/opex.13.003583, 2005.

Keller, M., Bustamante, M., Gash, J., and Dias, P., Amazonia and Global Change. Washington, DC: American Geophysical Union, 565 p, 2009.

Kesselmeier, J., Kuhn, U., Rottenberger, S., Biesenthal, T., Wolf, A., Schebeske, G., Andreae, M. O., Ciccioli, P., Brancaleoni, E., Frattoni, M., Oliva, S. T., Botelho, M. L., Silva, C. M. A., and Tavares, T. M., Concentrations and species composition of atmospheric volatile organic compounds (VOCs) as observed during the wet and dry season in Rondonia (Amazonia): J. Geophys. Res., 107, 8053, doi:10.1029/2000JD000267, 2002.

Kilcoyne, A. L. D., Tyliszczak, T., Steele, W. F., Fakra, S., Hitchcock, P., Franck, K., Anderson, E., Harteneck, B., Rightor, E. G., Mitchell, G. E., Hitchcock, A. P., Yang, L., Warwick, T., and Ade, H., Interferometer-controlled scanning transmission X-ray microscopes at the Advanced Light Source: Journal of Synchrotron Radiation, 10, 125-136, doi:10.1107/s0909049502017739, 2003.

Kirchhoff, V. W. J. H., Setzer, A. W., and Pereira, M. C., Biomass burning in Amazonia: Seasonal effects on atmospheric O_3 and CO: Geophys. Res. Lett., 16, 469-472, 1989.

Kirchhoff, V. W. J. H., daSilva, I. M. O., and Browell, E. V., Ozone measurements in Amazonia: Dry season versus wet season: J. Geophys. Res., 95, 16,913-16,926, 1990.

Krusche, N., and Oliveira, A. P., Characterization of coherent structures in the atmospheric surface layer: Boundary-Layer Meteorology, 110, 191-211, doi:10.1023/a:1026096805679, 2004.

Kuhn, U., Ganzeveld, L., Thielmann, A., Dindorf, T., Welling, M., Sciare, J., Roberts, G., Meixner, F. X., Kesselmeier, J., Lelieveld, J., Ciccioli, P.,

3389 Lloyd, J., Trentmann, J., Artaxo, P., and Andreae, M. O., Impact of
3390 Manaus City on the Amazon Green Ocean atmosphere: Ozone production,
3391 precursor sensitivity and aerosol load: Atmos. Chem. Phys., 10, 9251–
3392 9282, 2010.

3393 Kulmala, M., Petäjä, T., Ehn, M., Thornton, J., Sipilä, M., Worsnop, D. R., and
3394 Kerminen, V. M., Chemistry of atmospheric nucleation: On the recent
3395 advances on precursor characterization and atmospheric cluster
3396 composition in connection with atmospheric new particle formation:
3397 Annu. Rev. Phys. Chem., 65, 21-37, doi:10.1146/annurev-physchem-
3398 040412-110014, 2014.

3399 Lapola, D. M., Martinelli, L. A., Peres, C. A., Ometto, J. P. H. B., Ferreira, M. E.,
3400 Nobre, C. A., Aguiar, A. P. D., Bustamante, M. M. C., Cardoso, M. F.,
3401 Costa, M. H., Joly, C. A., Leite, C. C., Moutinho, P., Sampaio, G.,
3402 Strassburg, B. B. N., and Vieira, I. C. G., Pervasive transition of the
3403 Brazilian land-use system: Nature Clim. Change, 4, 27-35,
3404 doi:10.1038/nclimate2056, 2014.

3405 Lawrence, D., and Vandecar, K., Effects of tropical deforestation on climate and
3406 agriculture: Nature Clim. Change, 5, 27-36, doi:10.1038/nclimate2430,
3407 2015.

3408 Le Quéré, C., Moriarty, R., Andrew, R. M., Peters, G. P., Ciais, P., Friedlingstein,
3409 P., Jones, S. D., Sitch, S., Tans, P., Arneth, A., Boden, T. A., Bopp, L.,
3410 Bozec, Y., Canadell, J. G., Chevallier, F., Cosca, C. E., Harris, I.,
3411 Hoppema, M., Houghton, R. A., House, J. I., Jain, A., Johannessen, T.,
3412 Kato, E., Keeling, R. F., Kitidis, V., Klein Goldewijk, K., Koven, C.,
3413 Landa, C. S., Landschützer, P., Lenton, A., Lima, I. D., Marland, G.,
3414 Mathis, J. T., Metzl, N., Nojiri, Y., Olsen, A., Ono, T., Peters, W., Pfeil,
3415 B., Poulter, B., Raupach, M. R., Regnier, P., Rödenbeck, C., Saito, S.,
3416 Salisbury, J. E., Schuster, U., Schwinger, J., Séférian, R., Segschneider, J.,
3417 Steinhoff, T., Stocker, B. D., Sutton, A. J., Takahashi, T., Tilbrook, B.,
3418 van der Werf, G. R., Viovy, N., Wang, Y. P., Wanninkhof, R., Wiltshire,
3419 A., and Zeng, N., Global carbon budget 2014: Earth Syst. Sci. Data
3420 Discuss., 7, 521-610, doi:10.5194/essdd-7-521-2014, 2014.

3421 Lelieveld, J., Butler, T. M., Crowley, J. N., Dillon, T. J., Fischer, H., Ganzeveld,
3422 L., Harder, H., Lawrence, M. G., Martinez, M., Taraborrelli, D., and
3423 Williams, J., Atmospheric oxidation capacity sustained by a tropical
3424 forest: Nature, 452, 737-740, doi:10.1038/nature06870, 2008.

3425 Levin, E. J. T., Prenni, A. J., Palm, B. B., Day, D. A., Campuzano-Jost, P.,
3426 Winkler, P. M., Kreidenweis, S. M., DeMott, P. J., Jimenez, J. L., and
3427 Smith, J. N., Size-resolved aerosol composition and its link to
3428 hygroscopicity at a forested site in Colorado: Atmos. Chem. Phys., 14,
3429 2657-2667, doi:10.5194/acp-14-2657-2014, 2014.

3430 Li, D., and Bou-Zeid, E., Coherent Structures and the Dissimilarity of Turbulent
3431 Transport of Momentum and Scalars in the Unstable Atmospheric Surface
3432 Layer: Boundary-Layer Meteorology, 140, 243-262, doi:10.1007/s10546-
3433 011-9613-5, 2011.

Lin, J. C., Matsui, T., Pielke, R. A., Sr., and Kummerow, C., Effects of biomass burning-derived aerosols on precipitation and clouds in the Amazon basin: a satellite-based empirical study: J. Geophys. Res., 111, D19204, doi:10.1029/2005JD006884, 2006.

Lindinger, W., Hansel, A., and Jordan, A., Proton-transfer-reaction mass spectrometry (PTR-MS): on-line monitoring of volatile organic compounds at pptv levels: Chemical Society Reviews, 27, 347-354, 1998.

Liptzin, D., and Silver, W. L., Effects of carbon additions on iron reduction and phosphorus availability in a humid tropical forest soil: Soil Biology & Biochemistry 41, 1696-1702, 2009.

Lloyd, J., Kolle, O., Fritsch, H., de Freitas, S. R., Silva Dias, M. A. F., Artaxo, P., Nobre, A. D., de Araújo, A. C., Kruijt, B., Sogacheva, L., Fisch, G., Thielmann, A., Kuhn, U., and Andreae, M. O., An airborne regional carbon balance for Central Amazonia: Biogeosciences, 4, 759-768, 2007.

Lohou, F., Druilhet, A., Campistron, B., Redelspergers, J. L., and Said, F., Numerical study of the impact of coherent structures on vertical transfers in the atmospheric boundary layer: Boundary-Layer Meteorology, 97, 361-383, doi:10.1023/a:1002641728075, 2000.

Lu, C. H., and Fitzjarrald, D. R., Seasonal and diurnal variations of coherent structures over a deciduous forest: Boundary-Layer Meteorology, 69, 43-69, doi:10.1007/bf00713294, 1994.

Mahrt, L., Stratified atmospheric boundary layers: Boundary-Layer Meteorology, 90, 375-396, doi:10.1023/a:1001765727956, 1999.

Mahrt, L., Characteristics of submeso winds in the stable boundary layer: Boundary-Layer Meteorology, 130, 1-14, doi:10.1007/s10546-008-9336-4, 2009.

Malhi, Y., and Wright, J., Spatial patterns and recent trends in the climate of tropical rainforest regions: Philosophical Transactions of the Royal Society of London Series B-Biological Sciences, 359, 311-329, doi:10.1098/rstb.2003.1433, 2004.

Malhi, Y., Wood, D., Baker, T. R., Wright, J., Phillips, O. L., Cochrane, T., Meir, P., Chave, J., Almeida, S., Arroyo, L., Higuchi, N., Killeen, T. J., Laurance, S. G., Laurance, W. F., Lewis, S. L., Monteagudo, A., Neill, D. A., Vargas, P. N., Pitman, N. C. A., Quesada, C. A., Salomao, R., Silva, J. N. M., Lezama, A. T., Terborgh, J., Martinez, R. V., and Vinceti, B., The regional variation of aboveground live biomass in old-growth Amazonian forests: Global Change Biology, 12, 1107-1138, doi:10.1111/j.1365-2486.2006.01120.x, 2006.

Martin, S. T., Andreae, M. O., Althausen, D., Artaxo, P., Baars, H., Borrmann, S., Chen, Q., Farmer, D. K., Guenther, A., Gunthe, S., Jimenez, J. L., Karl, T., Longo, K., Manzi, A., Pauliquevis, T., Petters, M., Prenni, A., Pöschl, U., Rizzo, L. V., Schneider, J., Smith, J. N., Swietlicki, E., Tota, J., Wang, J., Wiedensohler, A., and Zorn, S. R., An overview of the Amazonian Aerosol Characterization Experiment 2008 (AMAZE-08): Atmos. Chem. Phys., 10, 11,415–11,438, 2010a.

Martin, S. T., Andreae, M. O., Artaxo, P., Baumgardner, D., Chen, Q., Goldstein, A. H., Guenther, A., Heald, C. L., Mayol-Bracero, O. L., McMurry, P. H., Pauliquevis, T., Pöschl, U., Prather, K. A., Roberts, G. C., Saleska, S. R., Dias, M. A. S., Spracklen, D., Swietlicki, E., and Trebs, I., Sources and properties of Amazonian aerosol particles: Rev. Geophys., 48, RG2002, doi:10.1029/2008RG000280, 2010b.

Martinez, M., Harder, H., Kubistin, D., Rudolf, M., Bozem, H., Eerdekens, G., Fischer, H., Klupfel, T., Gurk, C., Konigstedt, R., Parchatka, U., Schiller, C. L., Stickler, A., Williams, J., and Lelieveld, J., Hydroxyl radicals in the tropical troposphere over the Suriname rainforest: airborne measurements: Atmos. Chem. Phys., 10, 3759-3773, 2010.

Martins, D. L., Schietti, J., Feldpausch, T. R., Luizao, F. J., Phillips, O. L., Andrade, A., Castilho, C. V., Laurance, S. G., Oliveira, A., Amaral, I. L., Toledo, J. J., Lugli, L. F., Purri Veiga Pinto, J. L., Oblitas Mendoza, E. M., and Quesada, C. A., Soil-induced impacts on forest structure drive coarse woody debris stocks across central Amazonia: Plant Ecology & Diversity, 8, 229-241, doi:10.1080/17550874.2013.879942, 2015.

Martins, J. A., Dias, M., and Goncalves, F. L. T., Impact of biomass burning aerosols on precipitation in the Amazon: A modeling case study: J. Geophys. Res., 114, D02207, doi:10.1029/2007jd009587, 2009.

Mayol-Bracero, O. L., Gabriel, R., Andreae, M. O., Kirchstetter, T. W., Novakov, T., Ogren, J., Sheridan, P., and Streets, D. G., Carbonaceous aerosols over the Indian Ocean during the Indian Ocean Experiment (INDOEX): Chemical characterization, optical properties and probable sources: J. Geophys. Res., 107, 8030, doi:10.1029/2000JD000039, 2002.

McMeeking, G. R., Fortner, E., Onasch, T. B., Taylor, J. W., Flynn, M., Coe, H., and Kreidenweis, S. M., Impacts of nonrefractory material on light absorption by aerosols emitted from biomass burning: J. Geophys. Res., 119, 12,272–12,286, doi:10.1002/2014JD021750, 2014.

McNaughton, K. G., and Brunet, Y., Townsend's hypothesis, coherent structures and Monin-Obukhov similarity: Boundary-Layer Meteorology, 102, 161-175, doi:10.1023/a:1013171312407, 2002.

Miller, J. B., Gatti, L. V., d'Amelio, M. T. S., Crotwell, A. M., Dlugokencky, E. J., Bakwin, P., Artaxo, P., and Tans, P. P., Airborne measurements indicate large methane emissions from the eastern Amazon basin: Geophys. Res. Lett., 34, L10809, doi:10.1029/2006GL029213, 2007.

Mölder, M., Grelle, A., Lindroth, A., and Halldin, S., Flux-profile relationships over a boreal forest - roughness sublayer corrections: Agricultural and Forest Meteorology, 98/99, 645-658, doi:10.1016/s0168-1923(99)00131-8, 1999.

Moosmüller, H., Chakrabarty, R. K., Ehlers, K. M., and Arnott, W. P., Absorption Angstrom coefficient, brown carbon, and aerosols: basic concepts, bulk matter, and spherical particles: Atmos. Chem. Phys., 11, 1217-1225, doi:10.5194/acp-11-1217-2011, 2011.

Morton, D. C., Nagol, J., Carabajal, C. C., Rosette, J., Palace, M., Cook, B. D., Vermote, E. F., Harding, D. J., and North, P. R. J., Amazon forests maintain consistent canopy structure and greenness during the dry season: Nature, 506, 221-224, doi:10.1038/nature13006, 2014.

Nappo, C. J., Sporadic breakdowns of stability in the PBL over simple and complex terrain: Boundary-Layer Meteorology, 54, 69-87, doi:10.1007/bf00119413, 1991.

Nappo, C. J., An Introduction to Atmospheric Gravity Waves. Amsterdam: Academic Press, 276 p, 2002.

Nelson, D. W., and Sommers, L. E., Total carbon and total nitrogen, in *Methods of Soil Analysis: Part 3 - Chemical Methods*, edited by D. L. Sparks, pp. 961-1010, American Society of Agronomy and Soil Science Society of America, Madison, Wisconsin, USA, 1996.

Nepstad, D., McGrath, D., Stickler, C., Alencar, A., Azevedo, A., Swette, B., Bezerra, T., DiGiano, M., Shimada, J., Seroa da Motta, R., Armijo, E., Castello, L., Brando, P., Hansen, M. C., McGrath-Horn, M., Carvalho, O., and Hess, L., Slowing Amazon deforestation through public policy and interventions in beef and soy supply chains: Science, 344, 1118-1123, doi:10.1126/science.1248525, 2014.

Ng, N. L., Herndon, S. C., Trimborn, A., Canagaratna, M. R., Croteau, P. L., Onasch, T. B., Sueper, D., Worsnop, D. R., Zhang, Q., Sun, Y. L., and Jayne, J. T., An Aerosol Chemical Speciation Monitor (ACSM) for Routine Monitoring of the Composition and Mass Concentrations of Ambient Aerosol: Aerosol Sci. Tech., 45, 780-794, doi:10.1080/02786826.2011.560211, 2011.

Nobre, C. A., and Borma, L. D., 'Tipping points' for the Amazon forest: Curr. Opin. Environ. Sust., 1, 28-36, doi:10.1016/j.cosust.2009.07.003, 2009.

Nobre, C. A., Obregón, G. O., Marengo, J. A., Fu, R., and Poveda, G., Characteristics of Amazonian climate: Main Features, in *Amazonia and Global Change*, edited by M. Keller, M. Bustamante, J. Gash, & P. Dias, pp. 149-162, American Geophysical Union, Washington, DC, 2009.

Nölscher, A. C., Williams, J., Sinha, V., Custer, T., Song, W., Johnson, A. M., Axinte, R., Bozem, H., Fischer, H., Pouvesle, N., Phillips, G., Crowley, J. N., Rantala, P., Rinne, J., Kulmala, M., Gonzales, D., Valverde-Canossa, J., Vogel, A., Hoffmann, T., Ouwersloot, H. G., de Arellano, J. V. G., and Lelieveld, J., Summertime total OH reactivity measurements from boreal forest during HUMPPA-COPEC 2010: Atmos. Chem. Phys., 12, 8257-8270, doi:10.5194/acp-12-8257-2012, 2012.

Nölscher, A. C., Butler, T., Auld, J., Veres, P., Muñoz, A., Taraborrelli, D., Vereecken, L., Lelieveld, J., and Williams, J., Using total OH reactivity to assess isoprene photooxidation via measurement and model: Atmospheric Environment, 89, 453-463, doi:10.1016/j.atmosenv.2014.02.024, 2014.

Novelli, P. C., and Masarie, K. A., Atmospheric Carbon Monoxide Dry Air Mole Fractions from the NOAA ESRL Carbon Cycle Cooperative Global Air

Sampling Network, 1988-2013, Version: 2014-07-02, ftp://aftp.cmdl.noaa.gov/data/trace_gases/co/flask/surface/ (2014).

Oliveira, P. E. S., Acevedo, O. C., Moraes, O. L. L., Zimermann, H. R., and Teichrieb, C., Nocturnal intermittent coupling between the interior of a pine forest and the air above it: Boundary-Layer Meteorology, 146, 45-64, doi:10.1007/s10546-012-9756-z, 2013.

Oliveira, P. H. F., Artaxo, P., Pires, C., De Lucca, S., Procopio, A., Holben, B., Schafer, J., Cardoso, L. F., Wofsy, S. C., and Rocha, H. R., The effects of biomass burning aerosols and clouds on the CO_2 flux in Amazonia: Tellus, 59B, 338-349, doi:10.1111/j.1600-0889.2007.00270.x, 2007.

Pacifico, F., Folberth, G. A., Sitch, S., Haywood, J. M., Rizzo, L. V., Malavelle, F. F., and Artaxo, P., Biomass burning related ozone damage on vegetation over the Amazon forest: a model sensitivity study: Atmos. Chem. Phys., 15, 2791-2804, doi:10.5194/acp-15-2791-2015, 2015.

Pan, Y. D., Birdsey, R. A., Fang, J. Y., Houghton, R., Kauppi, P. E., Kurz, W. A., Phillips, O. L., Shvidenko, A., Lewis, S. L., Canadell, J. G., Ciais, P., Jackson, R. B., Pacala, S. W., McGuire, A. D., Piao, S. L., Rautiainen, A., Sitch, S., and Hayes, D., A large and persistent carbon sink in the World's forests: Science, 333, 988-993, doi:10.1126/science.1201609, 2011.

Patton, E. G. (1997). *Large-Eddy Simulation of Turbulent Flow Above and Within a Plant Canopy*, University of California at Davis, 132 p.

Paw U, K. T., Brunet, Y., Collineau, S., Shaw, R. H., Maitani, T., Qiu, J., and Hipps, L., On coherent structures in turbulence above and within agricultural plant canopies: Agricultural and Forest Meteorology, 61, 55-68, 1992.

Pella, E., Elemental organic analysis. 2. State of the art: American Laboratory, 22, 28-32, 1990.

Phillips, O. L., Aragao, L., Lewis, S. L., Fisher, J. B., Lloyd, J., Lopez-Gonzalez, G., Malhi, Y., Monteagudo, A., Peacock, J., Quesada, C. A., van der Heijden, G., Almeida, S., Amaral, I., Arroyo, L., Aymard, G., Baker, T. R., Banki, O., Blanc, L., Bonal, D., Brando, P., Chave, J., de Oliveira, A. C. A., Cardozo, N. D., Czimczik, C. I., Feldpausch, T. R., Freitas, M. A., Gloor, E., Higuchi, N., Jimenez, E., Lloyd, G., Meir, P., Mendoza, C., Morel, A., Neill, D. A., Nepstad, D., Patino, S., Penuela, M. C., Prieto, A., Ramirez, F., Schwarz, M., Silva, J., Silveira, M., Thomas, A. S., ter Steege, H., Stropp, J., Vasquez, R., Zelazowski, P., Davila, E. A., Andelman, S., Andrade, A., Chao, K. J., Erwin, T., Di Fiore, A., Honorio, E., Keeling, H., Killeen, T. J., Laurance, W. F., Cruz, A. P., Pitman, N. C. A., Vargas, P. N., Ramirez-Angulo, H., Rudas, A., Salamao, R., Silva, N., Terborgh, J., and Torres-Lezama, A., Drought sensitivity of the Amazon rainforest: Science, 323, 1344-1347, doi:10.1126/science.1164033, 2009.

Pleysier, J. L., and Juo, A. S. R., A single-extraction method using silver-thiourea for measuring exchangeable cations and effective CEC in soils with variable charges: Soil Science, 129, 205-211, 1980.

Pöhlker, C., Wiedemann, K., Sinha, B., Shiraiwa, M., Gunthe, S., Smith, M., Su, H., Artaxo, P., Chen, Q., Cheng, Y., Elbert, W., Gilles, M. K., Kilcoyne, A. L. D., Moffet, R. C., Weigand, M., Martin, S. T., Pöschl, U., and Andreae, M. O., Biogenic potassium salt particles as seeds for secondary organic aerosol in the Amazon: Science, 337, 1075-1078, 2012.

Pöhlker, C., Saturno, J., Krüger, M. L., Förster, J.-D., Weigand, M., Wiedemann, K. T., Bechtel, M., Artaxo, P., and Andreae, M. O., Efflorescence upon humidification? X-ray microspectroscopic in-situ observation of changes in aerosol microstructure and phase state upon hydration: Geophys. Res. Lett., 41, 3681-3689, doi:10.1002/2014GL059409, 2014.

Pöschl, U., Martin, S. T., Sinha, B., Chen, Q., Gunthe, S. S., Huffman, J. A., Borrmann, S., Farmer, D. K., Garland, R. M., Helas, G., Jimenez, J. L., King, S. M., Manzi, A., Mikhailov, E., Pauliquevis, T., Petters, M. D., Prenni, A. J., Roldin, P., Rose, D., Schneider, J., Su, H., Zorn, S. R., Artaxo, P., and Andreae, M. O., Rainforest aerosols as biogenic nuclei of clouds and precipitation in the Amazon: Science, 329, 1513-1516, 2010.

Poulter, B., Aragao, L., Heyder, U., Gumpenberger, M., Heinke, J., Langerwisch, F., Rammig, A., Thonicke, K., and Cramer, W., Net biome production of the Amazon Basin in the 21st century: Global Change Biology, 16, 2062-2075, doi:10.1111/j.1365-2486.2009.02064.x, 2010.

Prospero, J. M., Glaccum, R. A., and Nees, R. T., Atmospheric transport of soil dust from Africa to South America: Nature, 289, 570-572, 1981.

Quesada, C. A., Lloyd, J., Schwarz, M., Patino, S., Baker, T. R., Czimczik, C., Fyllas, N. M., Martinelli, L., Nardoto, G. B., Schmerler, J., Santos, A. J. B., Hodnett, M. G., Herrera, R., Luizao, F. J., Arneth, A., Lloyd, G., Dezzeo, N., Hilke, I., Kuhlmann, I., Raessler, M., Brand, W. A., Geilmann, H., Moraes Filho, J. O., Carvalho, F. P., Araujo Filho, R. N., Chaves, J. E., Cruz Junior, O. F., Pimentel, T. P., and Paiva, R., Variations in chemical and physical properties of Amazon forest soils in relation to their genesis: Biogeosciences, 7, 1515-1541, doi:10.5194/bg-7-1515-2010, 2010.

Quesada, C. A., Phillips, O. L., Schwarz, M., Czimczik, C. I., Baker, T. R., Patino, S., Fyllas, N. M., Hodnett, M. G., Herrera, R., Almeida, S., Alvarez Davila, E., Arneth, A., Arroyo, L., Chao, K. J., Dezzeo, N., Erwin, T., di Fiore, A., Higuchi, N., Honorio Coronado, E., Jimenez, E. M., Killeen, T., Lezama, A. T., Lloyd, G., Lopez-Gonzalez, G., Luizao, F. J., Malhi, Y., Monteagudo, A., Neill, D. A., Nunez Vargas, P., Paiva, R., Peacock, J., Penuela, M. C., Pena Cruz, A., Pitman, N., Priante Filho, N., Prieto, A., Ramirez, H., Rudas, A., Salomao, R., Santos, A. J. B., Schmerler, J., Silva, N., Silveira, M., Vasquez, R., Vieira, I., Terborgh, J., and Lloyd, J., Basin-wide variations in Amazon forest structure and function are mediated by both soils and climate: Biogeosciences, 9, 2203-2246, doi:10.5194/bg-9-2203-2012, 2012.

Rammig, A., Jupp, T., Thonicke, K., Tietjen, B., Heinke, J., Ostberg, S., Lucht, W., Cramer, W., and Cox, P., Estimating the risk of Amazonian forest

dieback: New Phytologist, 187, 694-706, doi:10.1111/j.1469-8137.2010.03318.x, 2010.

Ramos, F. M., Bolzan, M. J. A., Sa, L. D. A., and Rosa, R. R., Atmospheric turbulence within and above an Amazon forest: Physica D - Nonlinear Phenomena, 193, 278-291, doi:10.1016/j.physd.2004.01.026, 2004.

Raupach, M. R., Finnigan, J. J., and Brunet, Y., Coherent eddies and turbulence in vegetation canopies: The mixing-layer analogy: Boundary-Layer Meteorology, 78, 351-382, doi:10.1007/bf00120941, 1996.

Restrepo-Coupe, N., da Rocha, H. R., Hutyra, L. R., da Araujo, A. C., Borma, L. S., Christoffersen, B., Cabral, O. M. R., de Camargo, P. B., Cardoso, F. L., Lola da Costa, A. C., Fitzjarrald, D. R., Goulden, M. L., Kruijt, B., Maia, J. M. F., Malhi, Y. S., Manzi, A. O., Miller, S. D., Nobre, A. D., von Randow, C., Abreu Sa, L. D., Sakai, R. K., Tota, J., Wofsy, S. C., Zanchi, F. B., and Saleska, S. R., What drives the seasonality of photosynthesis across the Amazon basin? A cross-site analysis of eddy flux tower measurements from the Brasil flux network: Agricultural and Forest Meteorology, 182, 128-144, doi:10.1016/j.agrformet.2013.04.031, 2013.

Richardson, A. D., Jenkins, J. P., Braswell, B. H., Hollinger, D. Y., Ollinger, S. V., and Smith, M.-L., Use of digital webcam images to track spring green-up in a deciduous broadleaf forest: Oecologia, 152, 323-334, doi:10.1007/s00442-006-0657-z, 2007.

Richey, J. E., Melack, J. M., Aufdenkampe, A. K., Ballester, V. M., and Hess, L. L., Outgassing from Amazonian rivers and wetlands as a large tropical source of atmospheric CO2: Nature, 416, 617-620, 2002.

Rissler, J., Swietlicki, E., Zhou, J., Roberts, G., Andreae, M. O., Gatti, L. V., and Artaxo, P., Physical properties of the sub-micrometer aerosol over the Amazon rain forest during the wet-to-dry season transition - Comparison of modeled and measured CCN concentrations: Atmos. Chem. Phys., 4, 2119-2143, 2004.

Rizzo, L. V., Correia, A. L., Artaxo, P., Procópio, A. S., and Andreae, M. O., Spectral dependence of aerosol light absorption over the Amazon Basin: Atmos. Chem. Phys., 11, 8899-8912, 2011.

Rizzo, L. V., Artaxo, P., Müller, T., Wiedensohler, A., Paixão, M., Cirino, G. G., Arana, A., Swietlicki, E., Roldin, P., Fors, E. O., Wiedemann, K. T., Leal, L. S. M., and Kulmala, M., Long term measurements of aerosol optical properties at a primary forest site in Amazonia: Atmos. Chem. Phys., 13, 2391-2413, doi:10.5194/acp-13-2391-2013, 2013.

Ro, C.-U., Osan, J., Szaloki, I., De Hoog, J., Worobiec, A., and Van Grieken, R. A., Monte Carlo program for quantitative electron-induced X-ray analysis of individual particles: Anal. Chem., 75, 851-859, 2003.

Roberts, G. C., Andreae, M. O., Zhou, J., and Artaxo, P., Cloud condensation nuclei in the Amazon Basin: "Marine" conditions over a continent?: Geophys. Res. Lett., 28, 2807-2810, 2001.

3699 Rocha, R. P., Morales, C. A., Cuadra, S. V., and Ambrizzi, T., Precipitation
3700 diurnal cycle and summer climatology assessment over South America:
3701 An evaluation of Regional Climate Model version 3 simulations: J.
3702 Geophys. Res., 114, D10108, doi:10.1029/2008JD010212, 2009.

3703 Rose, D., Gunthe, S. S., Mikhailov, E., Frank, G. P., Dusek, U., Andreae, M. O.,
3704 and Pöschl, U., Calibration and measurement uncertainties of a
3705 continuous-flow cloud condensation nuclei counter (DMT-CCNC): CCN
3706 activation of ammonium sulfate and sodium chloride aerosol particles in
3707 theory and experiment: Atmos. Chem. Phys., 8, 1153-1179, 2008.

3708 Rose, D., Gunthe, S. S., Su, H., Garland, R. M., Yang, H., Berghof, M., Cheng, Y.
3709 F., Wehner, B., Achtert, P., Nowak, A., Wiedensohler, A., Takegawa, N.,
3710 Kondo, Y., Hu, M., Zhang, Y., Andreae, M. O., and Pöschl, U., Cloud
3711 condensation nuclei in polluted air and biomass burning smoke near the
3712 mega-city Guangzhou, China - Part 2: Size-resolved aerosol chemical
3713 composition, diurnal cycles, and externally mixed CCN-inactive soot
3714 particles: Atmos. Chem. Phys., 11, 2817-2836, 2011.

3715 Rummel, U., Ammann, C., Kirkman, G. A., Moura, M. A. L., Foken, T., Andreae,
3716 M. O., and Meixner, F. X., Seasonal variation of ozone deposition to a
3717 tropical rainforest in southwest Amazonia: Atmos. Chem. Phys., 7, 5415-
3718 5435, 2007.

3719 Saatchi, S., Asefi-Najafabady, S., Malhi, Y., Aragão, L. E. O. C., Anderson, L. O.,
3720 Myneni, R. B., and Nemani, R., Persistent effects of a severe drought on
3721 Amazonian forest canopy: Proc. Natl. Acad. Sci., 110, 565-570,
3722 doi:10.1073/pnas.1204651110, 2013.

3723 Salati, E., and Vose, P. B., Amazon Basin - A system in equilibrium: Science,
3724 225, 129-138, doi:10.1126/science.225.4658.129, 1984.

3725 Santos, I. A., and Buchmann, J., A qualitative review emphasizing climatic
3726 aspects of the Amazon and Northeast Brazil: Anu. Inst. Geocienc. , 33
3727 2010.

3728 Schafer, J. S., Holben, B. N., Eck, T. F., Yamasoe, M. A., and Artaxo, P.,
3729 Atmospheric effects on insolation in the Brazilian Amazon: Observed
3730 modification of solar radiation by clouds and smoke and derived single
3731 scattering albedo of fire aerosols: J. Geophys. Res., 107, 8074,
3732 doi:10.1029/2001JD000428, 2002.

3733 Schimel, D., Stephens, B. B., and Fisher, J. B., Effect of increasing CO_2 on the
3734 terrestrial carbon cycle: Proc. Natl. Acad. Sci., 112, 436-441,
3735 doi:10.1073/pnas.1407302112, 2015.

3736 Schkolnik, G., Falkovich, A. H., Rudich, Y., Maenhaut, W., and Artaxo, P., New
3737 analytical method for the determination of levoglucosan, polyhydroxy
3738 compounds, and 2-methylerythritol and its application to smoke and
3739 rainwater samples: Environ. Sci. Technol., 39, 2744-2752, 2005.

3740 Schöngart, J., Wittmann, F., and Worbes, M., Biomass and net primary production
3741 of Central Amazonian floodplains forests, in *Amazonian floodplain*
3742 *forests: ecophysiology, biodiversity and sustainable management*, edited

by W. Junk, M. T. F. Piedade, F. Wittmann, J. Schöngart, & P. Parolin, pp. 347-388, Springer New York, 2010.

Sena, E. T., Artaxo, P., and Correia, A. L., Spatial variability of the direct radiative forcing of biomass burning aerosols and the effects of land use change in Amazonia: Atmos. Chem. Phys., 13, 1261-1275, doi:10.5194/acp-13-1261-2013, 2013.

Serafimovich, A., Thomas, C., and Foken, T., Vertical and horizontal transport of energy and matter by coherent motions in a tall spruce canopy: Boundary-Layer Meteorology, 140, 429-451, doi:10.1007/s10546-011-9619-z, 2011.

Silva Dias, M. A., Rutledge, S., Kabat, P., Silva Dias, P. L., Nobre, C., Fisch, G., Dolman, A. J., Zipser, E., Garstang, M., Manzi, A. O., Fuentes, J. D., Rocha, H. R., Marengo, J., Plana-Fattori, A., Sá, L. D. A., Alvalá, R. C. S., Andreae, M. O., Artaxo, P., Gielow, R., and Gatti, L., Clouds and rain processes in a biosphere-atmosphere interaction context in the Amazon Region: J. Geophys. Res., 107, 8072, doi:10.1029/2001JD000335, 2002.

Sinha, V., Williams, J., Crowley, J. N., and Lelieveld, J., The comparative reactivity method - a new tool to measure total OH reactivity in ambient air: Atmos. Chem. Phys., 8, 2213-2227, 2008.

Soares-Filho, B. S., Nepstad, D. C., Curran, L. M., Cerqueira, G. C., Garcia, R. A., Ramos, C. A., Voll, E., McDonald, A., Lefebvre, P., and Schlesinger, P., Modelling conservation in the Amazon basin: Nature, 440, 520-523, 2006.

Sorbjan, Z., and Czerwinska, A., Statistics of turbulence in the stable boundary layer affected by gravity waves: Boundary-Layer Meteorology, 148, 73-91, doi:10.1007/s10546-013-9809-y, 2013.

Soudani, K., and Francois, C., Remote sensing: A green illusion: Nature, 506, 165-166, doi:10.1038/nature13052, 2014.

Spracklen, D. V., Arnold, S. R., and Taylor, C. M., Observations of increased tropical rainfall preceded by air passage over forests: Nature, 489, 282-285, doi:10.1038/nature11390, 2012.

Steeneveld, G. J., Holtslag, A. A. M., Nappo, C. J., de Wiel, B., and Mahrt, L., Exploring the possible role of small-scale terrain drag on stable boundary layers over land: Journal of Applied Meteorology and Climatology, 47, 2518-2530, doi:10.1175/2008jamc1816.1, 2008.

Steeneveld, G. J., Nappo, C. J., and Holtslag, A. A. M., Estimation of orographically induced wave drag in the stable boundary layer during the CASES-99 experimental campaign: Acta Geophysica, 57, 857-881, doi:10.2478/s11600-009-0028-3, 2009.

Steiner, A. L., Pressley, S. N., Botros, A., Jones, E., Chung, S. H., and Edburg, S. L., Analysis of coherent structures and atmosphere-canopy coupling strength during the CABINEX field campaign: Atmos. Chem. Phys., 11, 11,921-11,936, doi:10.5194/acp-11-11921-2011, 2011.

3785 Steinkamp, K., and Gruber, N., A joint atmosphere-ocean inversion for the
3786 estimation of seasonal carbon sources and sinks: Global Biogeochemical
3787 Cycles, 27, 732-745, doi:10.1002/gbc.20064, 2013.

3788 Stephens, B. B., Gurney, K. R., Tans, P. P., Sweeney, C., Peters, W., Bruhwiler,
3789 L., Ciais, P., Ramonet, M., Bousquet, P., Nakazawa, T., Aoki, S.,
3790 Machida, T., Inoue, G., Vinnichenko, N., Lloyd, J., Jordan, A., Heimann,
3791 M., Shibistova, O., Langenfelds, R. L., Steele, L. P., Francey, R. J., and
3792 Denning, A. S., Weak northern and strong tropical land carbon uptake
3793 from vertical profiles of atmospheric CO2: Science, 316, 1732-1735,
3794 doi:10.1126/science.1137004, 2007.

3795 Stickler, C. M., Coe, M. T., Costa, M. H., Nepstad, D. C., McGrath, D. G., Dias,
3796 L. C. P., Rodrigues, H. O., and Soares-Filho, B. S., Dependence of
3797 hydropower energy generation on forests in the Amazon Basin at local and
3798 regional scales: Proc. Natl. Acad. Sci. USA, 110, 9601-9606,
3799 doi:10.1073/pnas.1215331110, 2013.

3800 Sun, J. L., Burns, S. P., Lenschow, D. H., Banta, R., Newsom, R., Coulter, R.,
3801 Frasier, S., Ince, T., Nappo, C., Cuxart, J., Blumen, W., Lee, X., and Hu,
3802 X. Z., Intermittent turbulence associated with a density current passage in
3803 the stable boundary layer: Boundary-Layer Meteorology, 105, 199-219,
3804 doi:10.1023/a:1019969131774, 2002.

3805 Sun, J. L., Lenschow, D. H., Burns, S. P., Banta, R. M., Newsom, R. K., Coulter,
3806 R., Frasier, S., Ince, T., Nappo, C., Balsley, B. B., Jensen, M., Mahrt, L.,
3807 Miller, D., and Skelly, B., Atmospheric disturbances that generate
3808 intermittent turbulence in nocturnal boundary layers: Boundary-Layer
3809 Meteorology, 110, 255-279, doi:10.1023/a:1026097926169, 2004.

3810 Sun, J. L., Mahrt, L., Banta, R. M., and Pichugina, Y. L., Turbulence regimes and
3811 turbulence intermittency in the stable boundary layer during CASES-99: J.
3812 Atmos. Sci., 69, 338-351, doi:10.1175/jas-d-11-082.1, 2012.

3813 Swap, R., Garstang, M., Greco, S., Talbot, R., and Källberg, P., Saharan dust in
3814 the Amazon Basin: Tellus, 44B, 133-149, 1992.

3815 Talbot, R. W., Andreae, M. O., Berresheim, H., Artaxo, P., Garstang, M., Harriss,
3816 R. C., Beecher, K. M., and Li, S. M., Aerosol chemistry during the wet
3817 season in Central Amazonia: The influence of long-range transport: J.
3818 Geophys. Res., 95, 16,955-16,969, 1990.

3819 Taraborrelli, D., Lawrence, M. G., Crowley, J. N., Dillon, T. J., Gromov, S.,
3820 Gross, C. B. M., Vereecken, L., and Lelieveld, J., Hydroxyl radical
3821 buffered by isoprene oxidation over tropical forests: Nature Geoscience, 5,
3822 190-193, doi:10.1038/ngeo1405, 2012.

3823 Targhetta, N. (2012). *Comparação florística e estrutural entre florestas de igapó*
3824 *e campinarana ao longo de gradientes hidroedáficos na Reserva de*
3825 *Desenvolvimento Sustentável do Uatumã, Amazônia Central.* MSc Thesis,
3826 INPA, Manaus, 96 p.

3827 ter Steege, H., Nigel, C. A., Sabatier, D., Baraloto, C., Salomao, R. P., Guevara, J.
3828 E., Phillips, O. L., Castilho, C. V., Magnusson, W. E., Molino, J. F.,
3829 Monteagudo, A., Vargas, P. N., Montero, J. C., Feldpausch, T. R.,

Coronado, E. N. H., Killeen, T. J., Mostacedo, B., Vasquez, R., Assis, R. L., Terborgh, J., Wittmann, F., Andrade, A., Laurance, W. F., Laurance, S. G. W., Marimon, B. S., Marimon, B. H., Vieira, I. C. G., Amaral, I. L., Brienen, R., Castellanos, H., Lopez, D. C., Duivenvoorden, J. F., Mogollon, H. F., Matos, F. D. D., Davila, N., Garcia-Villacorta, R., Diaz, P. R. S., Costa, F., Emilio, T., Levis, C., Schietti, J., Souza, P., Alonso, A., Dallmeier, F., Montoya, A. J. D., Piedade, M. T. F., Araujo-Murakami, A., Arroyo, L., Gribel, R., Fine, P. V. A., Peres, C. A., Toledo, M., Gerardo, A. A. C., Baker, T. R., Ceron, C., Engel, J., Henkel, T. W., Maas, P., Petronelli, P., Stropp, J., Zartman, C. E., Daly, D., Neill, D., Silveira, M., Paredes, M. R., Chave, J., Lima, D. D., Jorgensen, P. M., Fuentes, A., Schongart, J., Valverde, F. C., Di Fiore, A., Jimenez, E. M., Mora, M. C. P., Phillips, J. F., Rivas, G., van Andel, T. R., von Hildebrand, P., Hoffman, B., Zent, E. L., Malhi, Y., Prieto, A., Rudas, A., Ruschell, A. R., Silva, N., Vos, V., Zent, S., Oliveira, A. A., Schutz, A. C., Gonzales, T., Nascimento, M. T., Ramirez-Angulo, H., Sierra, R., Tirado, M., Medina, M. N. U., van der Heijden, G., Vela, C. I. A., Torre, E. V., Vriesendorp, C., Wang, O., Young, K. R., Baider, C., Balslev, H., Ferreira, C., Mesones, I., Torres-Lezama, A., Giraldo, L. E. U., Zagt, R., Alexiades, M. N., Hernandez, L., Huamantupa-Chuquimaco, I., Milliken, W., Cuenca, W. P., Pauletto, D., Sandoval, E. V., Gamarra, L. V., Dexter, K. G., Feeley, K., Lopez-Gonzalez, G., and Silman, M. R., Hyperdominance in the Amazonian tree flora: Science, 342, 325, doi:10.1126/science.1243092, 2013.

Thomas, C., and Foken, T., Detection of long-term coherent exchange over spruce forest using wavelet analysis: Theoretical and Applied Climatology, 80, 91-104, doi:10.1007/s00704-004-0093-0, 2005.

Thomas, C., and Foken, T., Flux contribution of coherent structures and its implications for the exchange of energy and matter in a tall spruce canopy: Boundary-Layer Meteorology, 123, 317-337, doi:10.1007/s10546-006-9144-7, 2007.

Tollefson, J., Battle for the Amazon: Nature, 520, 20-23, 2015.

Tota, J., Fitzjarrald, D. R., and da Silva Dias, M. A. F., Amazon rainforest exchange of carbon and subcanopy air flow: Manaus LBA Site - A complex terrain condition: Scientific World Journal, 2012, 165067, doi:10.1100/2012/165067, 2012.

Trebs, I., Mayol-Bracero, O. L., Pauliquevis, T., Kuhn, U., Sander, R., Ganzeveld, L., Meixner, F. X., Kesselmeier, J., Artaxo, P., and Andreae, M. O., Impact of the Manaus urban plume on trace gas mixing ratios near the surface in the Amazon Basin: Implications for the NO-NO_2-O_3 photo-stationary state and peroxy radical levels: J. Geophys. Res., 117, doi:10.1029/2011JD016386, 2012.

Tuch, T. M., Haudeck, A., Müller, T., Nowak, A., Wex, H., and Wiedensohler, A., Design and performance of an automatic regenerating adsorption aerosol dryer for continuous operation at monitoring sites: Atmos. Meas. Tech., 2, 417-422, 2009.

3876 Tuomisto, H., Ruokolainen, K., Aguilar, M., and Sarmiento, A., Floristic patterns
3877 along a 43-km long transect in an Amazonian rain forest: Journal of
3878 Ecology, 91, 743-756, doi:10.1046/j.1365-2745.2003.00802.x, 2003.

3879 Valeriano, M. M., Topodata: Guia para utilização de dados geomorfológicos
3880 locais do projeto de produtividade em pesquisa modelagem de dados
3881 topográficos SRTM. INPE Sao Jose dos Campos, Brazil. (2008).

3882 Van de Wiel, B. J. H., Ronda, R. J., Moene, A. F., De Bruin, H. A. R., and
3883 Holtslag, A. A. M., Intermittent turbulence and oscillations in the stable
3884 boundary layer over land. Part I: A bulk model: J. Atmos. Sci., 59, 942-
3885 958, 2002.

3886 van Eijck, A. (2013). *Atmospheric degradation of reactive biogenic VOCs and
3887 their role in aerosol formation: Modeling activities, laboratory
3888 experiments and field studies in different vegetation zones*, Ph.D. Diss.,
3889 University of Mainz, Germany, 113 p.

3890 van Gorsel, E., Harman, I. N., Finnigan, J. J., and Leuning, R., Decoupling of air
3891 flow above and in plant canopies and gravity waves affect
3892 micrometeorological estimates of net scalar exchange: Agricultural and
3893 Forest Meteorology, 151, 927-933, doi:10.1016/j.agrformet.2011.02.012,
3894 2011.

3895 Vendrasco, E. P., Dias, P. L. S., and Freitas, E. D., A case study of the direct
3896 radiative effect of biomass burning aerosols on precipitation in the Eastern
3897 Amazon: Atmos. Res., 94, 409-421, doi:10.1016/j.atmosres.2009.06.016,
3898 2009.

3899 Vestenius, M., Hellen, H., Levula, J., Kuronen, P., Helminen, K. J., Nieminen, T.,
3900 Kulmala, M., and Hakola, H., Acidic reaction products of monoterpenes
3901 and sesquiterpenes in atmospheric fine particles in a boreal forest: Atmos.
3902 Chem. Phys., 14, 7883-7893, doi:10.5194/acp-14-7883-2014, 2014.

3903 Vieira, I. C. G., Toledo, P. M., Silva, J. M. C., and Higuchi, H., Deforestation and
3904 threats to the biodiversity of Amazonia: Brazilian Journal of Biology, 68,
3905 949-956, 2008.

3906 Wan, F., and Porte-Agel, F., A large-eddy simulation study of turbulent flow over
3907 multiscale topography: Boundary-Layer Meteorology, 141, 201-217,
3908 doi:10.1007/s10546-011-9648-7, 2011.

3909 Wang, X., Piao, S., Ciais, P., Friedlingstein, P., Myneni, R. B., Cox, P., Heimann,
3910 M., Miller, J., Peng, S., Wang, T., Yang, H., and Chen, A., A two-fold
3911 increase of carbon cycle sensitivity to tropical temperature variations:
3912 Nature, 506, 212-215, doi:10.1038/nature12915, 2014.

3913 Wendisch, M., Pöschl, U., Andreae, M. O., Machado, L. A. T., Albrecht, R.,
3914 Schlager, H., Rosenfeld, D., Buchholz, B., Ebert, V., Fisch, G., Curtius, J.,
3915 Frank, F., Kohl, R., Rose, D., Hüneke, T., Knecht, M., Pfeilsticker, K.,
3916 Longo, K., Afchine, A., Costa, A., Krämer, M., Jaervinen, E., Schnaiter,
3917 M., Ehrlich, A., Jäkel, E., Krisna, T. C., Kanter, S., Rosenow, D., Werner,
3918 F., Mertes, S., Kästner, U., Dorf, M., Klimach, T., Krüger, M., Nillius, B.,
3919 Pöhlker, C., Schneider, J., Schulz, C., Borrmann, S., Mahnke, C.,
3920 Molleker, S., Weigel, R., Ewald, F., Kölling, T., Mayer, B., Zinner, T.,

Fix, A., Fütterer, D., Jurkat, T., Kenntner, M., Sauer, D., Paul Stock, Voigt, C., Weinzierl, B., Ziereis, H., Barbosa, H., Artaxo, P., Souza, R. A. F. d., and Yamasoe, M. A., The ACRIDICON–CHUVA observational study of tropical convective clouds and precipitation using the new German research aircraft HALO: Bull. Am. Meteorol. Soc., 2015, under review.

Williams, C. A., Scanlon, T. M., and Albertson, J. D., Influence of surface heterogeneity on scalar dissimilarity in the roughness sublayer: Boundary-Layer Meteorology, 122, 149-165, doi:10.1007/s10546-006-9097-x, 2007.

Williams, E., Rosenfeld, D., Madden, N., Gerlach, J., Gears, N., Atkinson, L., Dunnemann, N., Frostrom, G., Antonio, M., Biazon, B., Camargo, R., Franca, H., Gomes, A., Lima, M., Machado, R., Manhaes, S., Nachtigall, L., Piva, H., Quintiliano, W., Machado, L., Artaxo, P., Roberts, G., Renno, N., Blakeslee, R., Bailey, J., Boccippio, D., Betts, A., Wolff, D., Roy, D., Halverson, J., Rickenbach, T., Fuentes, J., and Avelino, E., Contrasting convective regimes over the Amazon: Implications for cloud electrification: J. Geophys. Res., 107, 8082, doi:10.1029/2001JD000380, 2002.

Wilson, K. L., and Birks, J. W., Mechanism and elimination of a water vapor interference in the measurement of ozone by UV absorbance: Environ. Sci. Technol., 40, 6361-6367, 2006.

Winderlich, J., Chen, H., Gerbig, C., Seifert, T., Kolle, O., Lavric, J. V., Kaiser, C., Hofer, A., and Heimann, M., Continuous low-maintenance CO2/CH4/H2O measurements at the Zotino Tall Tower Observatory (ZOTTO) in Central Siberia: Atmos. Meas. Tech., 3, 1113-1128, doi:10.5194/amt-3-1113-2010, 2010.

Winderlich, J., Gerbig, C., Kolle, O., and Heimann, M., Inferences from CO_2 and CH_4 concentration profiles at the Zotino Tall Tower Observatory (ZOTTO) on regional summertime ecosystem fluxes: Biogeosciences, 11, 2055-2068, doi:10.5194/bg-11-2055-2014, 2014.

Wittmann, F., Householder, E., Piedade, M. T. F., de Assis, R. L., Schöngart, J., Parolin, P., and Junk, W. J., Habitat specifity, endemism and the Neotropical distribution of Amazonian white-water floodplain trees: Ecography, 36, 690-707, 2013.

Yañez-Serrano, A. M., Nölscher, A. C., Williams, J., Wolff, S., Alves, E., Martins, G. A., Bourtsoukidis, E., Brito, J., Jardine, K., Artaxo, P., and Kesselmeier, J., Diel and seasonal changes of biogenic volatile organic compounds within and above an Amazonian rainforest: Atmos. Chem. Phys., 15, 3359–3378, doi:10.5194/acp-15-3359-2015, 2015.

Zemp, D. C., Schleussner, C. F., Barbosa, H. M. J., van der Ent, R. J., Donges, J. F., Heinke, J., Sampaio, G., and Rammig, A., On the importance of cascading moisture recycling in South America: Atmos. Chem. Phys., 14, 13,337-13,359, doi:10.5194/acp-14-13337-2014, 2014.

Zeri, M., and Sa, L. D. A., Horizontal and vertical turbulent fluxes forced by a gravity wave event in the nocturnal atmospheric surface layer over the

Amazon forest: Boundary-Layer Meteorology, 138, 413-431, doi:10.1007/s10546-010-9563-3, 2011.

Zeri, M., Sa, L. D. A., Manzi, A. O., Araujo, A. C., Aguiar, R. G., von Randow, C., Sampaio, G., Cardoso, F. L., and Nobre, C. A., Variability of carbon and water fluxes following climate extremes over a tropical forest in southwestern Amazonia: Plos One, 9, e88130, doi:10.1371/journal.pone.0088130, 2014.

Zhang, K., Castanho, A. D. d. A., Galbraith, D. R., Moghim, S., Levine, N., Bras, R. L., Coe, M., Costa, M. H., Malhi, Y., Longo, M., Knox, R. G., McKnight, S., Wang, J., and Moorcroft, P. R., The fate of Amazonian ecosystems over the coming century arising from changes in climate, atmospheric CO_2 and land-use: Global Change Biology, doi:10.1111/gcb.12903, 2015, in press.

Zhou, J., Swietlicki, E., Hansson, H.-C., and Artaxo, P., Submicrometer aerosol particle size distribution and hygroscopic growth measured in the Amazon rain forest during the wet season: J. Geophys. Res., 107, 8055, doi:10.129/2000JD000203, 2002.

Zilitinkevich, S. S., Elperin, T., Kleeorin, N., Rogachevskii, I., and Esau, I., A hierarchy of energy- and flux-budget (EFB) turbulence closure models for stably-stratified geophysical flows: Boundary-Layer Meteorology, 146, 341-373, doi:10.1007/s10546-012-9768-8, 2013.

Author emails

Meinrat O. Andreae (m.andreae@mpic.de)
Otàvio C. Acevedo (otavio@ufsm.br)
Alessandro Araùjo (alessandro.araujo@gmail.com)
Paulo Artaxo (artaxo@if.usp.br)
Cybelli G. G. Barbosa (cybelli.barbosa@gmail.com)
Henrique M. J. Barbosa
Joel Brito (jbrito@if.usp.br)
Samara Carbone (carbone@if.usp.br)
Xuguang Chi (xuguang.chi@mpic.de)
Bruno Barçante Ladvocat Cintra (brunoladvocat@yahoo.com.br)
Naara Ferreira da Silva (naara_fs@hotmail.com)
Nelson L. Dias (nelsonluisdias@gmail.com)
Cléo Quaresma Dias-Júnior (cleoquaresma@hotmail.com)
Florian Ditas (f.ditas@mpic.de)
Reiner Ditz (reiner.ditz@mpic.de)
Ana F. L. Godoi (anaflgodoi@gmail.com)
Ricardo H. M. Godoi (rhmgodoi@hotmail.com)
Martin Heimann (martin.heimann@bgc-jena.mpg.de)
Thorsten Hoffmann (t.hoffmann@uni-mainz.de)
Jürgen Kesselmeier (j.kesselmeier@mpic.de)
Tobias Könemann (tobias.koenemann@gmail.com)
Mira Krüger (m.kruger@mpic.de)
Aline Pontes Lopes <alineplopes@gmail.com>
Jost V. Lavric (jlavric@bgc-jena.mpg.de)
Antonio O. Manzi (manzi@inpa.gov.br)
Demétrius. L. Martins <emaildemetrius@gmail.com>
Eugene F. Mikhailov <eugene.mikhailov@spbu.ru>
Daniel Moran (daniel.moran@mpic.de)
Bruce Walker Nelson <bnelsonbr@gmail.com>
Anke C. Nölscher (a.noelscher@mpic.de)
Daniele Santos Nogueira (danielesn84@yahoo.com.br)
Maria T. F. Piedade (maitepp@inpa.gov.br)
Christopher Pöhlker (c.pohlker@mpic.de)
Ulrich Pöschl (u.poschl@mpic.de)
Carlos Alberto Quesada <quesada.beto@gmail.com>
Nina Ruckteschler (n.ruckteschler@mpic.de)
Chul-Un Ro (curo@inha.ac.kr)
Leonardo D. A. Sá (leodeane@uol.com.br)
Marta de Oliveira Sá (martasa.inpa@gmail.com)
Claudomiro Batista Sales (cbsales1@hotmail.com)
Rosa Maria Nascimento dos Santos (rosa.maria.sto@gmail.com)
Jorge Saturno (j.saturno@mpic.de)
Jochen Schöngart (j.schoengart@mpic.de)
Matthias Sörgel (m.soergel@mpic.de)
Luciana V. Rizzo
Cledenilson Mendonca de Souza (cledenilsonms@gmail.com)
Rodrigo Augusto Ferreira de Souza (souzaraf@gmail.com)

Hang Su (h.su@mpic.de)
Natália Targhetta (natalia.targhetta@gmail.com)
Julio Tóta (totaju@gmail.com)
Ivonne Trebs (ivonne.trebs@list.lu)
Susan Trumbore (trumbore@bgc-jena.mpg.de)
Anna van Eijck (anna.v.eijck@gmail.com)
David Walter (david.walter@mpic.de)
Zhibin Wang (zhibin.wang@mpic.de)
Bettina Weber (b.weber@mpic.de)
Jonathan Williams (jonathan.williams@mpic.de)
Jan Winderlich (jan.winderlich@mpic.de)
Florian Wittmann (F-Wittmann@web.de)
Stefan Wolff (stefan.wolff@mpic.de)
Ana María Yáñez-Serrano (ayanezserrano@yahoo.es)

Deleted: ¶

Tables

Formatted: Heading 1, Indent: Left: 0 cm, Hanging: 0.76 cm

Table 1: Location and specifications of the towers and masts at the ATTO site.

Towers/masts	Coordinates (WGS 84)	Base elevation [m]	Height [m]
Walk-up tower	S 02° 08.647’ W 58° 59.992’	130	80
Triangular mast	S 02° 08.602’ W 59° 00.033’	130	81
ATTO Tall Tower	S 2° 08.752' W 59° 00.335’	130	325

Table 2: Overview of (micro)-meteorological sensors, trace gas and aerosol instrumentation installed at the walk-up tower.

Quantity	**Instrument**	**Height a.g.l./depth [m]**	**Institution**
Soil heat flux	Heat flux sensor (HFP01, Hukseflux, Netherlands)	0.05	INPA, EMBRAPA, MPIC
Soil moisture	Water content reflectometer (CS615, Campbell Scientific Inc., USA)	0.1; 0.2; 0.3; 0.4; 0,6; 1.0	INPA, EMBRAPA
Soil temperature	Thermistor (108, Campbell Scientific Inc., USA)	0.1; 0.2; 0.4	INPA, EMBRAPA, MPIC
Shortwave radiation (incoming and reflected)	Pyranometer (CMP21,Kipp & Zonen, Netherlands)	75.0	INPA, EMBRAPA
Longwave radiation (atmospheric and terrestrial)	Pyrgeometer (CGR4, Kipp & Zonen, Netherlands)	75.0	INPA, EMBRAPA
PAR (incoming and reflected)	Quantum sensor (PAR LITE, Kipp & Zonen, Netherlands)	75.0	USP
Net radiation	Net radiometer (NR-LITE2, Kipp & Zonen, Netherlands)	75.0	INPA, EMBRAPA
Ultra violet radiation	UV radiometer (CUV5, Kipp & Zonen, Netherlands)	75.0	INPA, EMBRAPA
Rainfall	Rain gauge (TB4, Hydrological Services Pty. Ltd., Australia)	81.0	INPA, EMBRAPA
Air temperature and relative humidity	Termohygrometer (CS215, Rotronic Measurement Solutions, UK)	81.0; 73.0; 55.0; 40.0; 36.0; 26.0; 12.0; 4.0; 1.5; 0.4	INPA, EMBRAPA
Atmospheric pressure	Barometer (PTB101B, Vaisala, Finnland)	75.0	INPA, EMBRAPA
Wind speed and direction	2D sonic anemometer (Windsonic, Gill Instruments Ltd., UK)	73.0; 65.0; 50.0; 42.0; 26.0; 19.0	INPA, EMBRAPA

Wind vector components (u, v, w)	3D sonic anemometer (Windmaster, Gill Instruments Ltd., UK)	81.0; 46.0; 36.0; 4.0; 1.0	INPA, EMBRAPA
CO_2 and H_2O molar density	IRGA (LI-7500A, LI-COR Inc., USA) IRGA (LI-7200, LI-COR Inc., USA)	81.0; 46.0 1.0	INPA, EMBRAPA
Vertical profile of CO_2, CH_4 and CO mixing ratios	G1301 (CFADS-109) and G1302 (CKADS-018; both Picarro Inc., USA)	4.0; 24.0; 38.0; 53.0; 79.0	MPI-BGC, MPI-C
Vertical profile of NO, NO_2, O_3, CO_2, and H_2O mixing ratios	CLD 780TR (Eco Physics, Switzerland), BLC (Droplet Measurement Technologies Inc., USA), TEI 49i (Thermo Electron Corp, USA), IRGA 7000 (LI-COR Inc., USA)	0.05; 0.5; 4.0; 12.0; 24.0; 38.3; 53.0; 79.3	INPA, MPI-C, UEA
Vertical profile of VOCs	Proton Transfer Mass Spectrometer (PTR-QMS 500, Ionicon, Austria)	0.05; 0.5; 4.0; 12.0; 24.0; 38.3; 53.0; 79.3	MPI-C, USP, INPA
Vertical profile of total reactivity to OH	Comparative Reaction Method, Proton Transfer Mass Spectrometer	0.05; 0.5; 4.0; 12.0; 24.0; 38.3; 53.0; 79.3	MPI-C
Black carbon equivalent	Multi Angle Absorption Photometer (model 5012, Thermo-Scientific, USA)	60.0	MPI-C
Refractory black carbon	Single Particle Soot Photometer (SP-2, Droplet Measurement Technologies, USA)	60.0	MPI-C
Black carbon equivalent	Aethalometer (model AE31 or AE33, Magee Scientific Corporation, USA)	60.0	USP
Aerosol scattering	Nephelometer (model 3563, TSI, USA) Ecotech Aurora 3000; wavelengths 450, 525, and 635 nm	60.0	USP
Aerosol number concentration	Condensation particle counter (model 3022A,TSI, USA)	60.0	MPI-C
Aerosol size distribution	Ultra-High Sensitivity Aerosol Spectrometer (Droplet Measurement Technologies,	60.0	MPI-C

Deleted: B

	USA)		
	Scanning Mobility Particle Sizer (SMPS, TSI model 3080, St. Paul, MN, USA; size range: 10-430 nm)	60.0	
	Optical Particle Sizer (OPS, TSI model 3330; size range: 0.3-10 µm)	60.0	
	Wide Range Aerosol Spectrometer (WRAS, Grimm Aerosol Technik, Ainring, Germany; size range: 6 nm - 32 µm)	3.0	
Primary Biological Aerosol Particles (PBAP)	Wideband Integrated Bioaerosol Spectrometer (WIBS-4, DMT)	60.0	MPI-C
Aerosol chemical composition	Aerosol Chemical Speciation Monitor (ACSM, Aerodyne, USA)	60.0	USP

Table 3: Tree species richness, forest structure, above-ground wood biomass (AGWB) and carbon stocks of the inventoried forest plots.

	Density	DBH	Tree height	Basal area	Species richness	AGWB[2]	Carbon stock[3]
		Mean±sd (max)	Mean±sd (max)				AGWB
	(Trees ha^{-1})	(cm)	(m)	(m^2 ha^{-1})	(spp. ha^{-1})	(Mg ha^{-1})	(Mg C ha^{-1})
Floodplain (igapó)[1]							
plot1	695	19.5±8.1 (136)	12.2±3.8 (27)	26.8	26	126	63
plot2	540	20.9±12.0 (78)	10.5±4.2 (29)	25.8	49	146	73
plot3	928	17.9±9.4 (117)	11.5±1.9 (18)	30.3	31	173	87
Mean±sd	**721±195**	**19.4±1.5**	**11.4±0.9**	**27.6±2.4**	**35±12**	**148±24**	**74±12**
Campina/campinarana							
plot 1	560	20.1±12.1 (90)	15.2±4.7 (34)	24.3	82	190	95
plot 2	503	17.2±10.4 (83)	11.2±3.6 (26)	16.3	46	98	49
plot 3	786	18.3±17.7 (162)	12.9±5.0 (33)	27.8	65	185	93
Mean±sd	**616±150**	**18.5±1.5**	**13.1±2.0**	**22.8±5.9**	**64±18**	**158±52**	**79±26**
Ancient fluvial terrace							
plot 1	516	20.9±11.2 (100)	14.9±3.0 (30)	22.7	135	181	91
plot 2	483	20.8±12.7 (117)	14.8±3.3 (32)	22.6	120	194	97
plot 3	492	21.1±14.6 (177)	14.8±3.5 (38)	25.4	126	232	116
Mean±sd	**497±17**	**20.9±0.2**	**14.8±0.1**	**23.6±1.6**	**127±8**	**202±27**	**101±13**
Terra firme							
plot 1	522	21.3±13.9 (152)	20.5±4.6 (40)	26.4	132	318	159
plot 2	644	20.5±12.0 (120)	20.4±4.3 (38)	28.6	142	335	168
plot 3	624	22.1±12.5 (96)	21.1±4.4 (36)	31.7	137	368	184
Mean±sd	**597±65**	**21.3±0.8**	**20.7±0.4**	**28.9±2.7**	**137±5**	**340±25**	**170±13**

[1] Mean flood height in the igapó floodplains: plot 1: 3.40±1.06 m; plot 2: 3.12±0.62 m; plot 3: 1.81±0.64 m

[2] Aboveground wood biomass (AGWB) was calculated using a pantropical allometric equation considering diameter (*DBH* in cm), tree height (*H* in m) and wood specific gravity (ρ in g cm^{-3}) as independent parameters (Feldpausch et al., 2012): $AGWB = -2.9205 + 0.9894 \times \ln (DBH^2 \times H \times \rho)$

[3] The carbon stock was estimated by 50% of the AGWB (Clark et al., 2001)

Table 4: Carbon stocks, soil bulk density, concentrations of K, Mg, Ca, P, Total reserve bases ($\sum_{RB}$), clay, silt, and sand, and Quesada's index of the forest plots.

	C stock (Mg ha^{-1}) [a]	Bulk density (g cm^{-3})	K (mmol$_c$ kg^{-1})[b]	Mg (mmol$_c$ kg^{-1})[b]	Ca (mmol$_c$ kg^{-1})[b]	P (mg kg^{-1})	$\sum_{RB}$ (mmol$_c$ kg^{-1} clay)^2	Clay (%)	Silt (%)	Sand (%)	Quesada's Index[c]
PLATEAUS											
1	143.7±8.7	0.9	0.3	0.4	0.4	84.8	1.7	85.1	5.2	9.7	0
2	160.7±7.6	0.9	0.4	0.4	0.8	125.9	1.8	86.2	4.6	9.2	0
3	164.1±6.9	0.9	0.4	0.3	0.8	121.4	1.0	84.6	3.8	12.1	0
Means	**156.2±10.9**	**0.9**	**0.4**	**0.4**	**0.7**	**100.2**	**1.5**	**85.3**	**4.5**	**10.4**	**0**
TERRACES											
1	140.2±6.4	1.2	0.3	0.4	0.6	92.5	4.9	52.8	12.4	34.8	3
2	129.4±6.8	1.1	0.3	0.4	0.7	181.1	5.1	70.7	7.1	24.8	2
3	140.8±5.9	1.1	0.4	0.5	0.8	129.1	5.5	68.3	6.4	25.4	1
Means	**136.8±6.4**	**1.0**	**0.3**	**0.4**	**0.7**	**161.1**	**5.2**	**74.3**	**6.6**	**19.3**	**2**

[a] Total cumulative C stock up to 2 m depth. Mean per plot and their respective standard deviations
[b] Mean nutrient concentration up to 30 cm depth
[c] Quesada's Index indicating soil physical constraints in which higher values of the index show stronger physical constraint. It is a semi-quantitative index and does not show intermediate values, therefore the value shown in the "means" line is the median value of the three plots.

Formatted: Font: Not Bold
Formatted: Font: Not Bold
Formatted Table
Formatted Table

Table 5: Percentage of occurrence of Cava's classes for dry and wet season obtained at the ATTO site and a comparison with the results found by Cava for the Duke Forest, North Carolina, USA.

Deleted: 4

Class	ATTO			Duke
	Wet	Dry	Avg.	Avg.
I	46.8 %	49.1 %	47.9 %	45.7 %
II	14.0 %	28.3 %	21.2 %	5.9 %
III	7.6 %	7.6 %	7.6 %	29.2 %
IV	3.8 %	3.7 %	3.75 %	1 %
V	27.8 %	11.3 %	19.6 %	18.2 %

Table 6: Distribution of Cava's classes associated with the turbulence regimes for the ATTO site nocturnal boundary layer.

Deleted: 5

	Regime 1		Regime 2		Regime 3	
	Wet	Dry	Wet	Dry	Wet	Dry
Class I	19.2 %	49 %	38.5 %	16 %	42.3 %	35 %
Class IV	100 %	67 %	0 %	0 %	0 %	33 %
Class V	25 %	50 %	25 %	27 %	50 %	23 %

Table 7: Summary of aerosol optical parameters for the dry and wet seasons. Average and standard deviations are calculated from 60-min data.

		Dry season		Wet season	
		Mean	Std. Dev.	**Mean**	Std. Dev.
Scattering coefficient (σ_s, Mm^{-1})	450 nm	**31**	15	**8.0**	7.4
	550 nm	**23**	11	**6.4**	6.5
	700 nm	**15**	8	**4.8**	5.3
Scattering Ångström Exponent ($å_s$)	450/700	**1.62**	0.26	**1.25**	0.71
Absorption coefficient (σ_a, Mm^{-1})	637 nm	**3.46**	2.32	**0.52**	1.25
Absorption Ångström Exponent ($å_a$)	470/960	**1.40***	0.26	**1.53***	0.36
Mass absorption cross-section (α_a, m^2/g)	637 nm			**13.5§**	

* Calculated by a log-log linear fit including the last six wavelengths measured by the Aethalometer ($R^2 > 0.99$).

§ Obtained by orthogonal regression ($R^2 = 0.92$)

Table 8: Relative abundance of single particle types obtained at top of the walk-up tower in April 2012 (in percent).

Deleted: 7

Date April 2012	Size fraction (μm)	Organic	Organic with S,K	Mineral	Biogenic	Salts	Soot
1	0.25~0.5	70	13	17	0	0	0
	0.5~1.0	0	27	71	1.2	0	0
	1.0~2.0	24	28	47	1.7	0	0
16	0.25~0.5	42	58	0	0	0	0
	0.5~1.0	60	32	8	0	0	0
	1.0~2.0	50	5.3	16	13	16	0
17	0.25~0.5	82	6.1	3	9.1	0	0
	0.5~1.0	37	27	6.7	17	13	0
	1.0~2.0	0	79	21	0	0	0
18	0.25~0.5	72	28	0	0	0	0
	0.5~1.0	41	36	21	2.4	0	0
	1.0~2.0	34	31	17	5.7	0	11